REPORT DOCUMENTATION PAGE

AFRL-SR-BL-TR-00-

0742

1. AGENCY USE ONLY *(Leave blank)*	2. REPORT DATE	3. REPORT TYPE AND DATES COVERED
	December, 1996	

4. TITLE AND SUBTITLE
1996 Summer Research Program (SRP), Graduate Student Research Program (GSRP), Final Reports, Volume 11, Arnold Eng. Development Center, US Air Force Academy, Wilford Hall Medical Center, and Wright Patterson Medical Center

5. FUNDING NUMBERS
F49620-93-C-0063

6. AUTHOR(S)
Gary Moore

7. PERFORMING ORGANIZATION NAME(S) AND ADDRESS(ES)
Research & Development Laboratories (RDL)
5800 Uplander Way
Culver City, CA 90230-6608

8. PERFORMING ORGANIZATION REPORT NUMBER

9. SPONSORING/MONITORING AGENCY NAME(S) AND ADDRESS(ES)
Air Force Office of Scientific Research (AFOSR)
801 N. Randolph St.
Arlington, VA 22203-1977

10. SPONSORING/MONITORING AGENCY REPORT NUMBER

11. SUPPLEMENTARY NOTES

12a. DISTRIBUTION AVAILABILITY STATEMENT
Approved for Public Release

12b. DISTRIBUTION CODE

13. ABSTRACT *(Maximum 200 words)*

The United States Air Force Summer Research Program (USAF-SRP) is designed to introduce university, college, and technical institute faculty members, graduate students, and high school students to Air Force research. This is accomplished by the faculty members (Summer Faculty Research Program, (SFRP)), graduate students (Graduate Student Research Program (GSRP)), and high school students (High School Apprenticeship Program (HSAP)) being selected on a nationally advertised competitive basis during the summer intersession period to perform research at Air Force Research Laboratory (AFRL) Technical Directorates, Air Force Air Logistics Centers (ALC), and other AF Laboratories. This volume consists of a program overview, program management statistics, and the final technical reports from the GSRP participants at the Arnold Engineering Development Center, US Air Force Academy, Wilford Hall Medical Center, and Wright Patterson Medical Center

14. SUBJECT TERMS
Air Force Research, Air Force, Engineering, Laboratories, Reports, Summer, Universities, Faculty, Graduate Student, High School Student

15. NUMBER OF PAGES

16. PRICE CODE

17. SECURITY CLASSIFICATION OF REPORT	18. SECURITY CLASSIFICATION OF THIS PAGE	19. SECURITY CLASSIFICATION OF ABSTRACT	20. LIMITATION OF ABSTRACT
Unclassified	Unclassified	Unclassified	UL

GENERAL INSTRUCTIONS FOR COMPLETING SF 298

The Report Documentation Page (RDP) is used in announcing and cataloging reports. It is important that this information be consistent with the rest of the report, particularly the cover and title page. Instructions for filling in each block of the form follow. It is important to ***stay within the lines*** to meet ***optical scanning requirements.***

Block 1. Agency Use Only *(Leave blank)*.

Block 2. Report Date. Full publication date including day, month, and year, if available (e.g. 1 Jan 88). Must cite at least the year.

Block 3. Type of Report and Dates Covered. State whether report is interim, final, etc. If applicable, enter inclusive report dates (e.g. 10 Jun 87 - 30 Jun 88).

Block 4. Title and Subtitle. A title is taken from the part of the report that provides the most meaningful and complete information. When a report is prepared in more than one volume, repeat the primary title, add volume number, and include subtitle for the specific volume. On classified documents enter the title classification in parentheses.

Block 5. Funding Numbers. To include contract and grant numbers; may include program element number(s), project number(s), task number(s), and work unit number(s). Use the following labels:

C - Contract	**PR** - Project
G - Grant	**TA** - Task
PE - Program Element	**WU** - Work Unit Accession No.

Block 6. Author(s). Name(s) of person(s) responsible for writing the report, performing the research, or credited with the content of the report. If editor or compiler, this should follow the name(s).

Block 7. Performing Organization Name(s) and Address(es). Self-explanatory.

Block 8. Performing Organization Report Number. Enter the unique alphanumeric report number(s) assigned by the organization performing the report.

Block 9. Sponsoring/Monitoring Agency Name(s) and Address(es). Self-explanatory.

Block 10. Sponsoring/Monitoring Agency Report Number. *(If known)*

Block 11. Supplementary Notes. Enter information not included elsewhere such as: Prepared in cooperation with....; Trans. of....; To be published in.... When a report is revised, include a statement whether the new report supersedes or supplements the older report.

Block 12a. Distribution/Availability Statement. Denotes public availability or limitations. Cite any availability to the public. Enter additional limitations or special markings in all capitals (e.g. NOFORN, REL, ITAR).

DOD -	See DoDD 5230.24, "Distribution Statements on Technical Documents."
DOE -	See authorities.
NASA -	See Handbook NHB 2200.2.
NTIS -	Leave blank.

Block 12b. Distribution Code.

DOD -	Leave blank.
DOE -	Enter DOE distribution categories from the Standard Distribution for Unclassified Scientific and Technical Reports.
	Leave blank.
NASA -	Leave blank.
NTIS -	

Block 13. Abstract. Include a brief *(Maximum 200 words)* factual summary of the most significant information contained in the report.

Block 14. Subject Terms. Keywords or phrases identifying major subjects in the report.

Block 15. Number of Pages. Enter the total number of pages.

Block 16. Price Code. Enter appropriate price code *(NTIS only)*.

Blocks 17. - 19. Security Classifications. Self- explanatory. Enter U.S. Security Classification in accordance with U.S. Security Regulations (i.e., UNCLASSIFIED). If form contains classified information, stamp classification on the top and bottom of the page.

Block 20. Limitation of Abstract. This block must be completed to assign a limitation to the abstract. Enter either UL (unlimited) or SAR (same as report). An entry in this block is necessary if the abstract is to be limited. If blank, the abstract is assumed to be unlimited.

UNITED STATES AIR FORCE

SUMMER RESEARCH PROGRAM -- 1996

GRADUATE STUDENT RESEARCH PROGRAM FINAL REPORTS

VOLUME 11

ARNOLD ENGINEERING DEVELOPMENT CENTER

UNITED STATES AIR FORCE ACADEMY

WILFORD HALL MEDCIAL CENTER

WRIGHT PATTERSON MEDICAL CENTER

RESEARCH & DEVELOPMENT LABORATORIES

5800 Uplander Way

Culver City, CA 90230-6608

Program Director, RDL
Gary Moore

Program Manager, AFOSR
Major Linda Steel-Goodwin

Program Manager, RDL
Scott Licoscos

Program Administrator, RDL
Johnetta Thompson

Program Administrator, RDL
Rebecca Kelly

Submitted to:

AIR FORCE OFFICE OF SCIENTIFIC RESFARCH

Bolling Air Force Base

Washington, D.C.

December 1996

PREFACE

Reports in this volume are numbered consecutively beginning with number 1. Each report is paginated with the report number followed by consecutive page numbers, e.g., 1-1, 1-2, 1-3; 2-1, 2-2, 2-3.

This document is one of a set of 16 volumes describing the 1996 AFOSR Summer Research Program. The following volumes comprise the set:

VOLUME	TITLE
1	Program Management Report
	Summer Faculty Research Program (SFRP) Reports
2A & 2B	Armstrong Laboratory
3A & 3B	Phillips Laboratory
4	Rome Laboratory
5A & 5B	Wright Laboratory
6	Arnold Engineering Development Center, Frank J. Seiler Research Laboratory, and Wilford Hall Medical Center, Air Logistic Centers
	Graduate Student Research Program (GSRP) Reports
7	Armstrong Laboratory
8	Phillips Laboratory
9	Rome Laboratory
10A & 10B	Wright Laboratory
11	Arnold Engineering Development Center, United States Air Force Academy, Wilford Hall Medical Center, and Wright Patterson Medical Center
	High School Apprenticeship Program (HSAP) Reports
12A & 12B	Armstrong Laboratory
13	Phillips Laboratory
14	Rome Laboratory
15A&B	Wright Laboratory
16	Arnold Engineering Development Center

SRP Final Report Table of Contents

SRP Final Report Table of Contents

SRP Final Report Table of Contents

SRP Final Report Table of Contents

SRP Final Report Table of Contents

SRP Final Report Table of Contents

SRP Final Report Table of Contents

SRP Final Report Table of Contents

INTRODUCTION

The Summer Research Program (SRP), sponsored by the Air Force Office of Scientific Research (AFOSR), offers paid opportunities for university faculty, graduate students, and high school students to conduct research in U.S. Air Force research laboratories nationwide during the summer.

Introduced by AFOSR in 1978, this innovative program is based on the concept of teaming academic researchers with Air Force scientists in the same disciplines using laboratory facilities and equipment not often available at associates' institutions.

The Summer Faculty Research Program (SFRP) is open annually to approximately 150 faculty members with at least two years of teaching and/or research experience in accredited U.S. colleges, universities, or technical institutions. SFRP associates must be either U.S. citizens or permanent residents.

The Graduate Student Research Program (GSRP) is open annually to approximately 100 graduate students holding a bachelor's or a master's degree; GSRP associates must be U.S. citizens enrolled full time at an accredited institution.

The High School Apprentice Program (HSAP) annually selects about 125 high school students located within a twenty mile commuting distance of participating Air Force laboratories.

AFOSR also offers its research associates an opportunity, under the Summer Research Extension Program (SREP), to continue their AFOSR-sponsored research at their home institutions through the award of research grants. In 1994 the maximum amount of each grant was increased from $20,000 to $25,000, and the number of AFOSR-sponsored grants decreased from 75 to 60. A separate annual report is compiled on the SREP.

The numbers of projected summer research participants in each of the three categories and SREP "grants" are usually increased through direct sponsorship by participating laboratories.

AFOSR's SRP has well served its objectives of building critical links between Air Force research laboratories and the academic community, opening avenues of communications and forging new research relationships between Air Force and academic technical experts in areas of national interest, and strengthening the nation's efforts to sustain careers in science and engineering. The success of the SRP can be gauged from its growth from inception (see Table 1) and from the favorable responses the 1996 participants expressed in end-of-tour SRP evaluations (Appendix B).

AFOSR contracts for administration of the SRP by civilian contractors. The contract was first awarded to Research & Development Laboratories (RDL) in September 1990. After

completion of the 1990 contract, RDL (in 1993) won the recompetition for the basic year and four 1-year options.

2. PARTICIPATION IN THE SUMMER RESEARCH PROGRAM

The SRP began with faculty associates in 1979; graduate students were added in 1982 and high school students in 1986. The following table shows the number of associates in the program each year.

YEAR	SRP Participation, by Year			TOTAL
	SFRP	GSRP	HSAP	
1979	70			70
1980	87			87
1981	87			87
1982	91	17		108
1983	101	53		154
1984	152	84		236
1985	154	92		246
1986	158	100	42	300
1987	159	101	73	333
1988	153	107	101	361
1989	168	102	103	373
1990	165	121	132	418
1991	170	142	132	444
1992	185	121	159	464
1993	187	117	136	440
1994	192	117	133	442
1995	190	115	137	442
1996	188	109	138	435

Beginning in 1993, due to budget cuts, some of the laboratories weren't able to afford to fund as many associates as in previous years. Since then, the number of funded positions has remained fairly constant at a slightly lower level.

3. RECRUITING AND SELECTION

The SRP is conducted on a nationally advertised and competitive-selection basis. The advertising for faculty and graduate students consisted primarily of the mailing of 8,000 52-page SRP brochures to chairpersons of departments relevant to AFOSR research and to administrators of grants in accredited universities, colleges, and technical institutions. Historically Black Colleges and Universities (HBCUs) and Minority Institutions (MIs) were included. Brochures also went to all participating USAF laboratories, the previous year's participants, and numerous individual requesters (over 1000 annually).

RDL placed advertisements in the following publications: *Black Issues in Higher Education, Winds of Change,* and *IEEE Spectrum.* Because no participants list either *Physics Today* or *Chemical & Engineering News* as being their source of learning about the program for the past several years, advertisements in these magazines were dropped, and the funds were used to cover increases in brochure printing costs.

High school applicants can participate only in laboratories located no more than 20 miles from their residence. Tailored brochures on the HSAP were sent to the head counselors of 180 high schools in the vicinity of participating laboratories, with instructions for publicizing the program in their schools. High school students selected to serve at Wright Laboratory's Armament Directorate (Eglin Air Force Base, Florida) serve eleven weeks as opposed to the eight weeks normally worked by high school students at all other participating laboratories.

Each SFRP or GSRP applicant is given a first, second, and third choice of laboratory. High school students who have more than one laboratory or directorate near their homes are also given first, second, and third choices.

Laboratories make their selections and prioritize their nominees. AFOSR then determines the number to be funded at each laboratory and approves laboratories' selections.

Subsequently, laboratories use their own funds to sponsor additional candidates. Some selectees do not accept the appointment, so alternate candidates are chosen. This multi-step selection procedure results in some candidates being notified of their acceptance after scheduled deadlines. The total applicants and participants for 1996 are shown in this table.

1996 Applicants and Participants			
PARTICIPANT CATEGORY	TOTAL APPLICANTS	SELECTEES	DECLINING SELECTEES
SFRP	572	188	39
(HBCU/MI)	(119)	(27)	(5)
GSRP	235	109	7
(HBCU/MI)	(18)	(7)	(1)
HSAP	474	138	8
TOTAL	1281	435	54

4. SITE VISITS

During June and July of 1996, representatives of both AFOSR/NI and RDL visited each participating laboratory to provide briefings, answer questions, and resolve problems for both laboratory personnel and participants. The objective was to ensure that the SRP would be as constructive as possible for all participants. Both SRP participants and RDL representatives found these visits beneficial. At many of the laboratories, this was the only opportunity for all participants to meet at one time to share their experiences and exchange ideas.

5. HISTORICALLY BLACK COLLEGES AND UNIVERSITIES AND MINORITY INSTITUTIONS (HBCU/MIs)

Before 1993, an RDL program representative visited from seven to ten different HBCU/Mis annually to promote interest in the SRP among the faculty and graduate students. These efforts were marginally effective, yielding a doubling of HBCI/MI applicants. In an effort to achieve AFOSR's goal of 10% of all applicants and selectees being HBCU/MI qualified, the RDL team decided to try other avenues of approach to increase the number of qualified applicants. Through the combined efforts of the AFOSR Program Office at Bolling AFB and RDL, two very active minority groups were found, HACU (Hispanic American Colleges and Universities) and AISES (American Indian Science and Engineering Society). RDL is in communication with representatives of each of these organizations on a monthly basis to keep up with the their activities and special events. Both organizations have widely-distributed magazines/quarterlies in which RDL placed ads.

Since 1994 the number of both SFRP and GSRP HBCU/MI applicants and participants has increased ten-fold, from about two dozen SFRP applicants and a half dozen selectees to over 100 applicants and two dozen selectees, and a half-dozen GSRP applicants and two or three selectees to 18 applicants and 7 or 8 selectees. Since 1993, the SFRP had a two-fold applicant

increase and a two-fold selectee increase. Since 1993, the GSRP had a three-fold applicant increase and a three to four-fold increase in selectees.

In addition to RDL's special recruiting efforts, AFOSR attempts each year to obtain additional funding or use leftover funding from cancellations the past year to fund HBCU/MI associates. This year, 5 HBCU/MI SFRPs declined after they were selected (and there was no one qualified to replace them with). The following table records HBCU/MI participation in this program.

SRP HBCU/MI Participation, By Year				
YEAR	SFRP		GSRP	
	Applicants	Participants	Applicants	Participants
1985	76	23	15	11
1986	70	18	20	10
1987	82	32	32	10
1988	53	17	23	14
1989	39	15	13	4
1990	43	14	17	3
1991	42	13	8	5
1992	70	13	9	5
1993	60	13	6	2
1994	90	16	11	6
1995	90	21	20	8
1996	119	27	18	7

6. SRP FUNDING SOURCES

Funding sources for the 1996 SRP were the AFOSR-provided slots for the basic contract and laboratory funds. Funding sources by category for the 1996 SRP selected participants are shown here.

1996 SRP FUNDING CATEGORY	SFRP	GSRP	HSAP
AFOSR Basic Allocation Funds	141	85	123
USAF Laboratory Funds	37	19	15
HBCU/MI By AFOSR (Using Procured Addn'l Funds)	10	5	0
TOTAL	188	109	138

SFRP - 150 were selected, but nine canceled too late to be replaced.
GSRP - 90 were selected, but five canceled too late to be replaced (10 allocations for the ALCs were withheld by AFOSR.)
HSAP - 125 were selected, but two canceled too late to be replaced.

7. COMPENSATION FOR PARTICIPANTS

Compensation for SRP participants, per five-day work week, is shown in this table.

1996 SRP Associate Compensation

PARTICIPANT CATEGORY	1991	1992	1993	1994	1995	1996
Faculty Members	$690	$718	$740	$740	$740	$770
Graduate Student (Master's Degree)	$425	$442	$455	$455	$455	$470
Graduate Student (Bachelor's Degree)	$365	$380	$391	$391	$391	$400
High School Student (First Year)	$200	$200	$200	$200	$200	$200
High School Student (Subsequent Years)	$240	$240	$240	$240	$240	$240

The program also offered associates whose homes were more than 50 miles from the laboratory an expense allowance (seven days per week) of $50/day for faculty and $40/day for graduate students. Transportation to the laboratory at the beginning of their tour and back to their home destinations at the end was also reimbursed for these participants. Of the combined SFRP and

GSRP associates, 65 % (194 out of 297) claimed travel reimbursements at an average round-trip cost of $780.

Faculty members were encouraged to visit their laboratories before their summer tour began. All costs of these orientation visits were reimbursed. Forty-five percent (85 out of 188) of faculty associates took orientation trips at an average cost of $444. By contrast, in 1993, 58 % of SFRP associates took orientation visits at an average cost of $685; that was the highest percentage of associates opting to take an orientation trip since RDL has administered the SRP, and the highest average cost of an orientation trip. These 1993 numbers are included to show the fluctuation which can occur in these numbers for planning purposes.

Program participants submitted biweekly vouchers countersigned by their laboratory research focal point, and RDL issued paychecks so as to arrive in associates' hands two weeks later.

In 1996, RDL implemented direct deposit as a payment option for SFRP and GSRP associates. There were some growing pains. Of the 128 associates who opted for direct deposit, 17 did not check to ensure that their financial institutions could support direct deposit (and they couldn't), and eight associates never did provide RDL with their banks' ABA number (direct deposit bank routing number), so only 103 associates actually participated in the direct deposit program. The remaining associates received their stipend and expense payments via checks sent in the US mail.

HSAP program participants were considered actual RDL employees, and their respective state and federal income tax and Social Security were withheld from their paychecks. By the nature of their independent research, SFRP and GSRP program participants were considered to be consultants or independent contractors. As such, SFRP and GSRP associates were responsible for their own income taxes, Social Security, and insurance.

8. CONTENTS OF THE 1996 REPORT

The complete set of reports for the 1996 SRP includes this program management report (Volume 1) augmented by fifteen volumes of final research reports by the 1996 associates, as indicated below:

1996 SRP Final Report Volume Assignments

LABORATORY	SFRP	GSRP	HSAP
Armstrong	2	7	12
Phillips	3	8	13
Rome	4	9	14
Wright	5A, 5B	10	15
AEDC, ALCs, WHMC	6	11	16

APPENDIX A – PROGRAM STATISTICAL SUMMARY

A. Colleges/Universities Represented

Selected SFRP associates represented 169 different colleges, universities, and institutions, GSRP associates represented 95 different colleges, universities, and institutions.

B. States Represented

SFRP -Applicants came from 47 states plus Washington D.C. and Puerto Rico. Selectees represent 44 states plus Puerto Rico.

GSRP - Applicants came from 44 states and Puerto Rico. Selectees represent 32 states.

HSAP - Applicants came from thirteen states. Selectees represent nine states.

Total Number of Participants	
SFRP	188
GSRP	109
HSAP	138
TOTAL	435

Degrees Represented			
	SFRP	GSRP	TOTAL
Doctoral	184	1	185
Master's	4	48	52
Bachelor's	0	60	60
TOTAL	188	109	297

SFRP Academic Titles	
Assistant Professor	79
Associate Professor	59
Professor	42
Instructor	3
Chairman	0
Visiting Professor	1
Visiting Assoc. Prof.	0
Research Associate	4
TOTAL	188

Source of Learning About the SRP		
Category	Applicants	Selectees
Applied/participated in prior years	28%	34%
Colleague familiar with SRP	19%	16%
Brochure mailed to institution	23%	17%
Contact with Air Force laboratory	17%	23%
IEEE Spectrum	2%	1%
BIIHE	1%	1%
Other source	10%	8%
TOTAL	100%	100%

APPENDIX B – SRP EVALUATION RESPONSES

1. OVERVIEW

Evaluations were completed and returned to RDL by four groups at the completion of the SRP. The number of respondents in each group is shown below.

Table B-1. Total SRP Evaluations Received

Evaluation Group	Responses
SFRP & GSRPs	275
HSAPs	113
USAF Laboratory Focal Points	84
USAF Laboratory HSAP Mentors	6

All groups indicate unanimous enthusiasm for the SRP experience.

The summarized recommendations for program improvement from both associates and laboratory personnel are listed below:

A. Better preparation on the labs' part prior to associates' arrival (i.e., office space, computer assets, clearly defined scope of work).

B. Faculty Associates suggest higher stipends for SFRP associates.

C. Both HSAP Air Force laboratory mentors and associates would like the summer tour extended from the current 8 weeks to either 10 or 11 weeks; the groups state it takes 4-6 weeks just to get high school students up-to-speed on what's going on at laboratory. (Note: this same argument was used to raise the faculty and graduate student participation time a few years ago.)

2. 1996 USAF LABORATORY FOCAL POINT (LFP) EVALUATION RESPONSES

The summarized results listed below are from the 84 LFP evaluations received.

1. LFP evaluations received and associate preferences:

Table B-2. Air Force LFP Evaluation Responses (By Type)

		How Many Associates Would You Prefer To Get ? (% Response)											
		SFRP				GSRP (w/Univ Professor)				GSRP (w/o Univ Professor)			
Lab	Evals Recv'd	0	1	2	3+	0	1	2	3+	0	1	2	3+
AEDC	0	-	-	-	-	-	-	-	-	-	-	-	-
WHMC	0	-	-	-	-	-	-	-	-	-	-	-	-
AL	7	28	28	28	14	54	14	28	0	86	0	14	0
FJSRL	1	0	100	0	0	100	0	0	0	0	100	0	0
PL	25	40	40	16	4	88	12	0	0	84	12	4	0
RL	5	60	40	0	0	80	10	0	0	100	0	0	0
WL	46	30	43	20	6	78	17	4	0	93	4	2	0
Total	84	32%	50%	13%	5%	80%	11%	6%	0%	73%	23%	4%	0%

LFP Evaluation Summary. The summarized responses, by laboratory, are listed on the following page. LFPs were asked to rate the following questions on a scale from 1 (below average) to 5 (above average).

2. LFPs involved in SRP associate application evaluation process:
    a. Time available for evaluation of applications:
    b. Adequacy of applications for selection process:
3. Value of orientation trips:
4. Length of research tour:
5. a. Benefits of associate's work to laboratory:
    b. Benefits of associate's work to Air Force:
6. a. Enhancement of research qualifications for LFP and staff:
    b. Enhancement of research qualifications for SFRP associate:
    c. Enhancement of research qualifications for GSRP associate:
7. a. Enhancement of knowledge for LFP and staff:
    b. Enhancement of knowledge for SFRP associate:
    c. Enhancement of knowledge for GSRP associate:
8. Value of Air Force and university links:
9. Potential for future collaboration:
10. a. Your working relationship with SFRP:
    b. Your working relationship with GSRP:
11. Expenditure of your time worthwhile:

(Continued on next page)

12. Quality of program literature for associate:
13. a. Quality of RDL's communications with you:
    b. Quality of RDL's communications with associates:
14. Overall assessment of SRP:

Table B-3. Laboratory Focal Point Reponses to above questions

	AEDC	*AL*	*FJSRL*	*PL*	*RL*	*WHMC*	*WL*
# Evals Recv'd	0	7	1	14	5	0	46
Question #							
2	-	86 %	0 %	88 %	80 %	-	85 %
2a	-	4.3	n/a	3.8	4.0	-	3.6
2b	-	4.0	n/a	3.9	4.5	-	4.1
3	-	4.5	n/a	4.3	4.3	-	3.7
4	-	4.1	4.0	4.1	4.2	-	3.9
5a	-	4.3	5.0	4.3	4.6	-	4.4
5b	-	4.5	n/a	4.2	4.6	-	4.3
6a	-	4.5	5.0	4.0	4.4	-	4.3
6b	-	4.3	n/a	4.1	5.0	-	4.4
6c	-	3.7	5.0	3.5	5.0	-	4.3
7a	-	4.7	5.0	4.0	4.4	-	4.3
7b	-	4.3	n/a	4.2	5.0	-	4.4
7c	-	4.0	5.0	3.9	5.0	-	4.3
8	-	4.6	4.0	4.5	4.6	-	4.3
9	-	4.9	5.0	4.4	4.8	-	4.2
10a	-	5.0	n/a	4.6	4.6	-	4.6
10b	-	4.7	5.0	3.9	5.0	-	4.4
11	-	4.6	5.0	4.4	4.8	-	4.4
12	-	4.0	4.0	4.0	4.2	-	3.8
13a	-	3.2	4.0	3.5	3.8	-	3.4
13b	-	3.4	4.0	3.6	4.5	-	3.6
14	-	4.4	5.0	4.4	4.8	-	4.4

3. 1996 SFRP & GSRP EVALUATION RESPONSES

The summarized results listed below are from the 257 SFRP/GSRP evaluations received.

Associates were asked to rate the following questions on a scale from 1 (below average) to 5 (above average) - by Air Force base results and over-all results of the 1996 evaluations are listed after the questions.

1. The match between the laboratories research and your field:
2. Your working relationship with your LFP:
3. Enhancement of your academic qualifications:
4. Enhancement of your research qualifications:
5. Lab readiness for you: LFP, task, plan:
6. Lab readiness for you: equipment, supplies, facilities:
7. Lab resources:
8. Lab research and administrative support:
9. Adequacy of brochure and associate handbook:
10. RDL communications with you:
11. Overall payment procedures:
12. Overall assessment of the SRP:
13. a. Would you apply again?
    b. Will you continue this or related research?
14. Was length of your tour satisfactory?
15. Percentage of associates who experienced difficulties in finding housing:
16. Where did you stay during your SRP tour?
    a. At Home:
    b. With Friend:
    c. On Local Economy:
    d. Base Quarters:
17. Value of orientation visit:
    a. Essential:
    b. Convenient:
    c. Not Worth Cost:
    d. Not Used:

SFRP and GSRP associate's responses are listed in tabular format on the following page.

Table B-4. 1996 SFRP & GSRP Associate Responses to SRP Evaluation

	Arnold	Brooks	Edwards	Eglin	Griffis	Hanscom	Kelly	Kirtland	Lackland	Robins	Tyndall	WPAFB	average
# res	6	48	6	14	31	19	3	32	1	2	10	85	257
1	4.8	4.4	4.6	4.7	4.4	4.9	4.6	4.6	5.0	5.0	4.0	4.7	4.6
2	5.0	4.6	4.1	4.9	4.7	4.7	5.0	4.7	5.0	5.0	4.6	4.8	4.7
3	4.5	4.4	4.0	4.6	4.3	4.2	4.3	4.4	5.0	5.0	4.5	4.3	4.4
4	4.3	4.5	3.8	4.6	4.4	4.4	4.3	4.6	5.0	4.0	4.4	4.5	4.5
5	4.5	4.3	3.3	4.8	4.4	4.5	4.3	4.2	5.0	5.0	3.9	4.4	4.4
6	4.3	4.3	3.7	4.7	4.4	4.5	4.0	3.8	5.0	5.0	3.8	4.2	4.2
7	4.5	4.4	4.2	4.8	4.5	4.3	4.3	4.1	5.0	5.0	4.3	4.3	4.4
8	4.5	4.6	3.0	4.9	4.4	4.3	4.3	4.5	5.0	5.0	4.7	4.5	4.5
9	4.7	4.5	4.7	4.5	4.3	4.5	4.7	4.3	5.0	5.0	4.1	4.5	4.5
10	4.2	4.4	4.7	4.4	4.1	4.1	4.0	4.2	5.0	4.5	3.6	4.4	4.3
11	3.8	4.1	4.5	4.0	3.9	4.1	4.0	4.0	3.0	4.0	3.7	4.0	4.0
12	5.7	4.7	4.3	4.9	4.5	4.9	4.7	4.6	5.0	4.5	4.6	4.5	4.6
Numbers below are percentages													
13a	83	90	83	93	87	75	100	81	100	100	100	86	87
13b	100	89	83	100	94	98	100	94	100	100	100	94	93
14	83	96	100	90	87	80	100	92	100	100	70	84	88
15	17	6	0	33	20	76	33	25	0	100	20	8	39
16a	-	26	17	9	38	23	33	4	-	-	-	30	
16b	100	33	-	40	-	8	-	-	-	-	36	2	
16c	-	41	83	40	62	69	67	96	100	100	64	68	
16d	-	-	-	-	-	-	-	-	-	-	-	0	
17a	-	33	100	17	50	14	67	39	-	50	40	31	35
17b	-	21	-	17	10	14	-	24	-	50	20	16	16
17c	-	-	-	-	10	7	-	-	-	-	-	2	3
17d	100	46	-	66	30	69	33	37	100	-	40	51	46

4. 1996 USAF LABORATORY HSAP MENTOR EVALUATION RESPONSES

Not enough evaluations received (5 total) from Mentors to do useful summary.

5. 1996 HSAP EVALUATION RESPONSES

The summarized results listed below are from the 113 HSAP evaluations received.

HSAP apprentices were asked to rate the following questions on a scale from 1 (below average) to 5 (above average)

1. Your influence on selection of topic/type of work.
2. Working relationship with mentor, other lab scientists.
3. Enhancement of your academic qualifications.
4. Technically challenging work.
5. Lab readiness for you: mentor, task, work plan, equipment.
6. Influence on your career.
7. Increased interest in math/science.
8. Lab research & administrative support.
9. Adequacy of RDL's Apprentice Handbook and administrative materials.
10. Responsiveness of RDL communications.
11. Overall payment procedures.
12. Overall assessment of SRP value to you.
13. Would you apply again next year? Yes (92 %)
14. Will you pursue future studies related to this research? Yes (68 %)
15. Was Tour length satisfactory? Yes (82 %)

	Arnold	Brooks	Edwards	Eglin	Griffiss	Hanscom	Kirtland	Tyndall	WPAFB	Totals
# resp	5	19	7	15	13	2	7	5	40	113
1	2.8	3.3	3.4	3.5	3.4	4.0	3.2	3.6	3.6	3.4
2	4.4	4.6	4.5	4.8	4.6	4.0	4.4	4.0	4.6	4.6
3	4.0	4.2	4.1	4.3	4.5	5.0	4.3	4.6	4.4	4.4
4	3.6	3.9	4.0	4.5	4.2	5.0	4.6	3.8	4.3	4.2
5	4.4	4.1	3.7	4.5	4.1	3.0	3.9	3.6	3.9	4.0
6	3.2	3.6	3.6	4.1	3.8	5.0	3.3	3.8	3.6	3.7
7	2.8	4.1	4.0	3.9	3.9	5.0	3.6	4.0	4.0	3.9
8	3.8	4.1	4.0	4.3	4.0	4.0	4.3	3.8	4.3	4.2
9	4.4	3.6	4.1	4.1	3.5	4.0	3.9	4.0	3.7	3.8
10	4.0	3.8	4.1	3.7	4.1	4.0	3.9	2.4	3.8	3.8
11	4.2	4.2	3.7	3.9	3.8	3.0	3.7	2.6	3.7	3.8
12	4.0	4.5	4.9	4.6	4.6	5.0	4.6	4.2	4.3	4.5
Numbers below are percentages										
13	60%	95%	100%	100%	85%	100%	100%	100%	90%	92%
14	20%	80%	71%	80%	54%	100%	71%	80%	65%	68%
15	100%	70%	71%	100%	100%	50%	86%	60%	80%	82%

IDENTIFICATION AND EVALUATION OF LOSS AND DEVIATION MODELS FOR USE IN COMPRESSOR STAGE PERFORMANCE PREDICTION

Joseph E. Cahill
Graduate Research Assistant
Department of Mechanical Engineering

Virginia Polytechnic Institute and State University
Graduate School
Blacksburg, VA 24061-0325

Final report for:
Graduate Student Research Program
Arnold Engineering Development Center
Arnold Air Force Base, TN

Sponsored by:
Air Force Office of Scientific Research
Bolling Air Force Base, DC
and
Arnold Engineering Development Center

September 1996

IDENTIFICATION AND EVALUATION OF LOSS AND DEVIATION MODELS FOR USE IN COMPRESSOR STAGE PERFORMANCE PREDICTION

Joseph E. Cahill
Graduate Research Assistant
Department of Mechanical Engineering
Virginia Polytechnic Institute and State University

Abstract

Simulations to model the compressor, a component of the gas turbine engine, have been developed to augment ground and altitude testing at AEDC. The models are based upon the conservation principals of continuity, momentum, and energy. To provide closure for these equations, a set of stage characteristics are required to capture the physics of the compressor since the blades have been replaced with semi actuator disk theory. Correlations of cascade experimental data is one method used to obtain these characteristics. These correlations specify pressure loss and flow turning caused by the blade. Current correlations used in the streamline curvature codes are inadequate for high speed transonic axial compressors. The objective of this project is to investigate and evaluate correlations available and ultimately discover sets of correlations which best fit the empirical data to be used in a streamline curvature code.

Introduction

In the turbine engine altitude test cells at AEDC, testing has been used to determine the performance of axial flow compressors in turbojet engines. This type of testing is expensive, time consuming, and sometimes rough on the engines. Simulations to model the compressor have been developed to augment this testing at AEDC. These computer models speed up the testing process by eliminating much of the physical testing, which in turn, also decreases the cost. The models require stage-by-stage characteristics to capture the physics of the compressor since the blades have been replaced with semi actuator disk theory. This theory replaces the blade geometry with an externally imposed discontinuity in flow properties over the axial spacing of the bladed region. For an axial flow compressor, the stage-by-stage characteristics are the pressure ratio and the efficiency with respect to corrected mass flow rate at varying speeds. The use of correlations is one method used to obtain these characteristics. These correlations specify blade loss and flow deviation from the exit blade geometry. Loss and deviation encompass the physical phenomena that the blade geometry impose on the flow field. Loss and deviation correlations implement theory from geometry effects, boundary layers, and shocks to try and match the empirical results. Current correlations located in the streamline curvature code are inaccurate for high speed transonic axial compressors. The correlations used in industry are most likely more accurate, but are generally proprietary information. However, additional correlations are available in the open literature. A list of some of these were found in an AGARD report. These need to be tested over a wide range operating conditions and compared against each other and the empirical data.

The first objective of this research and the goal of this summer's research was to:

1) Acquire the knowledge of computer codes needed to evaluate the correlations.
2) Prepare the existing meanline and a streamline curvature codes as tools for the testing of correlations.
3) Develop a technical approach.
4) Log out a detailed plan for future

This has been completed. The second part will be to research and study the correlations available. The final task , which is the heart of the authors master of science thesis, will be to program, test, and report on the quality of the meanline correlations at different operating conditions. These correlations will then be

tested away from the meanline. If time permits, some of the correlations may be adjusted/improved to better fit the experimental data.

Approach

An intense study of two computer codes that simulate the performance of axial flow compressors was conducted. These codes were a compressible meanline code, and a streamline curvature code. Both of these codes can use correlations to solve stage-by-stage characteristics. The initial goal of this project was to learn and understand how the programs ran and prepare them for the correlation study. This was accomplished by, first, reviewing the theory intertwined in the programs for completeness and correctness. A review of the actual FORTRAN coding was conducted, which identified some errors. These errors were then removed. Modifications were made which made the codes more user friendly and expandable. The meanline code was also updated to handle more input situations and compute source terms. Last, test cases were executed to test the code for correctness and robustness.

Meanline Code

Theory

The meanline program is a compressible 1-D, steady state, stage by stage characteristics solver developed by Alan Hale at AEDC. However, it has the capability to become a pseudo 2-D solver, if the positions of streamtubes and their respective inputs are known. The meanline code approximates many flow phenomena using assumptions that allow and support its theory. It assumes ideal gas with constant properties, steady state, inviscid flow, adiabatic walls before and after the blade, and constant rhothalpy through the blades. As mentioned before, the blade rows are replaced with semi actuator disk theory. All the losses and inefficiencies that consummate in the span of the blade are modeled in loss and deviation.

Structure and Input

Figure 1 is a flowchart of the meanline code. It begins with an input file. The input file contains all the necessary geometry, gas properties, and flowfield information required to solve the stage characteristics. It also determines the path that the program will take. The subroutines *Stag_Beta* and *MassFF* are called when certain inputs that are necessary to run the code are not directly specified. These inputs can be determined from other parameters that are given. The subroutine *StackBld* is used when adjacent blade rows need to be combined. This is possible by using the exit flowfield information as input

flowfield information for the following blade row. After these subroutines have been used or passed, the main routines of the code are prompted. These routines cross the blade and compute the downstream flowfields. There are two options available to the user. The option where *Eff_cnvg* and *PR_cnvg* are called calculates loss, deviation angle, and the downstream flowfield from the known stage characteristics, pressure ratio and efficiency. The other option uses correlations to calculate the stage characteristics and the downstream flowfield. After all the downstream information has been determined, the code will calculate power, and force requirements. Finally, the code outputs information to both the screen and a file.

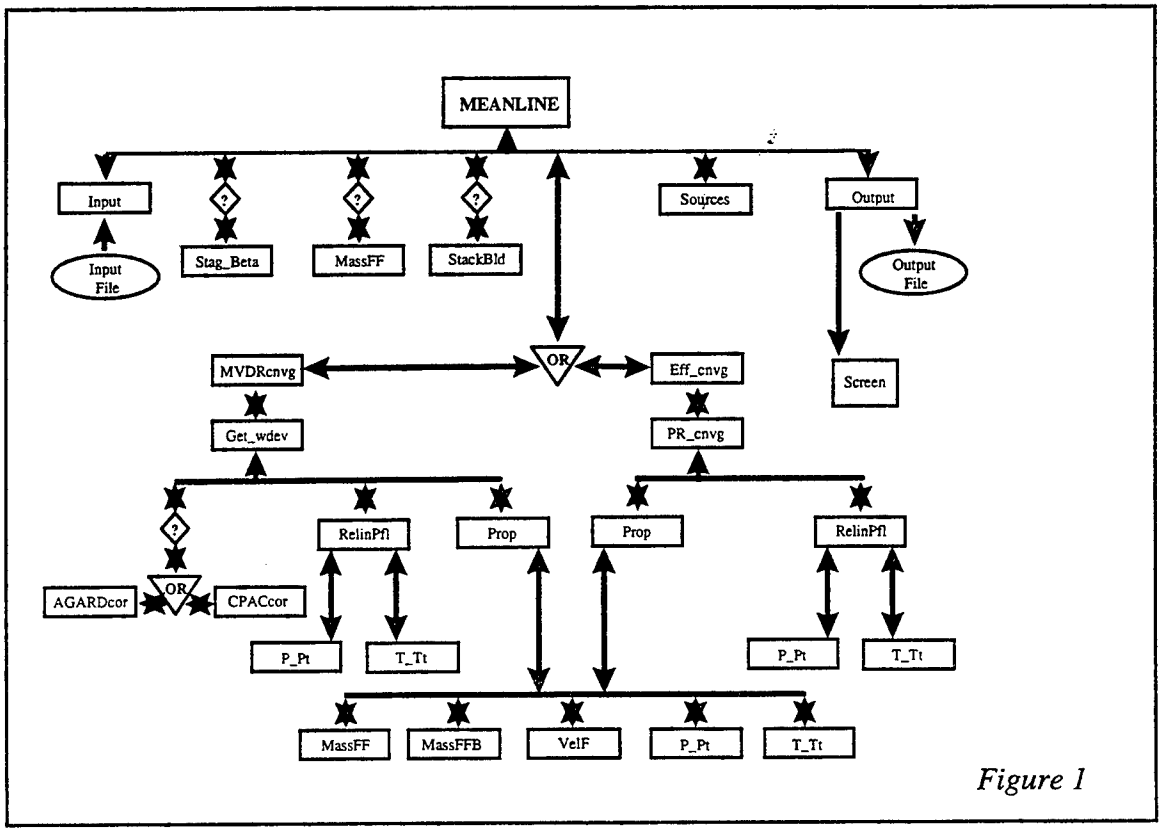

Figure 1

Streamline Curvature Code Theory

The streamline curvature code called CPAC, originally written by Dick Hearsey, and later modified by Alan Hale, also has the ability to use correlations. CPAC is a 2-D compressible, steady state, stage characteristic solver. It assumes steady state flow of an inviscid, perfect gas. Streamlines are determined by solving the conservation of mass and the conservation of momentum simultaneously with the assumption that total enthalpy and entropy are constant along a streamline. CPAC also uses the outer and

inner casing as the final streamlines. In order to establish closure, CPAC assumes that the inlet and exit streamline curvature is zero. CPAC uses semi actuator disk theory to model the affects of the blade.

Velocity Density Ratio

Background

While I was working with the meanline code, I came across a variable called axial velocity density ratio, AVDR. This variable was used inaccurately according to its definition. After a thorough investigation, it became apparent that AVDR does not hold the same properties in an annular cascade with radial effects as it did with a linear cascade. This posed a slight problem which eventually gave birth to a new definition called the meridional velocity density ratio, MVDR. MVDR holds similar properties in an annular cascade as AVDR does with a linear cascade. This is what the meanline uses, and it is consistent with its definition and sound in its theory.

Linear Cascade Theory

AVDR is a useful quantity to know when dealing with cascade flow. The ratio of areas perpendicular to the relative flow entering and exiting the blade row can be calculated directly if the AVDR and the relative flow angles are known This ratio is necessary when computing the relative mass flow functions, which is one method used to cross the blade. Eq(1) represents the definition of absolute velocity density ratio

$$Eq(1) \quad AVDR = (\rho_2 V_{x2}) / (\rho_1 V_{x1})$$

where ρ is the density, V_x is the absolute axial velocity, and (1) and (2) stand for the inlet and exit of the blade row respectively. Because the blade velocity is perpendicular to the flow the absolute axial velocity and the relative axial velocity (W_x) are equivalent.

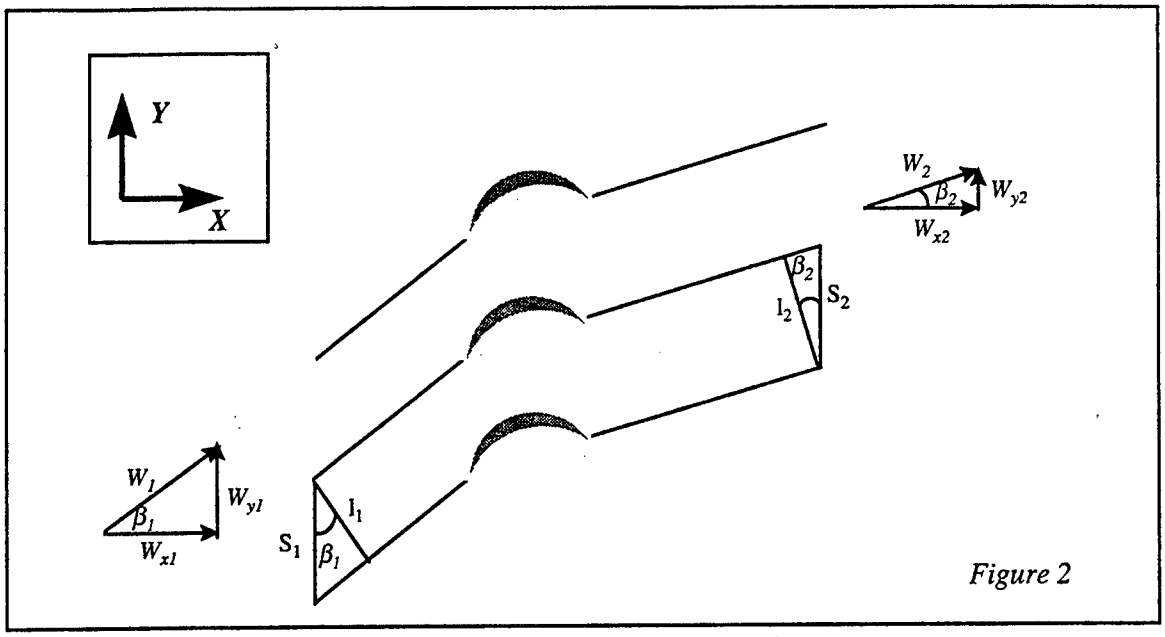

Figure 2

An illustration of a linear cascade is shown in figure 2. Assuming uniform properties, we can solve for A1/ A2 in terms of AVDR and β_1 and β_2. Below is a derivation of A1/A2 where A1 and A2 refer to the cross sectional areas that are perpendicular to the relative flow at the blade at the inlet and exit respectively, A_s is the cross sectional area of the streamtube normal to the axial, β is the relative flow angle, d is the uniform depth, mdot is the mass flow, and the remaining variables are defined in the figure above..

Eq(2) $A_{1s}/A_{2s} = (S_1*d_1) / (S_2*d_2)$

Eq(3) $A_1/A_2 = (l_1*d_1) / (l_2*d_2)$

Eq(4) $l_1 = S_1* \text{Cos}(\beta_1)$ and $l_2 = S_2* \text{Cos}(\beta_2)$

$\therefore$ Eq(5) $A_1/A_2 = A_{1s}/A_{2s}* \text{Cos}(\beta_1) / \text{Cos}(\beta_2)$

By conservation of mass we know that

Eq(6) $\text{mdot} = (\rho A_s V_x)_1 = (\rho A_s V_x)_2$

$\therefore$ Eq(7) $A_{1s}/A_{2s} = (\rho V_x)_2 / (\rho V_x)_1 =$ **AVDR**

Combining Eq(5) and Eq(7) results in

Eq(8) $A_1/A_2 =$ **AVDR*** $\text{Cos}(\beta_1) / \text{Cos}(\beta_2)$

Note that A1s and A2s do not include boundary layers. Therefore, **AVDR** can not be measured strictly from the geometry of the casing, although this is usually a good approximation.

Annular Cascade Theory

When dealing with annular cascades with radial affects Eq(6) and Eq(7) do not satisfy continuity. Therefore, Eq(8) is also incorrect. However, if we define a new variable called the meridional velocity density ratio, MVDR, a similar result proceeds. The meridional velocity is the vector sum of the axial and radial velocity vectors. Below is the equation.

$$Eq(9) \quad MVDR = (\rho_2 V_{m2}) / (\rho_1 V_{m1})$$

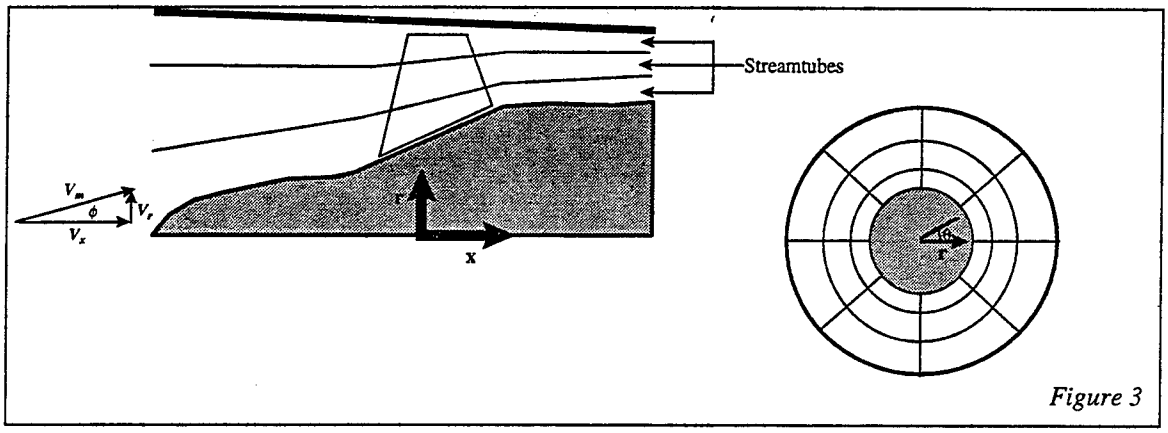

Figure 3

Figure 3 shows the front and side views of an annulus. One difference between linear cascade flow and annular flow with radial effects is that the relative flow angles are taken with respect to the meridional velocity and not the axial. Assuming uniform properties, axisymmetric flow the derivation of A1/A2 is as follows where Am is the cross sectional area of the streamtube that is normal to the meridional velocity.

$$Eq(10) \quad mdot = (\rho A_m V_m)_1 = (\rho A_m V_m)_2$$

$$Eq(11) \quad A_1/A_2 = A_{1m}/A_{2m} * \cos(\beta_1) / \cos(\beta_2)$$

$$Eq(12) \quad A_1/A_2 = \mathbf{MVDR} * \cos(\beta_1) / \cos(\beta_2)$$

There exist a relationship between AVDR and MVDR for a annular cascade. It is shown in eq(13)

Eq(13) **MVDR = AVDR** * $\cos(\phi_2)/\cos(\phi_1)$

Detailed Plan

In order to accurately test the correlations, experimental data for a stage is required. Currently, sets of data are available for both a rotor (Rotor 1-B), and a stage (Stage 35). This data will act as a control to validate the results from the correlations. There exist two correlations that have been coded and prepared for the meanline code. These will be the first correlations tested in the meanline code. After running the full range of speeds and operating conditions, the results will be documented and compared with the experimental data. Next, a thorough investigation of other existing correlations in the open literature will be conducted. The correlations which fit the conditions of transonic axial compressor will be coded and tested at the meanline. After all the meanline testing is completed, the results will be compared and the optimum loss and deviation correlations for each speed and inlet condition will be determined.

The purpose of the meanline analysis is to provide an easy method to quickly gather insight of the behavior and quality of the correlations. It is hypothesized that the correlations which represent the data the best at the meanline will also do a good job for the majority of the flowfield. This is because the loss and deviation at the meanline is a function of the behavior of the flowfield in the entire span of the blade.

Next, I want to explore radially away from the meanline. This will be done by testing the correlations using the streamline curvature code. It is expected that the correlations will not be reliable at the hub and tip. However, it is desirable to know how well the correlations work away from the meanline, and where they fail. This knowledge would be valuable for future work.

Conclusions

The overall goal of this effort is to improve the loss and deviation models currently used in the streamline curvature code. My task is to investigate and evaluate correlations available in the open literature and determine if improvements can be made by implementing them into the models. During the AFOSR program I prepared tools to test the correlations. They are the meanline and streamline curvature codes. I also have gathered several correlations which need to be reviewed and tested. After my task is completed, recommendations will be provided.

References

1) DYNATECH R/D Co., "HT0300-A Computer Program for the Design and Analysis of Axial Turbomachinery," Parts I-II, Cambridge, Massachusetts, March 17, 1970

2) M. Cetin, A.S. Ucer, Ch. Hirsch, and G.K. Serovy, "Application of Modified Loss and Deviation Correlations to Transonic Axial Compressors" AGARD Report No. 745 November 1987.

3) Lonnie Reid and Royce D. Moore, "Performance of Single-Stage Axial-Flow Transonic Compressor with Rotor and Stator Aspect Ratios of 1.19 and 1.26, and with design Pressure Ratio of 1.82" NASA Technical Paper 1338 November 1978.

4) D.R. Seyler and J.P. Gostelow, "Single Stage Experimental Evaluation of High Mach Number Compressor Rotor Blading" NASA Lewis Research Center September 22, 1967.

DYNAMICALLY MODELING THE AEDC 16S SUPERSONIC WIND TUNNEL

Peter A. Montgomery
Graduate Research Assistant
Department of Aerospace and Mechanical Engineering

University of Tennessee Space Institute
B.H. Goetthert Parkway
Tullahoma, TN 37388

Final Report for:
Graduate Student Research Program
Arnold Engineering Development Center

Sponsored by:
Air Force Office of Scientific Research
Bolling Air Force Base, Washington, DC

and

Arnold Engineering Development Center

August 1996

DYNAMICALLY MODELING THE AEDC 16S SUPERSONIC WIND TUNNEL

Peter A. Montgomery
Graduate Research Assistant
Department of Aerospace and Mechanical Engineering
University of Tennessee Space Institute

Abstract

The 16S supersonic wind tunnel facility at the Arnold Engineering Development Center (AEDC) was modeled dynamically using the one dimensional, time dependent, compressible Euler equations with source terms. The purpose for constructing the 16S model was to determine the source (or sources) of flow unsteadiness observed during some operational conditions in the 16S test section. The approach taken in the development of the 16S model was to modify an existing Euler flow solver that was developed for application to gas turbine engine compressors. Individual models were implemented that represent the 16S components to provide the source term information. These models included wall friction, compressors, screens, heat exchangers, and other pressure loss devices.

DYNAMICALLY MODELING THE AEDC 16S SUPERSONIC WIND TUNNEL

Peter A. Montgomery

Introduction

Flow quality is crucial in the accuracy of data taken in any wind tunnel. The 16S supersonic wind tunnel at Arnold Engineering Development Center currently experiences flow unsteadiness, during some operational conditions, in the 16S test section. Although likely sources of the unsteadiness have been determined, a much more rigorous examination of the overall flow path is desired before modifications are made to the tunnel. The task for this summer was to begin building a dynamic computational model of the 16S test circuit based on the 1-D Euler equations.

A similar dynamic model and simulation of the 16T wind tunnel facility was recently developed using as a basis the DYNTECC dynamic compression system computer code ([1] Hale & Davis). The resulting code, called AFAST (Aerodynamic Facility Analysis Simulation Technique), was put through several sample runs and obtained results that compared favorably with steady-state model results and facility test data. The work this summer was to begin making the necessary modifications to AFAST and its various geometry and data files such that it could operate for the 16S tunnel.

The DYNTECC (DYNamic Turbine Engine Compressor Code), developed at AEDC, is a one-dimensional, time-dependent, stage-by-stage axial compression system mathematical model and simulation which is able to analyze a

generic compression system. It uses a finite difference numerical technique to simultaneously solve the mass, momentum, and energy equations (i.e., Euler equations) with source terms (mass bleed, blade forces, and shaft work) within a given domain of interest that has been separated into individual control volumes. The governing equations are derived by the application of mass, momentum, and energy conservation to the elemental control volume:

$$\frac{\partial U}{\partial t} + \frac{\partial F}{\partial x} = G$$

where:

$$U = \begin{bmatrix} S\rho \\ \rho Su \\ SE \end{bmatrix} ; F = \begin{bmatrix} \rho Su \\ \rho Su^2 + SP \\ u(SE + SP) \end{bmatrix} ; G = \begin{bmatrix} -W_{Bx} \\ F_x \\ Q_x + SW_x - H_{Bx} \end{bmatrix}$$

The specific flow variables are density ρ, static pressure P, total energy per unit volume E, and the axial flow velocity, u. The cross-sectional area of the flow path is defined as S. The source term for the conservation of mass equation is the bleed flow rate distribution W_{Bx}. The conservation of momentum equation source term is F_x, which is the axial force distribution acting on the control volume. The conservation of energy equation source terms include the heat transfer rate into the control volume fluid Q_x, the shaft work distribution applied to the control volume SW_x, and the enthalpy change due to the bleed flow distribution H_{Bx}. (For a more complete description see [2] Garrard, G. D.)

To provide stage force (F_x) and shaft work (SW_x) inputs to the momentum and energy equations, sets of steady-state stage characteristics must be provided. The heat addition (Q_x) to the energy equation uses a set

of steady-state wall heat transfer equations and cooler performance maps. Several other equations are required to obtain closure of the equation set. These include the ideal gas equation of state and the isentropic flow relationships. A constant ratio of specific heats is also assumed.

When the need for a dynamic model of the 16T wind tunnel system was identified, it was recognized that the tunnel circuit is basically a compression system, and as such it could be modeled using DYNTECC. Modifications were needed to allow simulation of a closed-circuit system and to provide the necessary physical geometry parameters and operating characteristics. Changing these geometry parameters and operating characteristics was necessary to create the 16S model. Further modifications were also needed to allow for multiple compressor operations. The 16T facility uses only one compressor while 16S has up to four that may operate at any one time. Also 16S has two coolers while the 16T system has only one.

Discussion of Problem

Variations in flow angularity are occurring in the 16S wind tunnel that lead to unsteady flow in the test section, during some operational conditions. It is suspected that this is caused by separation of the flow from the tunnel walls upstream of the test section, perhaps in the upstream diffuser. To better validate this assumption, a computer model needs to be generated that can show conditions conducive to separation

in the areas suspected. It may also show some other possibilities not considered before, as well as provide a means to try various fixes, such as adding strategically placed screens, etc. to the tunnel in the computer model to see if that will solve the problem. If it doesn't work in the model, then another solution possibility can be tried until a viable option has been found. Only at that point does it make sense to physically modify the tunnel. The computer model therefore serves to validate assumptions about where the flow unsteadiness is actually occurring and how it might be fixed without spending time and money going down a potentially incorrect path of solution.

Methodology

A general schematic of the 16S wind tunnel system is shown in figure 1. The system was first broken up into 125 control volumes. These were chosen to include volumes between varying cross-sectional areas, volumes where mass is introduced or leaves the tunnel, and volumes where significant pressure losses occur, such as due to flow across screens or turning vanes. Each of the two coolers has its own control volume, and each of the four compressors in 16S is contained entirely within its own control volume as well. The compressors are modeled using pressure ratios and efficiencies as a function of inlet guide vane angle, which can be varied, and the current configuration being used. Modifications to the code were therefore made to determine first which compressor

Figure 1: **TUNNEL 16S**

Potential Measurement Locations

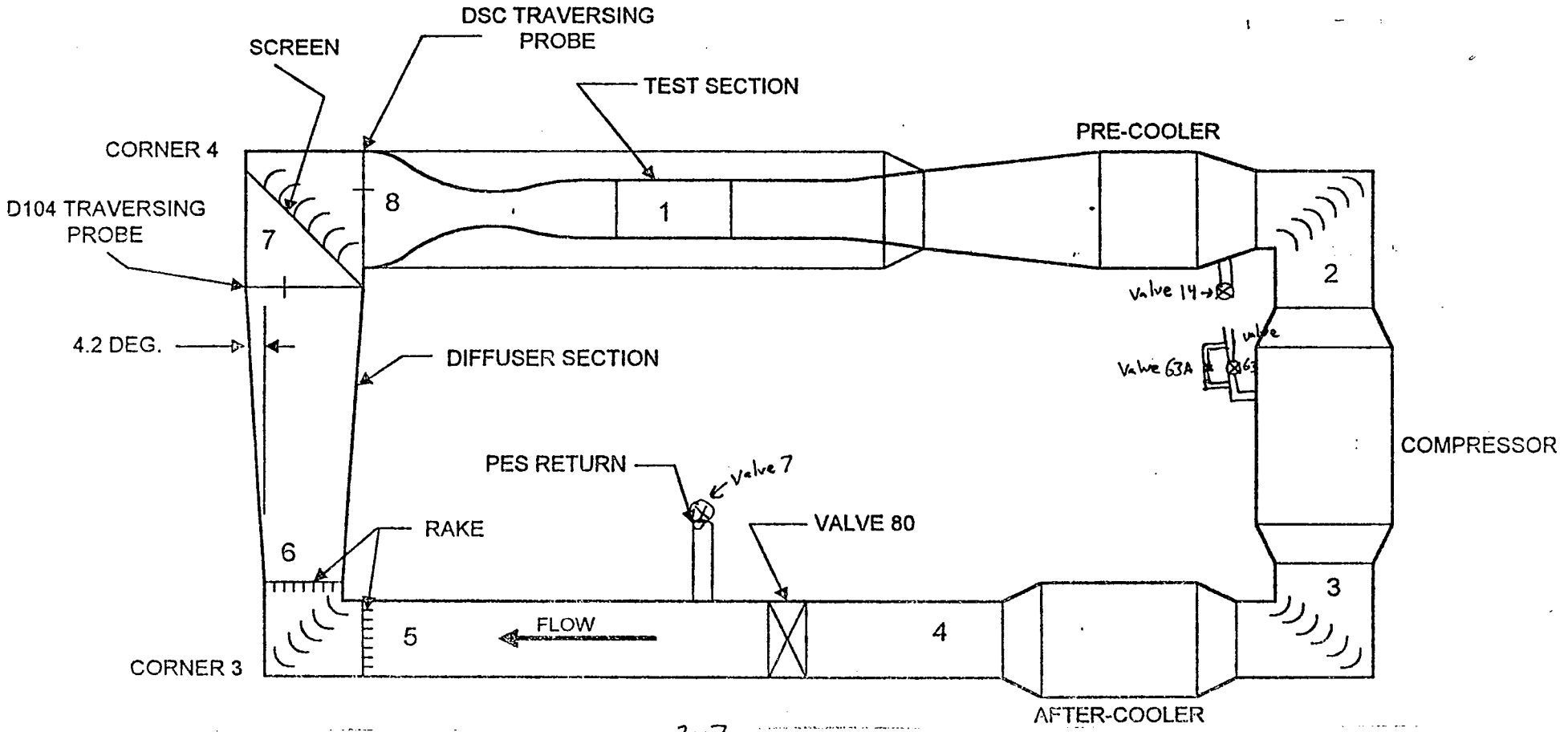

configuration was being utilized, and then bring in the appropriate data to be used in the remainder of the calculations. The 16S tunnel also has two coolers, as opposed to 16T having only one. The new cooler characteristics needed to be determined, and the necessary code modifications made to handle the extra cooler. Each cooler was entirely contained in a single control volume for the model.

The first step in building the 16S model was to determine the wind tunnel geometry. This was accomplished through extensive examination of the original plans and memos concerning any changes made to the tunnel over the years. Consultation with wind tunnel test engineers was also helpful. The 16S tunnel has a 16 ft square test section with a rectangular nozzle feeding the flow into it and a rectangular diffuser accepting the outflow. The rest of the tunnel is circular in diameter with a maximum diameter of 55 ft., for the corner and section just before the rectangular nozzle. Given the shape of the cross section around the tunnel, the cross-sectional areas at the beginning of each control volume were determined. Node points were assigned at each location where cross-sectional area changed from that at the previous node point as well as at critical pressure loss locations, such as on either side of screens and turning vanes. A total of 125 node points were selected with node 1 chosen to be just downstream of valve 80 in the back leg of the tunnel.

The compressor configuration is shown in figure 2. All of the flow into

Barrel	Hub Diameter	Tip Diameter	No. of Stages of Compression	Hub Speed Ft./Sec.	Tip Speed Ft./Sec.
C 2	18	27.8	4	565	872
C 3	18	25.4	4	565	797
C 4	18	23.9	4	565	750
C 5	18	22.3→20.9	6	565	700 → 656

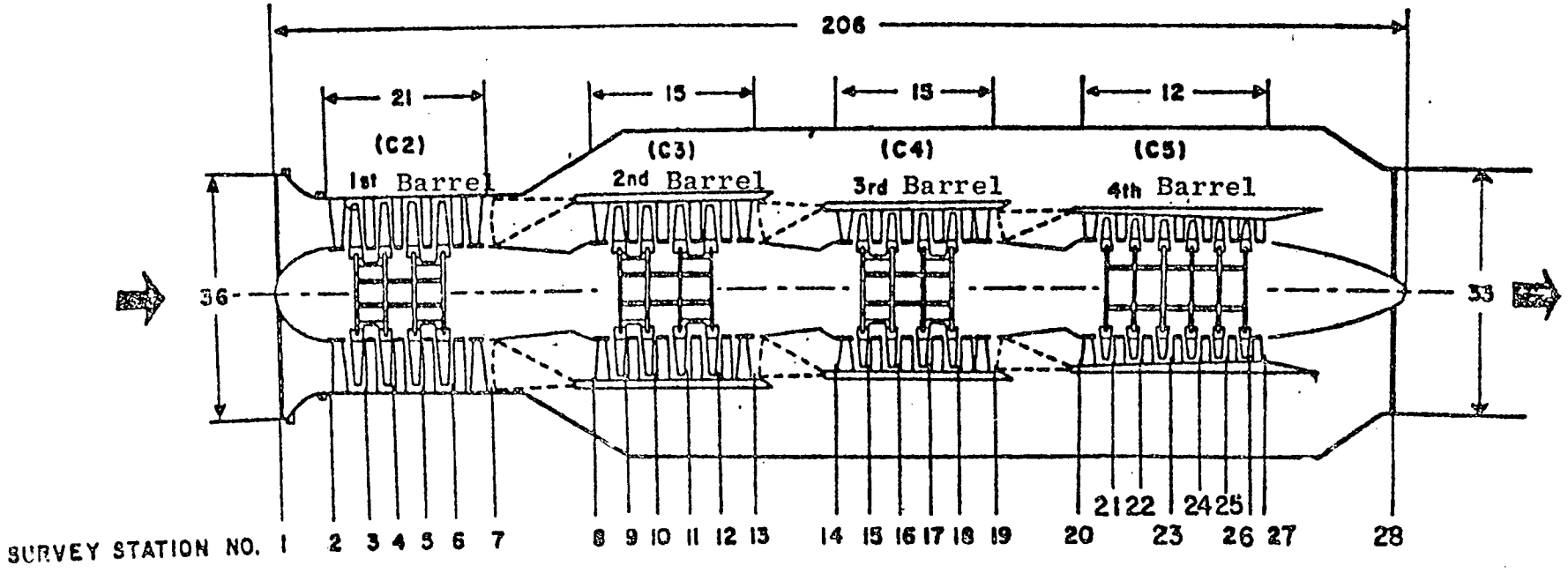

Dimensions in Feet
Not to Scale

Figure 2. Compressor Dimensions and Longitudinal Survey Stations

the compressor section is guided into compressor C2. (Note: The 16T compressor is referred to as C1 so the four compressors in 16S are referred to as C2-C5) Where the flow goes after exiting C2 depends on the setting of the iris valves in front of C3. If the valves are open (Note: By open, it is meant that the valve is in the horizontal position in the drawing such that all the flow out of one compressor goes into the other.), then all of the flow passes through C3 as well. This operation of C2 and C3 together, if no other compressors are operating, is called "two-barrel" operation. Test engineers have indicated that this is the base configuration used for flow speeds from Mach 1.6 to 2.4. If the valves after C3 are closed, then the flow is routed around C4 and C5 into an outer shell that surrounds the inner core of compressors. The cross-sectional area used in the model at the nodes at the face of C4 and C5 would then be the area of the duct at that point minus the area of the compressor shell. The same is true at the node corresponding to the C5 entrance. If instead the valves in front of C4 are open then the flow is forced completely into the compressor, and the model uses the cross-sectional area of the compressor only at that node. If the iris valves at C5 are then closed the outer shell cross-sectional area is used as discussed for C4 earlier. This is termed "three barrel" operation and flow speeds up to Mach 2.8 are achieved in this configuration. If the valves before C5 are open then all four compressors are in use and "four barrel" operation is taking place with flow speeds up to Mach 3.4 being provided. The cross sectional areas of all the compressors are used at each node and the outer bypass shell is

completely ignored. To handle each configuration, this decision making process for which cross-sectional areas are utilized was written into the code.

Characteristics for each 16S cooler were gathered and are shown in figures 3 and 4. Cooler K2 (the precooler) cools the flow before compression and has a set exit temperature of 100 degrees F. Cooler K3 (the aftercooler) cools the flow after compression and has an exit temperature that is varied to a desired value.

Pressure control for the 16S wind tunnel was explored leading to a determination of mass bleeds needed in the code. About ten percent of the flow is pulled out through valve 14 just after the exit of cooler K2. Some of this loss is replaced through valve 7 in the back leg of the tunnel after valve 80. This replacement is made with dry air but only for flow speeds up to Mach 2. Above Mach 2 valve 7 is closed, and there is no replacement made. Flow is also reintroduced into the tunnel in the outer shell of the compressor, above C3, C4, and C5. Valve 63 stays open to provide constant flow here and valve 63A, which is smaller, is varied to control the pressure as desired. Mass bleeds were therefore introduced into the code for the control volumes around the areas where these flows enter and exit.

Results

A detailed accurate model of the AEDC 16S supersonic wind tunnel has been created and a dynamic program modified for use. Upon completion of

Figure 3: K2 Characteristics, CPR=6,

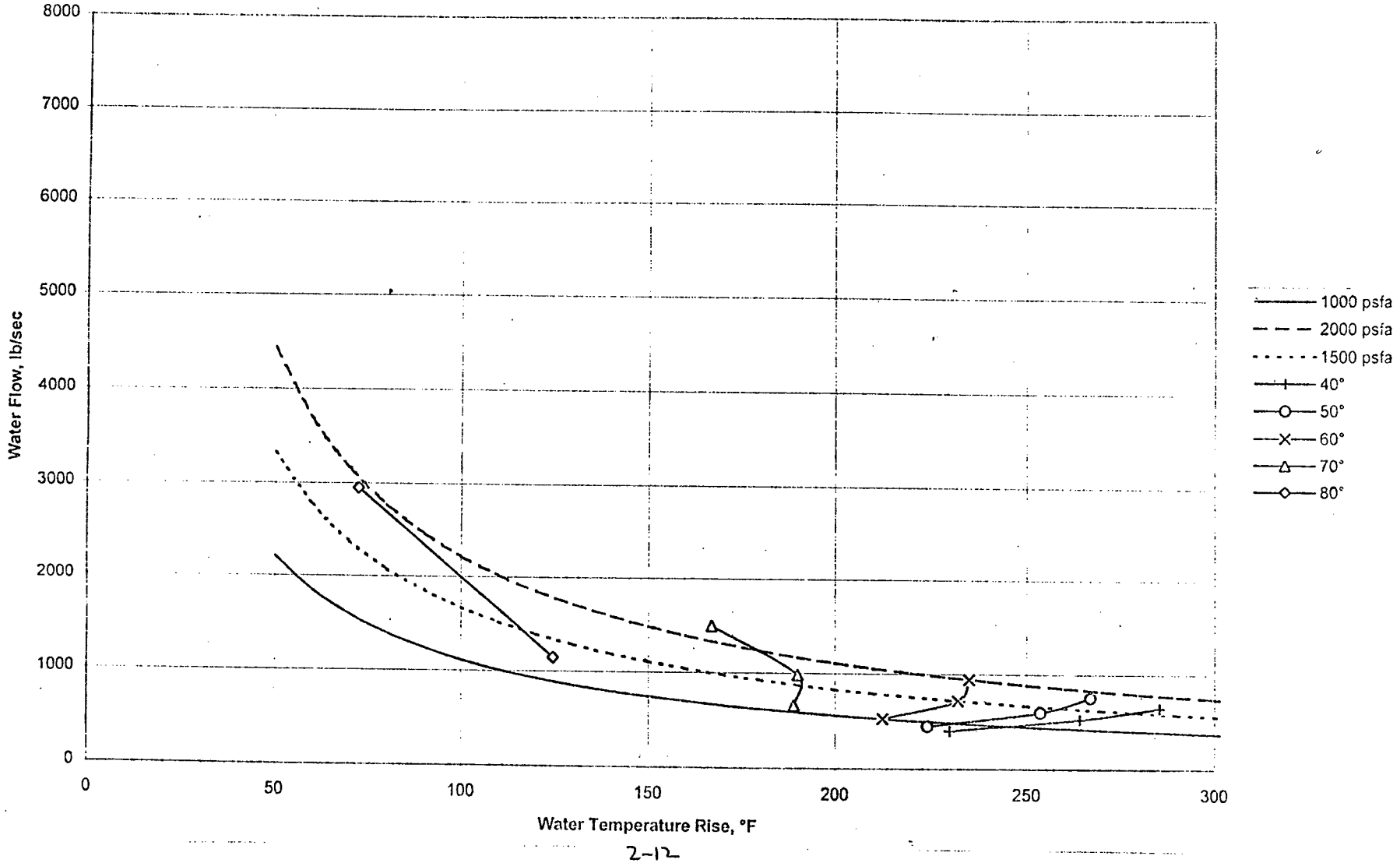

Figure 4: K3 Characteristics, CPR=6,

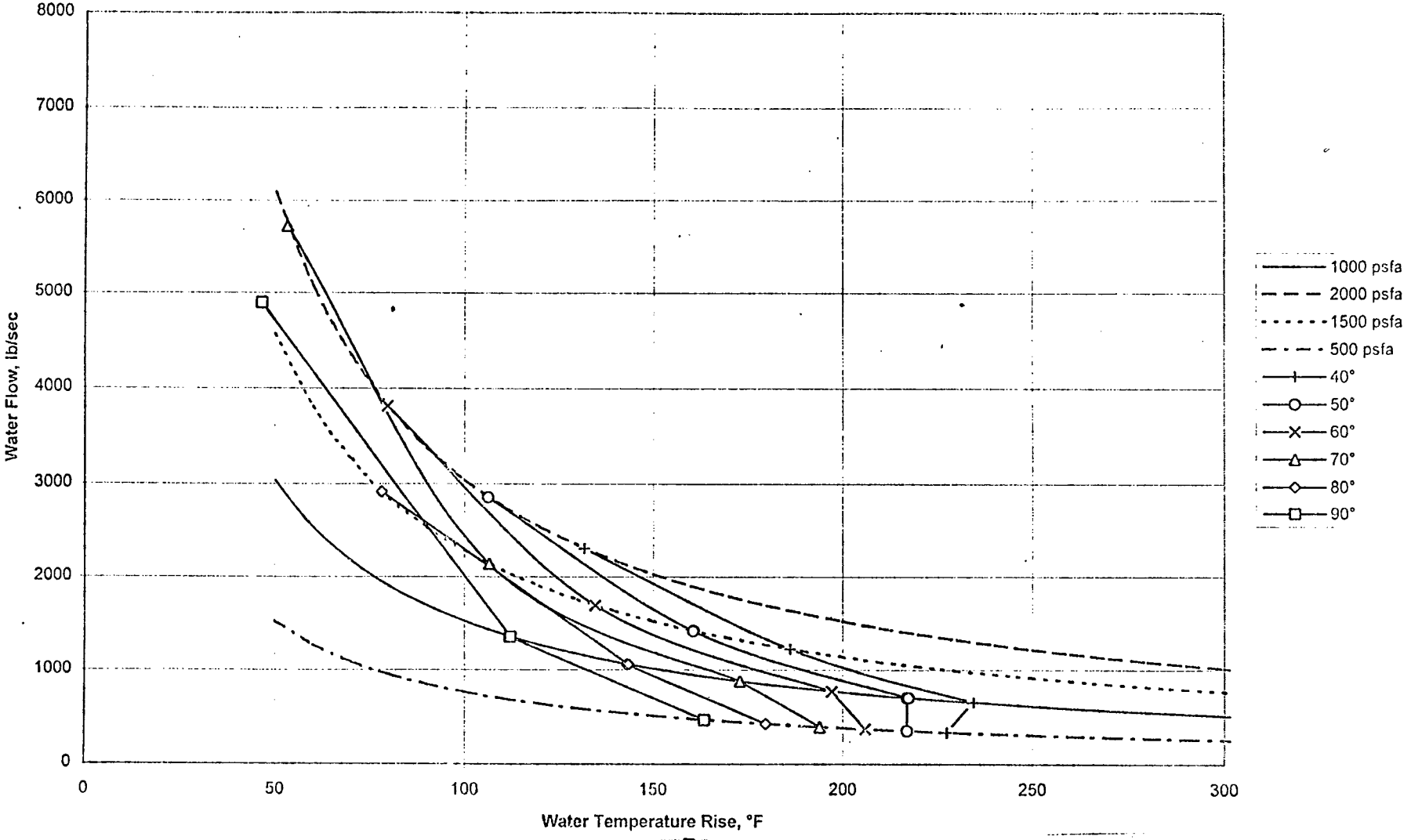

the debugging process, a 1-D dynamic model of the 16S tunnel will be available for study of possible areas of flow separation, and ways to minimize the effect of flow into the test section. This will lead to physical modifications in the tunnel and improvements to the flow steadiness through the 16S test section.

Table 1 lists the information about 16S brought together for use by the model. It contains node locations, cross-sectional areas at each node, volume between the current node and the next one, and pressure drops across turning vanes, screens, etc. The x column is distance from the start of the test section, where negative values indicate upstream direction and positive distances are downstream of the test section. The delta-x column indicates distance to the next node. Note that the node spacing in the main diffuser, test section, and fixed diffuser at the exit of the test section is very small. This is due to the fact that very precise information about the flow through these areas is desired to validate flow separation assumptions.

Conclusions

All indications from the 16T model are that this is a very effective way to model wind tunnels. The work done this summer in development of a similar model for the 16S tunnel should further validate the use of such 1-D dynamic computer models. The savings of time and money alone in the reduction of flow unsteadiness, such as has been observed in 16S, make this approach well worth further study. A detailed complete model of the 16S wind tunnel is now available for a variety of conceived uses.

Table 1: 16S Geometry and Pressure Losses

Node	X	Delta-X	Diameter	Area	Volume	Delta-P	Comments
1	-715.744	11.33	20	314.1593	3559.424		Valve-80
2	-704.414	40	20	314.1593	16153.68		Expansion
3	-664.414	148.08	25.25	500.7404	79407.45		Mass in from PES
4	-516.334	80.53	27	572.5553	45404.26		Corner 103 (1st leg to turning vanes (81.03' - 0.5'))
5	-435.804	1	27	572.5553	572.5553	0.11q	Turning Vanes
6	-434.804	21.64	27	572.5553	11686.48		Corner 103 (2nd leg from vanes to exit (22.14' - 0.5'))
		Diffuser					
7	-413.164	9.5	27	572.5553	5726.778		
8	-403.664	9.5	28.40284	633.5974	6321.361		
9	-394.164	9.5	29.80568	697.7307	6945.311		
10	-384.664	9.5	31.20851	764.9553	7598.628		
11	-375.164	9.5	32.61135	835.2712	8281.313		
12	-365.664	9.5	34.01419	908.6783	8993.364		
13	-356.164	9.5	35.41703	985.1766	9734.782		
14	-346.664	9.5	36.81987	1064.766	10505.57		
15	-337.164	9.5	38.2227	1147.447	11305.72		
16	-327.664	9.5	39.62554	1233.219	12135.24		
17	-318.164	9.5	41.02838	1322.083	12994.12		
18	-308.664	9.5	42.43122	1414.037	13882.38		
19	-299.164	9.5	43.83406	1509.083	14799.99		
20	-289.664	9.5	45.23689	1607.22	15746.98		
21	-280.164	9.5	46.63973	1708.449	16723.33		
22	-270.664	9.5	48.04257	1812.768	17729.05		
23	-261.164	9.5	49.44541	1920.179	18764.14		
24	-251.664	9.5	50.84825	2030.682	19828.6		
25	-242.164	9.5	52.25108	2144.275	20922.42		
26	-232.664	9.5	53.65392	2260.96	22022.5		
27	-223.164	40	55	2375.829	93945.95		Corner 104 (1st leg up to screen (40.50' - 0.5'))

Table 1 (continued): 16S Geometry and Pressure Losses

Node	X	Delta-X	Diameter	Area	Volume	Delta-P	Comments
28	-183.164	1	55	2375.829	2375.829	2.00q	Screen
29	-182.164	50.98	55	2375.829	120032.6		Corner 104 (2nd leg from screen to nozzle)
			Nozzle-Test Section-Diffuser System				
30	-131.184	7.88434	55	2375.829	16963.26		
31	-123.3	7.88434	49.63252	1934.74	13663.96		
32	-115.416	7.88434	44.26504	1538.904	10721.46		
33	-107.531	7.88434	38.89756	1188.323	8997.417		
34	-99.647	11.5487	37.3333	597.3328			Note: Square Cross-Section (16 ft. height)
35	-88.0983	2.4479	28.1626	450.6016			
36	-85.6504	2.5034	24.6866	394.9856			
37	-83.147	2.5844	21.372	341.952			
38	-80.5626	2.6649	18.32	293.12			
39	-77.8977	2.7917	15.9476	255.1616			
40	-75.106	2.8693	14.256	228.096			
41	-72.2367	2.9052	13.2004	211.2064			
42	-69.3315	2.9166	12.6512	202.4192			
43	-66.4149	2.9186	12.4316	198.9056			
44	-63.4963	2.9179	12.4166	198.6656			Throat Location
45	-60.5784	2.9154	12.5646	201.0336			
46	-57.663	2.9122	12.845	205.52			
47	-54.7508	2.9099	13.2332	211.7312			
48	-51.8409	2.9093	13.6888	219.0208			
49	-48.9316	2.9106	14.1594	226.5504			
50	-46.021	3.0115	14.5938	233.5008			
51	-43.0095	2.9833	14.9722	239.5552			
52	-40.0262	4.0005	15.2722	244.3552			
53	-36.0257	4.0022	15.5544	248.8704			
54	-32.0235	4.0029	15.7172	251.4752			
55	-28.0206	4.003	15.7924	252.6784			

Table 1 (continued): 16S Geometry and Pressure Losses

Node	X	Delta-X	Diameter	Area	Volume	Delta-P	Comments
56	-24.0176	4.0029	15.8266	253.2256			
57	-20.0147	4.003	15.8518	253.6288			
58	-16.0117	4.0029	15.8812	254.0992			
59	-12.0088	4.0029	15.912	254.592			
60	-8.0059	4.0029	15.9414	255.0624			
61	-4.003	4.003	15.971	255.536			
62	0	2	16	256			End of Nozzle/Start of Test Section
63	2	2	15.96509	255.4415			
64	4	2	15.93019	254.883			
65	6	2	15.89528	254.3244			
66	8	2	15.86037	253.7659			
67	10	2	15.82546	253.2074			
68	12	2	15.79056	252.6489			
69	14	2	15.75565	252.0904			
70	16	2	15.72074	251.5318			
71	18	2	15.68583	250.9733			
72	20	2	15.65093	250.4148			
73	22	2	15.61602	249.8563			
74	24	2	15.58111	249.2978			
75	26	2	15.5462	248.7392			
76	28	2	15.5113	248.1807			
77	30	2	15.47639	247.6222			
78	32	2	15.44148	247.0637			
79	34	2	15.40657	246.5052			
80	36	2	15.37167	245.9466			
81	38	2	15.33676	245.3881			
82	40	1	15.30185	244.8296			End of Test Section/Start of Diffuser
83	41	23.5	15.46875	247.5			(Contour M=1.6)
84	64.5	20	15.79188	252.6701			
85	84.5	16	16.27188	260.3501			

Table 1 (continued): 16S Geometry and Pressure Losses

Node	X	Delta-X	Diameter	Area	Volume	Delta-P	Comments
86	100.5	16	16.35188	261.6301			
87	116.5	24.5	16.28813	260.6101			
88	141	1.25	17.36	277.76			End of Variable Diffuser/Start Fixed Diffuser
89	142.25	4.666667	17.4625	279.4			
90	146.9167	3.666667	17.59444	281.5111			
91	150.5833	2.916667	17.63056	282.0889			
92	153.5	9.333333	17.69444	283.1111			
93	162.8333	5.135417	19.59028	313.4444			
94	167.9688	3.28125	20.85417	333.6667			
95	171.25	3.25	22.20833	387.3662	1328.986		
96	174.5	3.25	23.42188	430.857	1474.735		
97	177.75	3.25	24.64583	477.0643	1583.123		
98	181	3.25	25.16146	497.2348	1706.279		
99	184.25	3.25	26.54167	553.2816	1840.482		
100	187.5	3.25	27.16146	579.4234	1972.981		
101	190.75	3.25	28.4375	635.1447	2157.966		
102	194	76.5	29.71	693.2585	17678.09		End of Fixed Diffuser
103	270.5	1	41.8	1372.279	1377.539	1.38q	Screen
104	271.5	23.5	41.96	1382.805	35453.8		
105	295	68.67	45.67	1638.143	163349.6	11.45q	Precooler K2 (included in single control volume)
106	363.67	39.42	55	2375.829	65027.15	10% mass	Mass out to PES
107	403.09	62.42	36	1017.876	63535.82		Corner 101 (1st leg up to screen (62.92' - 0.5'))
108	465.51	1	36	1017.876	1017.876	1.38q	Screen
109	466.51	22.75	36	1017.876	23156.68		Corner 101 (2nd leg from screen to exit (23.25' - 0.5'))
		Compressors					
110	489.26	15	36	763.407	10782.1		Compressor Inlet
111	504.26	17.737	27.8	352.5181	6252.614	See Map	Compressor C2
112	521.997	38.655	27.8	352.5181	11659.29		Inlet to C3

Table 1 (continued): 16S Geometry and Pressure Losses

Node	X	Delta-X	Diameter	Area	Volume	Delta-P	Comments		
113	560.652	11.04	25.4	252.2385	2784.713	See Map	Compressor C3	Area	Volume
114	571.692	32.86	25.4	252.2385	7324.621		Inlet to C4 **If valves closed:**	1231.701	29071.54
115	604.552	10.903	23.9	194.1583	2116.908	See Map	Compressor C4	1037.542	11312.32
116	615.455	32.054	23.9	194.1583	5282.334		Inlet to C5	1037.542	22996.91
117	647.509	8.9	22.3	136.1016	997.6423	See Map	Compressor C5	1095.599	9750.831
118	656.409	38.991	20.9	1231.701	41778.06		Exit of compressor system		
119	695.4	23.23	33	855.2986	19275.15		Corner 102 (1st leg up to vanes (23.73' - 0.5'))		
120	718.63	1	33	855.2986	855.2986	0.11q	Turning Vanes		
121	719.63	45.5	33	855.2986	38322.65		Corner 102 (2nd leg from vanes to exit (46.00' - 0.5'))		
122	765.13	49.92	33	855.2986	61187.33				
123	815.05	116.92	45.67	1638.143	213941.5	10.48q	Aftercooler K3 (included in single control volume)		
124	931.97	140.83	27	572.5553	80632.96				
125	1072.8	10.83	27	572.5553	4732.095				

Units: X, Delta-X, and Diameter in ft.
Area in sq. ft.
Volume in cu. ft.

References

1. Hale, A. A. and Davis, M. W., "DYNamic Turbine Engine Compressor Code DYNTECC - Theory and Capabilities," AIAA-92-3190, Presented at the AIAA/SAE/ASME/ASEE 28th Joint Propulsion Conference and Exhibit, Nashville, TN, July 6-8, 1992.

2. Garrard, G. D., "ATEC: The Aerodynamic Turbine Engine Code for the Analysis of Transient and Dynamic Turbine Engine System Operations," Ph. D. Dissertation, The University of Tennessee, Knoxville, August, 1995.

INITIAL SOFTWARE DEVELOPMENT AND PERFORMANCE STUDY OF THE CADDMAS HIGH SPEED, HIGH VOLUME STORAGE BOARD

Gregory G. Nordstrom
Graduate Student
Department of Electrical Engineering

Vanderbilt University
401 24th Avenue South
Nashville, TN 37212

Final Report for:
Graduate Student Research Program
Arnold Engineering Development Center

Sponsored by:
Air Force Office of Scientific Research
Bolling Air Force Base, DC

and

Arnold Engineering Development Center

August 1996

INITIAL SOFTWARE DEVELOPMENT AND PERFORMANCE STUDY OF THE CADDMAS HIGH SPEED, HIGH VOLUME STORAGE BOARD

Gregory G. Nordstrom
Graduate Student
Department of Electrical Engineering
Vanderbilt University

Abstract

A high-speed, high-volume TMS320C44-to-PC storage board has been created to support the Computer Assisted Dynamic Data Monitoring and Analysis System (CADDMAS) currently being developed at Arnold Engineering Development Center. Software was written to test the board's features, and a parametric study of the board's performance was conducted to analyze its capabilities and to provide feedback to the board's designers for future revisions. The software is discussed, and a report on the board's performance is given.

INITIAL SOFTWARE DEVELOPMENT AND PERFORMANCE STUDY OF THE CADDMAS HIGH SPEED, HIGH VOLUME STORAGE BOARD

Gregory G. Nordstrom

Introduction

The Computer Assisted Dynamic Data Analysis and Monitoring System (CADDMAS) under development at Arnold Engineering Development Center (AEDC) is a high-speed, real-time, parallel-processing dynamic data acquisition and processing system used to support ground-based testing and qualification of gas turbine engines. The various engineering analysis outputs of the CADDMAS, both on-screen and hard copy, are available in real-time, allowing on-line test direction. The CADDMAS also performs real-time, on-line engine health monitoring. Refer to [1] for a complete description of the CADDMAS.

One of the CADDMAS requirements is to store the digital data generated during a test period. Because of the high volumes and data rates involved, a study was undertaken in 1994 which produced an initial CADDMAS mass storage system (MSS) design – a distributed, parallel data storage and retrieval system built primarily from off-the-shelf components [2]. The study recommended designing and building a PC-based storage board which could interface the CADDMAS to multiple PCs (such a board was not available commercially). Each PC would be equipped with a Peripheral Component Interconnect (PCI) bus and a Small Computer Systems Interconnect (SCSI) bus with one or more attached disk drives.

as amended

as amended

The recommended storage board was designed and constructed in early 1996, but only a minimum of software was developed ~~[3]~~. Before any further MSS designs could be done, the board's features needed to be fully tested and verified, and the board's performance measured. Additionally, a library of software routines needed to be created so that the board could be integrated into the CADDMAS. This paper describes the software design chosen for the board, discusses the data and control flow used within the board, and outlines some of the software tools developed to measure the board's performance and to facilitate integration of the board into the CADDMAS. The results of these performance measurements are given, and recommendations for further work are also made.

Background

During the testing phase of jet engine's development cycle, many ground-based performance tests are performed. A typical engine test is made up of several "air-on" test periods of up to 12 hours in duration. During these air-on periods, engines are run through simulated missions and maneuvers as the engine's performance is analyzed. During these air-on periods data are continuously available from sensors mounted in the test cell and on the running engine.

Data acquisition during a 12 hour test period is broken down into a series of "data points" that are created by setting the external engine operating environment and then capturing and processing both environmental (i.e. test cell) and engine (i.e. strain gauge) data streams as the engine is run through simulated mission maneuvers. During such maneuvers the CADDMAS processes the data from these parallel streams, allowing the test conductor to analyze the engine's performance and, to a limited degree, modify the nature and direction of the test.

Typically an air-on data point lasts several minutes. During this period, analog signals from the engine under test are digitized and organized into blocks of 1024 dwords (32-bit data samples). Each 1024 dword block is appended to a 64-dword header, resulting in a total block size of 1088 dwords. These data blocks flow from a front-end processor (FEP) into the rest of the CADDMAS. One FEP can handle two high-speed CADDMAS data channels, and generates one 1088-dword block every 4mS. This results in a per-FEP data rate of 262,000 dwords/sec (1,088,000 bytes/sec). Therefore, once the number of channels and duration of air-on periods have been specified for a given CADDMAS application, the aggregate data storage requirements may be calculated using this per-FEP data rate.

Software Development

Fig. 1 shows the overall software design which was developed to support the storage board's operation. A description of the diagram follows.

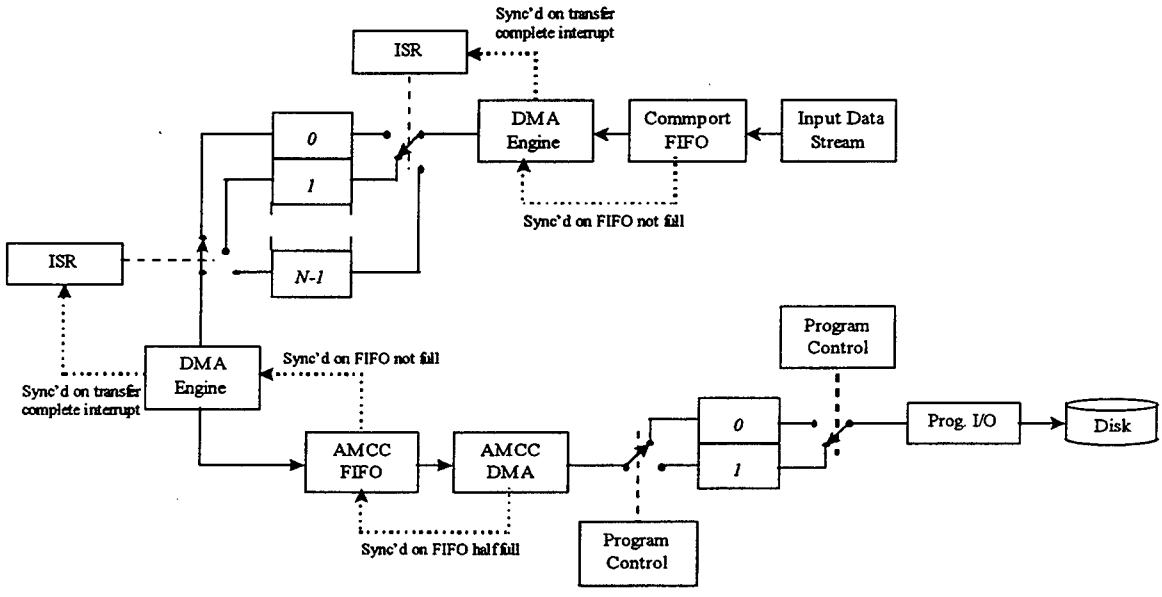

Fig. 1. MSS Functional Block Diagram

Blocks of data enter the storage board via one of four C44 commports. The C44 has six DMA engines which can be synchronized to commports and/or external pins on the processor. (A synchronized DMA engine can manage the movement of data between the commport and the C44's memory independently of the C44 processor.) For the purposes of this discussion, only one commport will be considered. Commport data is DMA'd into one of several C44 memory blocks. An interrupt service routine (ISR) is invoked when the DMA has transferred a block of incoming data to the C44's memory. This ISR updates the DMA engine's destination pointer and causes another block transfer to begin. Note that if all C44 memory blocks are already full (i.e. all blocks contain data not yet transferred to the PC's memory), the oldest block *not currently being emptied* is selected for disposal and the DMA engine is reprogrammed to begin filling that block with new data. Also, a "dropped data block" message is generated. Currently that message is in the form of a unique 32-bit value which is inserted in the data stream.

(see Fig. 2)

Full C44 memory blocks are transferred to the S5933's FIFO by another DMA engine. Once a block has been transferred to the S5933's FIFO, another ISR is invoked which updates the outgoing DMA engine's source pointer and begins another transfer (if, of course, one or more full blocks exist). This DMA engine is synchronized to the S5933's FIFO via one of the C44's external interrupt pins.

Data is transferred out of the S5933 FIFO, and into the PC's memory, by the S5933's DMA engine. This DMA engine is synchronized on the "S5933 FIFO half full" signal (the FIFO can hold a maximum of eight dwords). In this way, there are always at least four dwords to transfer – the minimum amount required to perform PCI burst transfers. Two buffers are created in the PC's memory space to hold data coming from the S5933. More than two buffers are not needed here because the C44's multi-buffer scheme "takes up the slack" when, on the PC side, data flow is momentarily interrupted as pointers are updated when switching between these two buffers. Notice that all data transfers between buffers and FIFOs are synchronized so that data "backs up" into the empty C44 memory buffers when the transfer is interrupted (in addition to buffer switching, interruptions occur due to operating system delays, asynchronous system interrupts, etc.) Finally, data is sent to the SCSI disk via PC program control. Because no custom SCSI controller programming is involved, but rather the Windows 95 and/or DOS-based SCSI device drivers are used, it is important that the disk and controller card drivers are manufacturer's most recent, insuring that the best performance is achieved.

The Windows 95 operating system is used on the PC. Because Windows 95 uses on-demand memory paging (virtual memory), the memory for the PC data buffers must be locked and Windows 95 must not be allowed to page it to disk. The technique used to guarantee this is as follows. When the PC is first booted, an extended memory manager is loaded (emm386.exe) which allows the PC's memory to be treated as extended memory (XMS memory). Next a program (xmsalloc.exe – see Table 1 for more

information) is run which reserves and locks a certain amount of this XMS memory, effectively "hiding" it from Windows 95. This program also creates a small disk file containing the size and starting physical address of this reserved XMS memory. That information is available to any program running under Windows 95, allowing the memory can be accessed using far pointer "C" functions.

A list of the software developed to verify the performance of the storage board is listed below, along with a brief description of what each program does. A much more detailed explanation of each program's operation is given as comments within each program. Additionally, the syntax and a brief description of the PC-based programs can be obtained by running each program and supplying the -h command line switch (C44 programs cannot access the display device, and as such, cannot give syntax descriptions of themselves).

Program Name	Platform	Description
amcc_out.c	C44	Sends simulated FEP blocks to the S5933's FIFO at an adjustable rate
clout.c	C44	Sends simulated FEP blocks to the C44's commport 1 at an adjustable rate
storage1.c	C44	Receives FEP blocks from a commport, buffers them in an adjustable size buffer, and sends them to the S5933's FIFO
amcclib.c	Pentium	A library of routines for configuring the S5933
xmsalloc.cc	Pentium	Allows XMS memory to be reserved and locked
xmsrel.cc	Pentium	Releases previously allocated XMS memory
reset.cc	Pentium	Resets up to four storage boards
status.cc	Pentium	Reports the status of up to four storage boards
bootc44.cc	Pentium	Allows C44 binary program images (.emp files) to be uploaded to the C44 via the PC
readfifo.cc	Pentium	Allows data to be read from one of four storage boards (via the S5933 FIFO)
c442mem.cc	Pentium	Measures the rate at which data can be transferred from the storage board to the PC's memory
mem2mem.cc	Pentium	Measures the PC's memory transfer rate for various data movement methods
diskrate.cc	Pentium	Measures the rate at which data can be transferred from the PC's memory to a disk file
end2end.cc	Pentium	Configures two storage boards (one as a sender, the other as a receiver), receives blocks of simulated FEP data, stores the blocks to disk, and measures the transfer rate.
analyze5.cc	Pentium	Analyzes previously stored blocks of data for consistency, missing blocks, etc.

Table 1. A Description of the Storage Board Developmental Software

Performance Analysis

Before discussing the performance of the storage system, the performance of each of the system's functional components must be understood.

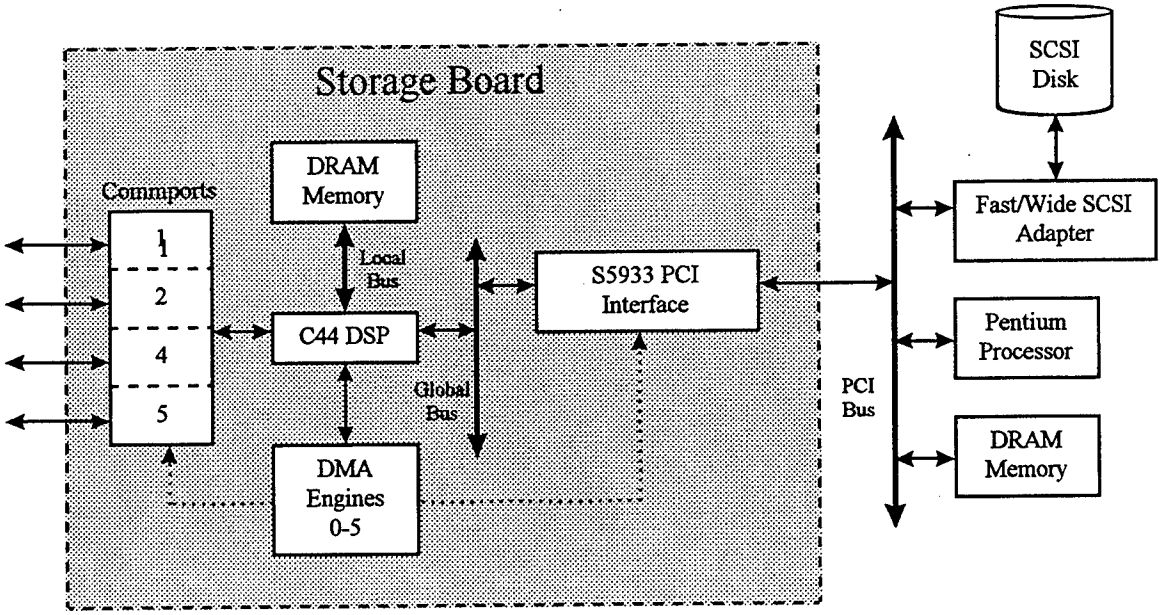

Fig. 2. Storage System Functional Block Diagram

Referring to Fig. 2, and recapping the process just described in the preceding section, FEP blocks arrive at the commports once every 4mS. The blocks are transferred via DMA to the C44's DRAM memory, where they are stored. Later, the blocks are transferred again via a separate DMA process to the S5933's FIFO. The S5933 has its own DMA engine which transfers data from the FIFO to the PC's DRAM memory. The PC then transfers the data to the SCSI controller card (and on to the SCSI disk) via program control. The critical data paths then become 1) C44 commport to C44 DRAM, 2) C44 DRAM to PC DRAM, and 3) PC DRAM to SCSI disk file. The performance of each of these paths was measured separately, then an end-to-end test was conducted to measure the performance of the entire system.

The transfer rate along the first path (C44 commport to C44 DRAM) is a function of commport speed, C44 DRAM cycle time, and DMA engine transfer rate, and is specified by Texas Instruments to be a maximum of 50Mbytes/sec ~~[3]~~. However, when using the C44's DMA engines to transfer data, significant overhead can be incurred when transferring relatively small blocks. On the storage board, there are 3M dwords of DRAM available to store program code and to create blocks for buffering incoming commport data. Because the fundamental unit of transfer within the CADDMAS is the FEP block (1088 dwords), a block size of 1088 dwords was chosen (remember, this is the block size used to transfer data within the C44's memory space, not necessarily the block size used by either the S5933 DMA controller or the PC's processor). Note that an integer multiple of 1088 dwords could be used, and undoubtedly better C44 transfer rate performance would result. However, this performance comes at a cost. The C44 DRAM buffer management algorithm specifies that if all incoming data blocks fill up, the

oldest block of data is dropped, and that block is used to buffer the next incoming block of data. In other words, if the last empty buffer overflows by even one dword, an entire block is lost. It was felt that this loss should be held to a minimum, at least for the time being. If at some time in the future a larger block size is acceptable, the C44 buffer management this can be easily changed, and a parametric study of transfer rate vs. block size performed.

To measure the performance along the two other data paths (C44 DRAM to PC DRAM and PC DRAM to SCSI disk), a second storage board was configured as a data generator, capable of generating simulated FEP data blocks at known rates. The output of this board was fed into the first storage board, and various data rates, representing from one to five FEPs, were simulated. The results of these measurements are shown below. Additionally, to ensure that the PC's memory transfer rate was not the limiting factor in the overall end-to-end transfer rate, it was necessary to measure the PC DRAM-to-PC DRAM data transfer time. Results of those measurements are also listed.

The first experiment conducted was to measure the transfer rate when moving data across the PCI bus. Transferring data from the C44 DRAM to the PC DRAM was done using the S5933's DMA engine. This DMA engine can be programmed to transfer data blocks of various sizes. The general scheme involved creating a pair of buffers in the PC's memory space, and transferring a block of data first to one, then the other, and continuing until the desired amount of data had been moved. A double-buffering scheme was used for this test so that the effects of buffer management, which represent transfer overhead, could be included in the performance measurement.

Block Size (bytes)	Transfer Rate ($x10^6$ bytes/sec)
4096	19.33
16384	19.50
65536	19.50
262144	19.60
1048576	19.70
4194304	19.70

Table 2. C44 DRAM to PC DRAM Performance.

As Table 2 shows, when moving data from the storage board into the PC's memory, the transfer rate is relatively insensitive to the S5933's DMA transfer block size, but there is a tendency for the transfer rate to drop as the block size becomes smaller. This is to be expected, since the transfer rate is a function of

the sum of the data transfer time (which is directly proportional to block size) and the double-buffer management overhead (which remains constant regardless of block size). As the block size decreases, the overhead term becomes more and more dominant. Block size should, therefore, be as large as the PC's memory and the S5933's DMA block size will allow. According to the PCI specification [4], the PCI bus is capable of transferring data at 133Mbytes/sec when using the burst transfer mode. Since the S5933 was programmed to use burst mode transfers for this experiment, it is reasonable to conclude that the PCI bus is not the limiting factor when transferring data from the storage board into the PC's DRAM. (The next test, PC DRAM to PC DRAM shows that the transfer rate observed in Table 2 is, in fact, limited by the PC's DRAM. The results of the PC DRAM to PC DRAM test are shown in Table 3 below.)

Transfer Mode	Transfer Rate ($x10^6$ bytes/sec)
bcopy()	6.52
memcpy()	12.70
memmove()	6.94
programmed I/O	14.10

Table 3. PC DRAM to PC DRAM Performance.

The PC DRAM to PC DRAM test involved transferring blocks of data from one area of the PC's memory to another. Several different methods were used, as indicated by the mode column of Table 3. All the modes are memory transfer modes available in the C programming language. Two assumptions must be stated at this point. First, it is assumed that the PC's hardware (i.e. the memory controller and bus controller) are capable of burst I/O when transferring data across the PCI bus. Also, it is assumed that the DRAM cycle time is equivalent whether reading or writing the DRAM. Since transferring data between two areas of memory involves *both* a read and a write operation, the transfer rates shown in Table 3 should be doubled to give the PC memory transfer rate. Using this somewhat simplified approach, it can be seen that PC DRAM transfer rates of between 13Mbytes/sec and 28Mbytes/sec are possible (such large variations in the measurement are acceptable here, due to the asynchronous use of the bus by the operating system). Table 3 indicates that no matter how fast the data is presented to the PCI bus by the S5933 PCI controller, the transfer is inherently limited by the rate at which data can be accepted by the PC's memory.

The final data path which was tested was the PC DRAM to SCSI disk. For this test, a Seagate ST32550 Barracuda 2LP SCSI drive, attached to an Adaptec AHA-2940W Fast/Wide PCI SCSI controller, was used as the target. (Additionally, a second set of tests was performed using a 540Mbyte Western Digital Caviar 2540 IDE hard drive, using the standard Windows 95 IDE driver. This transfer rates were significantly lower than the SCSI drive in all cases, and so the results are not reported.) Also, since the

tests were conducted in a Windows 95 DOS window, Adaptec's ASPI8DOS.SYS driver was loaded by the operating system before beginning the tests.

For this test, a block of data was first created in the PC's DRAM, and then transferred to the disk using a C program loop as shown below (the filename parameter is a pointer to a previously opened binary file).

```
for(i=0;i<ITERATIONS;i++){
      write(filename, (const void*)d_array, BLOCK_SIZE);
}
```

Here the C function `write()` was chosen after a comparison between `write()` and `fwrite()` revealed that `write()` is much faster (in some cases, up to twice as fast) when transferring data from PC DRAM to the SCSI disk. The speed increase is due to the fact that `fwrite()` uses of an extra layer of memory buffering. Table 4 lists the results of these tests.

Block Size (bytes)	Transfer Rate ($x10^6$ bytes/sec)
512	2.62
1024	4.50
2048	4.52
4096	5.71
8192	2.63
16384	3.52
65536	3.68
262144	3.58
1048576	3.50

Table 4. PC DRAM to SCSI Disk Performance.

Clearly the performance peaks at a block size of 4096 bytes. For block sizes below this, the expected performance decrease is undoubtedly due to the overhead of buffer management. However, the decrease *above* a block size of 4096 bytes is a bit puzzling. It is reasonable to expect that block sizes which are integer multiples of 4096 would have similar performance as the 4096 byte block. Two possible explanations for this behavior are compiler/operating system interactions, and/or interaction between the operating system and the SCSI disk driver. This can be easily verified by compiling the code using another 32-bit C compiler and repeating the tests (all tests in this report were done using the djgpp port of the popular gcc C++ compiler). Because of the definite performance improvement when using a block

size of 4096 bytes, that size was chosen for use to transfer data from the PC DRAM to the SCSI disk in the end-to-end test discussed below.

The end-to-end test simulated the real-life environment in which the storage board will operate. A second storage board was configured as a data generator, capable of generating simulated FEP blocks at various rates. Binary data files of 67,108,864 bytes were created by sending data into the storage board, passing that data as described above to the C44 memory, then to the PC memory, and finally to the SCSI disk drive. Overall performance is indicated in Table 5.

Number of Simulated FEPs	Lost Blocks	Rate ($x10^6$ bytes/sec)
1	0	1.086
2	0	2.17
3	0	2.89
4	0	4.26
5	many	4.24

Table 5. End-to-End Performance.

Conclusions and Recommendations

The results of these tests indicate that a single PC with a single fast hard drive and controller can reliably support storage of data from up to eight high-speed CADDMAS channels. Because this work was designed to measure overall throughput, no data-specific optimizations were performed. However, it is known that the 1024 dwords of data contained in an FEP block, while delivered to the storage board as 32-bit values, are really just 16-bit values extended to 32 bits by a previous process. Because of this, a relatively fast and simple packing operation will result in a significant increase in storage system performance. For example, data arrives at the storage board from the FEP at a rate of one block (1088 dwords) every 4mS, yielding an incoming data rate of ((1024+64) x 4 bytes)/4mS, or 1,088,000 bytes per second. If 1024 of those 1088 dwords can be packed as two 16-bit samples per dword, the outgoing data rate is reduced to (((512+64) x 4 bytes)/4mS, or 576,000 bytes per second. Assuming the overhead required to do the packing is inconsequential (a realistic assumptions, since the packing operation can be done very rapidly, and the C44 processor is idle most of the time -- the C44 DMA engines do virtually all of the work required to move data through the storage board), this could result in a data storage speedup of 1088000/576000, or 1.89. This means that instead of being able to support eight high-speed channels, the single storage board/single SCSI disk setup could support closer to 15 channels. A more realistic expectation might be 12 channels, or 6 FEP boards. This is for storage only. Another factor to consider is

that the CADDMAS must support *simultaneous* storage and playback of data, and must maintain a 20-minute circular buffer (also called a "crash buffer") in case of catastrophic engine failure during a test.

When considering the performance of each segment along the critical data path through the storage board and finally onto the disk, it can be seen that the SCSI disk/controller is the bottleneck. Because the SCSI-2 bus specification allows for up to 10Mbytes/sec transfer rates, it can be assumed that the disk drive, and not the controller, is the real choke point in the system. This can be remedied by 1) obtaining a SCSI drive with faster transfer rates, and/or 2) attaching multiple drives to a single controller. Last year, SCSI controller and drive manufacturers announced hardware supporting the Ultra SCSI standard, capable of supporting SCSI bus transfers up to 40Mbytes/sec across the 16-bit Ultra SCSI bus. And last month, manufacturers announced controller cards based on the Ultra2 SCSI standard, which supports transfer rates of up to 80Mbytes on a single 16-bit Ultra2 SCSI bus. As of this writing, drive manufacturers have not developed a single drive that can keep up with such controllers. However, because up to 15 devices may be attached to a single Ultra or Ultra2 SCSI bus, multiple drive configurations promise to provide significant improvements over the system described in this paper.

Therefore, recommendation for future work are as follows. Modification of the C44 algorithms to allow packing of the data samples as described above. The use of two or more SCSI-2 disks, and modification of the software described in this paper to support multiple disks. Of course, further performance tests must be done in support of both of these efforts. Once a multi-disk system has been built and it performance measured, a prototype storage system can be developed using state-of-the-art hardware components, such as a faster PC (the PC used in this test runs at 90Mhz), the use of EDO RAM in the PC (the current PC does not use EDO RAM), and multiple Ultra or Ultra2 SCSI disk drives and an Ultra or Ultra2 controller (the Ultra2 controller can be purchased right now and is backward compatible with both SCSI-2 and Ultra drives).

A final consideration, now that the system has been proved feasible, is to design the user interface and to begin integrating the storage board into the CADDMAS. Many of the software routines written this summer were based on data structures and methods already in use in the current CADDMAS. Issues of control and data flow must be addressed, as well as expected data rates and volumes when supporting actual testing.

References

[1] Thomas F. Tibbals, Theodore A. Bapty, Ben A. Abbott. **CADDMAS: A Real-Time Parallel System for Dynamic Data Analysis**. *International Gas Turbine and Aeroengine Congress and Exposition*, 1994.

[2] Gregory G. Nordstrom. **CADDMAS Mass Storage System**. A technical memorandum to Sverdrup Technology. Summer, 1994.

[3] Bruce W. Bomar. **TMS320C44 Storage Board**. A technical memorandum to Sverdrup Technology. Spring, 1996.

[4] **TMS320C4x User's Guide**. Texas Instruments Incorporated, 1996.

[5] Edward Solari, George Willse. **PCI Hardware and Software Architecture and Design**. Annabooks, 1995.

remove as amended.

Bibliography

S5933 PCI Controller Data Book. Applied Micro Circuits Corporation. Spring, 1996.

TMS320 Floating-Point DSP Optimizing C Compiler. Texas Instruments, Houston, TX. 1995

Lance Leventhal. **80386 Programming Guide.** Bantam Books, NY. 1988.

PCI BIOS Specification, Revision 2.1. PCI Special Interest Group. August 26, 1994.

DOS Protected Mode Interface Specification 0.9. July 26, 1990.

Rosemarie Piedra. **Mastering the C4x DMA.** Texas Instruments, Houston, TX. 1994

Leor Brenman. **Setting Up TMS320 DSP Interrupts in C.** Texas Instruments, Houston, TX.

Robert Collins. **Protected Mode Basics.** Internet document
http://www.x86.org/art...sics/tspec_a1_doc.html. 1996.

ROLLING MOMENT OF INERTIA AND THREE DIMENSIONAL BOUNDARY LAYER STUDY

Jeff Random
Graduate Research Assistant
Department of Mechanical and Industrial Engineering

Montana State University
PO Box 173800
Bozeman, MT 59715

Final Report for:
Graduate Student Research Program
Arnold Engineering Development Center

Sponsored by:
Air Force Office of Scientific Research
Bolling Air Force Base, DC

and

Arnold Engineering Development Center

September 1996

ROLLING MOMENT OF INERTIA AND THREE-DIMENSIONAL BOUNDARY LAYER STUDY

Jeff Random
Graduate Research Assistant
Department of Mechanical Engineering
Montana State University

Abstract

A method for experimentally determining rolling moment of inertia for cylindrical bodies is discussed with analysis of experimental uncertainty. The roll-acceleration method was used where a weight was attached to the model and released which caused the model to accelerate in roll. The effect various weight sizes is considered. A description of a three-dimensional boundary layer study is also included. An array of thermocouples was installed on the test article in attempt to detect the presence and wavelength of standing vortices. An array of film probes was used at the maximum energy point in the boundary layer at various locations to measure the wavelength and velocity of cross flow instabilities.

ROLLING MOMENT OF INERTIA AND 3-D BOUNDARY LAYER STUDY

INTRODUCTION

This report was written to describe activities experienced and performed by the author at the Arnold Engineering Air Force Center (AEDC), von Karman Gas Dynamics Facility (VKF) wind tunnel facility through the months of June to August of 1996. The work was made possible by the Air Force Office of Scientific Research (AOFSR) through Research Development Laboratories (RDL).

Two major topics will be discussed in this report. Experimental determination of moment of inertia for a cylindrical body rotating about its longitudinal axis and a three-dimensional boundary layer study performed for Wright Laboratory, Wright Patterson Air Force Base, Ohio. The activities undertaken by the author include active involvement in the moment of inertia measurements, and mostly observations in the three dimensional boundary layer study. In order to enhance readability the figures are located at the end of this report.

PART I. EXPERIMENTAL DETERMINATION OF ROLLING MOMENT OF INERTIA

Background

Muzzle fired artillery rounds are released with a high rate of spin to dampen the effects of structural inaccuracies and to spin stabilize the projectile. Wind tunnel tests are often performed with scale models of these projectiles to measure the effects of viscous drag and to measure the effect of the possible Magnus force. If the spin rate is great enough, the projectile is subject to a Magnus force that acts in a direction normal to the plane formed by the axis of the projectile rotation and the incident velocity field. The magnitude of this force is a function of the spin rate, the flight velocity, and the shape of the missile. Although the magnitude of the Magnus force is small (1/10 to 1/100 of the normal force), it can have a detrimental effect to range and accuracy[1].

For a spinning system it is necessary to determine the moment of inertia of the system rotating about its axis in order to properly interpret the data. Analytical methods for determining moment of inertia are tedious and time consuming. For rotating systems it is possible to determine the rolling moment of inertia through experiment.

Description of Test Article and Experimental Setup

As shown in Figure 1, the test article was a scale model of a missile prototype that consisted of a long, cylindrical body mounted on a rigid sting. The model was attached to the sting through a pair of

roller bearings mounted to a six degree of freedom balance. Provisions for attaching one of five flare configurations were present at the rear of the model. The sting was mounted to a massive bulkhead to reduce vibration. A turbine fin ring at the base of the model provided a surface onto which a stream of high pressure air was directed to spin the model at rates of up to 2800 rpm. The model was fitted with an internal photo-diode to serve as a tachometer, outputting one pulse per revolution. The photo-diode signal was routed to a circuit that activated one of two timers: the first pulse started the first timer, the second pulse stopped the first timer and started the second timer, and the third pulse stopped the second timer. The timers then displayed the time elapsed for the first and second revolutions.

Test Procedure

The roll-acceleration method was used to determine the rolling moment of inertia of the cylinder about its longitudinal axis. The model was first balanced statically and dynamically in roll for all fin configurations by adding small amounts of weight at strategic points on the model interior. String was wound around the circumference with successive, equally spaced wraps with the distance from the roll axis to the centerline of the string accurately measured. A weight was attached to the free end of the string and then released. As the model accelerated in roll under the influence of the hanging weight, the internal photo-diode sent a signal for each revolution to the timing circuit. The timing circuit then reported the time to complete each of the two revolutions.

Calculations

The average acceleration is given as

$$a = \frac{4\pi r(P_2 t_1 - P_1 t_2)}{(t_2^2 t_1 - t_1^2 t_2)} \tag{1}$$

where r is the radius of the cylinder, t_1 is the time through P_1 revolutions, and t_2 is the time through P_2 revolutions. Equation (2) derived by Smith and Jenke[2] provides the theoretical calculation to determine the moment of inertia for a rotating body,

$$I_x = \frac{wr^2}{a} - \frac{wr^2}{g} - \frac{w_T r^2}{a} \tag{2}$$

where r is the radius, w is a weight, a is the acceleration of the weight, g is the acceleration due to gravity, and w_T is a tare weight.

The tare weight is an unknown quantity and can be eliminated by repeating the experiment with two or more weights. Considering two weights (w_A and w_B) the following process will eliminate the tare weight. For weight A,

$$a_A I_x = w_A r^2 - \frac{a_A w_A r^2}{g} - w_T r^2 \tag{3}$$

and for weight B,

$$a_B I_x = w_B r^2 - \frac{a_B w_B r^2}{g} - w_T r^2 . \tag{4}$$

Subtracting equation (4) from equation (5), we have the operational result:

$$I_x = \frac{r^2}{(a_A - a_B)}\left[(w_A - w_B) - \left(\frac{a_A w_A - a_B w_B}{g}\right)\right]. \tag{5}$$

Equation 5 results in the moment of inertia for a rolling body and eliminates the effect of the tare weight when two or more weights are used.

A practical question is what choice of weights should be made for calculation of moment of inertia. It is apparent from Equation (5) that the choice of weights should be made such that the difference between them is as large as possible. For a pair of weights that are nearly equal, the fraction outside the brackets is extremely large in comparison to the quantity inside the brackets. This in effect amplifies any uncertainties in the weight and acceleration measurements. For two weights that differ significantly in size, the fraction outside the brackets is smaller in magnitude and the term inside the brackets is larger. Uncertainties in weight and acceleration measurements are now much less significant in relation to the difference between the two weights.

Results

Three weights were chosen ranging from 20g up to 131.5g to evaluate the moment of inertia for this particular model with all flare configurations. Each weight was dropped five times and an overall average acceleration for each weight was computed. Equation (5) was used three times to determine the moment of inertia calculated using each possible combination of weights. The three values were averaged resulting in a mean rolling moment of inertia.

As an additional step, the experimental uncertainty was determined by applying Equation (5) for every possible combination of acceleration values, resulting in 25 inertia computations for each pair of weight groups with five drops. This process resulted in a population of 75 independent inertia calculations when three weights were used. Figure 2 displays the population of inertia computations produced by dropping three weights five times each for the 30 degree flare attachment on the model. Each group of vertical bars represents a group of computations involving two weights. For example, the second block represents the results from using Weight 1 with Weight 3 acceleration data. Note the scale of the vertical

axis in Figure 2; the entire range of the vertical axis is about 1.8% of the mean. The experimental uncertainty associated with this group of computations was calculated to be 0.23%.

In order to quantify the effect of weight choice, a single model configuration was chosen (no flare attachments) and five weights (ranging from 21g to 584 g) were dropped five times each, and Equation (5) was used 250 times to produce a population of 250 independent inertia calculations. Figure 3 shows all inertia calculations from this set. The spikes appearing in the fourth, seventh, ninth and tenth groups were all caused by a single anomalous measurement that occurred during the first weight drop in Group 5. The effect of weight matching can be observed by comparing the average levels of the individual groups in Figure 3. The fifth group of bars (2&3) was calculated using the two smallest weights and resulted in an average value less than the entire population average. The last five groups on the right side of the chart were computed using combinations of large weights that differed significantly. The result was a set of inertia calculations that was much more behaved (more tightly grouped) and consistent between sets. The overall uncertainty for this set is 0.25%.

Concluding Remarks

When experimentally determining the roll moment of inertia of a slender object, weights should be chosen such that a wide range of accelerations can be observed. Ideally, the differences in acceleration should be large enough to drive the fraction outside the brackets in Equation (5) to a value close to or below unity. Small weights furnish acceptable results provided they are heavy enough to overcome the static friction in the bearings. It is important to not compare two groups that have similarly small weights when applying Equation (5). Large weights should also be used with similar caution. The best results will be produced when the two groups under consideration were produced by weights that differ significantly in magnitude.

PART II. THREE-DIMENSIONAL HYPERSONIC BOUNDARY LAYER STUDY

Background

The stability and transition characteristics of three-dimensional boundary layers differ significantly from those of two-dimensional boundary layers. The most fundamental difference is that in addition to the traveling instability waves present in two-dimensional or axisymmetric flow, three-dimensional flows may contain stationary cross flow instabilities[3]. An objective of this investigation was to measure the angles of the traveling instability waves with an array of hot film anemometers, and to detect the presence and wavelength of cross-flow vortices on the cold wall model.

Previous tests at AEDC involved a 7 degree half angle cone at angles of attack that produced some 3-dimensionality but measurements were limited to leeward and windward surfaces only. For the present investigation, a new model was constructed that produced a three dimensional flow without the need to change the model attitude, allowing for measurements at various peripheral locations on the model surface.

Description of Test Facility

Tunnel B is a 50-in hypersonic tunnel capable of both Mach 6 and Mach 8 flows. Mach 8 was used for this investigation. The tunnel is closed circuit with axisymmetric contoured nozzle, and can be operated continually over a range of pressure levels[4]. Stagnation temperature sufficient to avoid liquefaction in the test section are obtained with a natural gas-fired combustion heater in combination with the heat of compression. The entire tunnel (throat, nozzle, test section, and diffuser) is cooled by integral, external water jackets.

Directly below the test section is an installation tank that houses the model injection system. The model and support can be completely retracted into the installation tank and sealed from the test section. The tank can be vented to atmosphere to allow for model adjustments while the wind tunnel remains in operation. After model changes are made, the tank is vented to the test section pressure, and the model is injected into the airstream. The minimum injection time is about 2 seconds, and the model is exposed to the airstream for about 0.9 sec before the model comes to rest at the tunnel centerline.

An air lock that houses the X-Z survey mechanism is located directly above the test section. The X-Z survey mechanism was designed and developed by AEDC and can be retracted into the airlock to allow for probe modifications while the tunnel remains in operation. As shown in Figure 4, three axes of motion are possible. The entire system translates along the x-axis (along the model axis at zero angle of attack), and the probing arm moves vertically along the Z direction (perpendicular to the model axis at zero angle of attack). To facilitate boundary layer surveys, the Z' axis provides for motion normal to the model surface and can be adjusted from 5 degrees (swept upstream) to -15 degrees (swept downstream). The probes are mounted to the foot of the Z' bar, and up to 10 inches of travel can be achieved along the Z' axis.

Description of Hardware

Test Article

The model used for this investigation was a sharp nosed cone with elliptical cross section constructed of 17-4 stainless steel. With an axis ratio of 2:1, the half angle of the cone created in the minor axis was seven degrees.

The model was instrumented with 59 Schmidt-Boelter heat transfer gages, 49 pressure orifices, and a ceramic insert fitted with an L-shaped array of thermocouples. The bulk of the instrumentation was

located in two adjacent quadrants on the model, bounded by the 270- to 0-degree rays, and 0- to 90-degree rays (quadrants I and IV in Figure 5). One pressure tap was located on the 180-degree ray at the rear of the model to ensure proper alignment with the flow. Otherwise, the surface bounded by the 90-to 270-degree rays (quadrants II and III in Figure 5) was free of instrumentation and presented a 'clean' surface for probing.

As an attempt to monitor cross-flow vortices for the cold wall case, a ceramic insert housing an L-shaped array of thermocouples was installed so the reference thermocouple was positioned on the 315-degree ray, centered at model station 32 (see Figure 6). The thermocouples were wired in such a way that the reference thermocouple (gage number 201) measured the actual temperature, while the remaining 14 thermocouples measured temperature differences relative to the reference thermocouple. This allowed for greater resolution in relative temperature measurements between the thermocouples.

Film Probes

Three hot film probes constructed at Montana State University were used for qualitative measurements to determine the frequency and wavelength of cross flow instabilities in the three dimensional boundary layer. The film probes were constructed with an Alumina body as the substrate, platinum leadwires, and a platinum film as the sensing element. Figure 7 shows the general features of a typical probe of this design. The probes were operated in constant-current mode at an overheat of 20%.

A probe holder was designed and fabricated at AEDC to hold the three probes so that the tips of the three probes were at the same height above the model (see Figure 8). Two probes were positioned side by side while the third probe was located below and behind the other two. The probe holder was mounted to the foot of the Z' axis of the X-Z survey mechanism. The Z' axis was rotated 8.8-degrees (downstream) relative to the Z axis. This positioned the three probe tips at the same height above the model surface. The probe holder was adjustable in roll to ensure probe alignment with the model surface for various model roll positions.

Test Procedures

Heat Transfer and Thermocouple Measurements

The first priority was to gather heat transfer measurements in order to determine the location of transition for the cold wall case. This information was important to ensure that probe measurements would take place at locations where the boundary layer was laminar. The process for obtaining heat transfer measurements was to inject the cold model into the airstream and collect data for roughly five to six seconds. The model was then retracted into the installation tank and allowed to cool. The procedure was repeated for a number of free stream unit Reynolds numbers ranging from 0.5- to $2.0X10^6$/ft.

Thermocouple data were recorded simultaneously in hopes of observing standing vortices. A PC was connected directly to the thermocouple array and was running custom software written by the instrumentation team using LabVIEW® for Microsoft Windows® that graphically displayed the temperature distribution in terms of color coding. With this display it was easy to see whether or not temperature distributions were present in real time. The data files were stored for future analysis.

Hot Film Probe Measurements

Based on the heat transfer data, model station 32 was chosen for probing with the hot films. The probing took place at various roll positions, ranging from 90 (major axis vertical) to 180 degrees (minor axis vertical). The probes were used to collect qualitative data at the maximum energy point in the boundary layer at each of the roll positions for future waveform analysis.

The maximum energy point (MEP) was defined as the location where the rms output of the film probes was maximized. To locate the MEP, the probe array was brought as close as possible to the model surface and then retracted normal to the model surface through the boundary layer. As the probes traversed the boundary layer, the rms voltage would increase, reach a maximum, and then begin to drop off. At this point the motion was reversed and the probes were returned to the point of maximum output where a continuous signal was recorded from all three probes. Previously, the rms voltage of only one probe in the array was monitored on an XY plotter with the x-axis connected to the probe output and the y-axis connected to the Z' position transducer. This was cumbersome because the output of only one probe could be monitored at a time (unless a number of plotters were used). To improve this method, another custom software package written with LabVIEW® was developed to simultaneously display the rms voltages of all three film probes. The software also included a counter feature that simplified the process of returning the probes to the maximum energy point.

The foregoing procedure was straight forward for roll positions of 90 and 180 degrees where the probing surface is located at the top of the silhouette. A high magnification camera was set up to display an enlarged view of the probing area and it was possible to bring the probes very close to the surface. At this point a datum was established in the Z' axis and the probes were raised normal to the model surface until the MEP was found. This allowed for a good approximation for the distance above the model. However, intermediate roll positions did not have this luxury and a slightly different method was used.

At the intermediate roll positions, view of the probing surface was obscured by the model itself (see Figure 9). In these situations, the probe array was lowered to the top of the silhouette, at which point a datum in the Z' axis was established. The probe array was lowered toward the surface, down to and through the MEP. The probes were then backed up to the MEP where a stream of data was recorded. The distance of the MEP above the model surface was inferred from calculations that predicted the distance along a normal from the line of sight over the silhouette down to the probing surface.

Results

As previously described, the thermocouple data acquisition system included a PC running a custom LabVIEW® program. As data was being collected, the computer displayed a graphical representation of the thermocouple temperatures in real time. It initially appeared that no significant temperature distributions were present for any of the flow conditions considered.

Subsequent data reduction pointed to the same result. Figure 10 displays a typical time history temperature distribution for the spanwise thermocouples, and Figure 11 displays a typical time history temperature distribution for the streamwise thermocouples. The spanwise thermocouples were located at model station 32, equally spaced between the 305- and 315-degree rays (gage numbers 211-217 in Figure 6). The streamwise thermocouples were aligned on the 315-degree ray, equally spaced between axial locations of 32.00- to 33.30-inches (gage numbers 202-208 in Figure 6). In Figures 10 and 11, the vertical axis represents the thermocouple temperature relative to the reference thermocouple (number 201, not included in the plots). The axis labeled 'Measurement Index' refers to the data point index, the first data point being taken just after the model has reached centerline in the flow. The last data point in the plot was taken just prior to the retraction of the model. Roughly ten data points were taken every second. These two data sets were recorded for a unit Reynolds number of $1.8X10^6$/ft. The picture remained relatively unchanged for unit Reynolds numbers ranging from 0.5- to $2.0X10^6$/ft.

Figure 12 displays the location of the MEP relative to the surface of the model for various roll positions with numerical results for boundary layer thickness included for reference . The roll position refers to the angular location that was located vertical when the probing takes place. As shown in Figure 13, probing on the leading edge refers to 90-degrees (major axis vertical), and 180-degrees refers to the orientation where the minor axis is vertical. The data point at about 104-degrees seems to fall out of line, but generally the points seem to follow a trend. The region near the leading edge exhibits an interesting shape in that the MEP appears to approach the model surface away from the leading edge but then begins to move away from the model surface after an angular position of about 104-degrees.

Concluding Remarks

It appears that no standing vortices were sensed by the thermocouple array or the heat transfer gages mounted on the model surface for the cold wall case. This does not mean that these phenomena do not exist. It is very possible that the resolution of the thermocouple array was not sufficient to sense these phenomena.

As previously stated, continuous streams of data were recorded for the hot film probes at the maximum energy point. Waveform analysis of these data sets has yet be performed to measure the frequency and speed of the cross flow instabilities.

REFERENCES

1 Kayser, L. D., Sturek, W. G., and Yanta, W. J., "Computations of Magnus Effects for a Yawed, Spinning Body of Revolution," AIAA Journal, Vol. 16, No. 7, July 1978, Pp687-92.

2 Smith, K., and Jenke, L., "Measurements of Moments of Inertia," Departmental Correspondece to Glen Burt, March 3, 1975.

3 Kimmel, R. L., Schwoerke, S. N., Klein, M. A., "Three-Dimensional Hypersonic Laminar Boundary Layer Computations for Transition Experiment Design," AIAA Paper 96-2080.

4 Test Facilities Handbook (Tenth Edition) "von Karman Gas Dynamics Facility, Vol. 3," Arnold Engineering Development Center, May 1974.

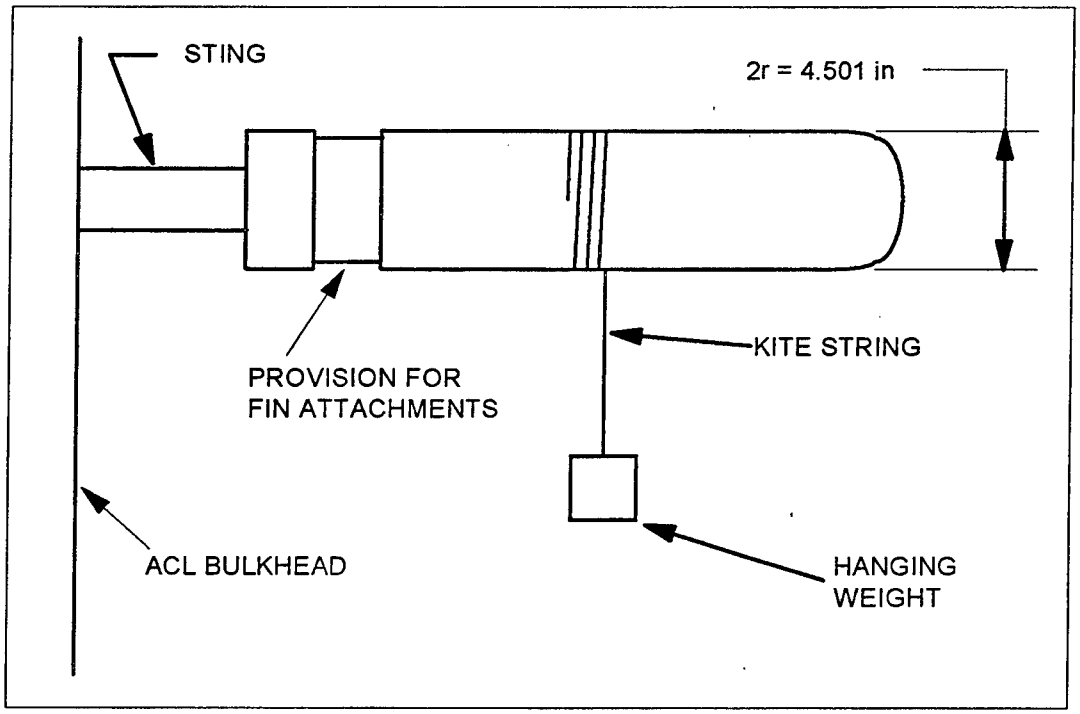

Figure 1. Setup for experimental determination of rolling moment of inertia.

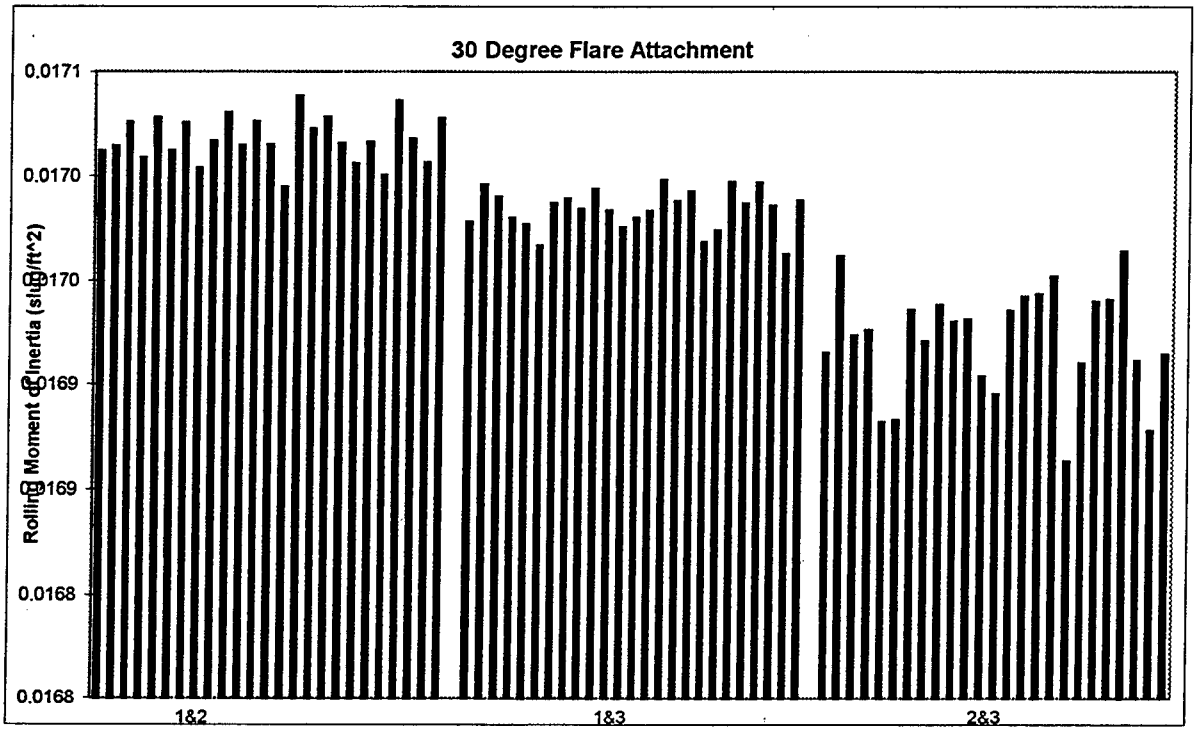

Figure 2. Individual inertia calculations for 30-degree flare configuration using three weights.

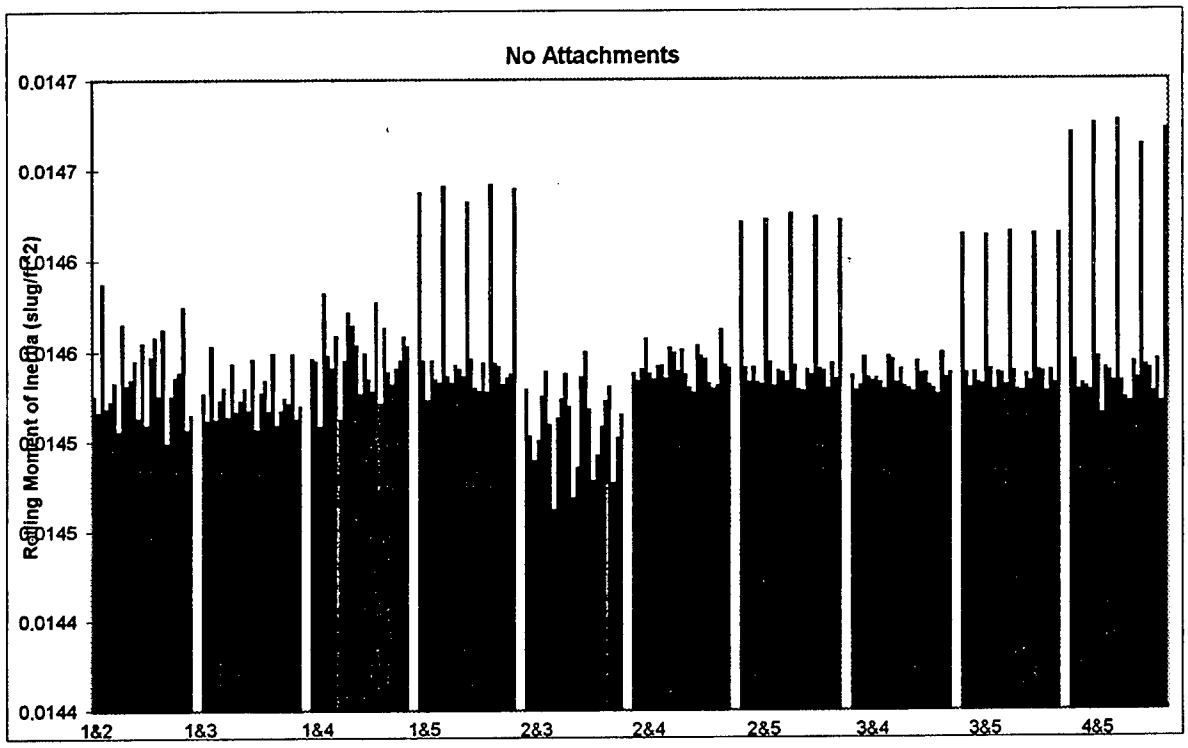

Figure 3. Individual inertia calculations for no attachment configuration using five weights.

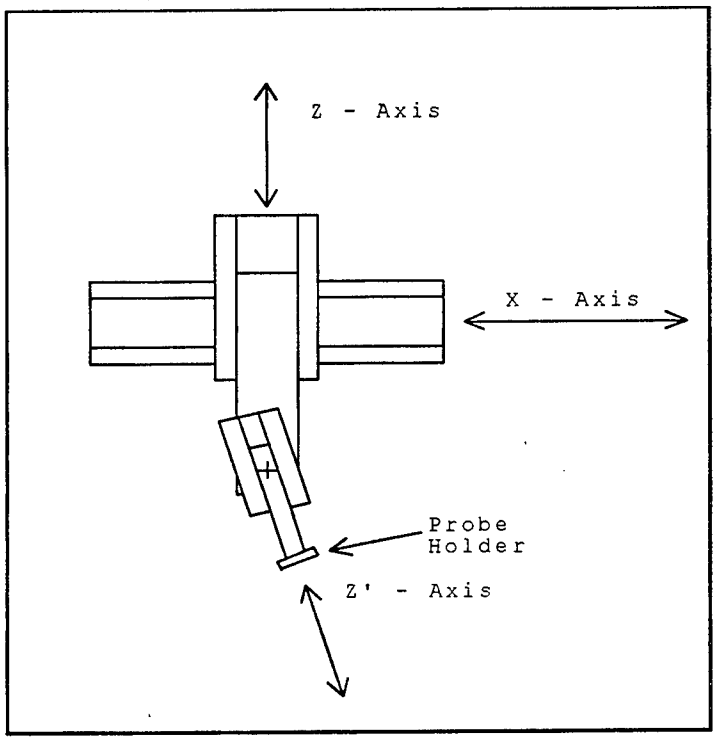

Figure 4. X-Z survey mechanism as viewed from the operator side of the test section

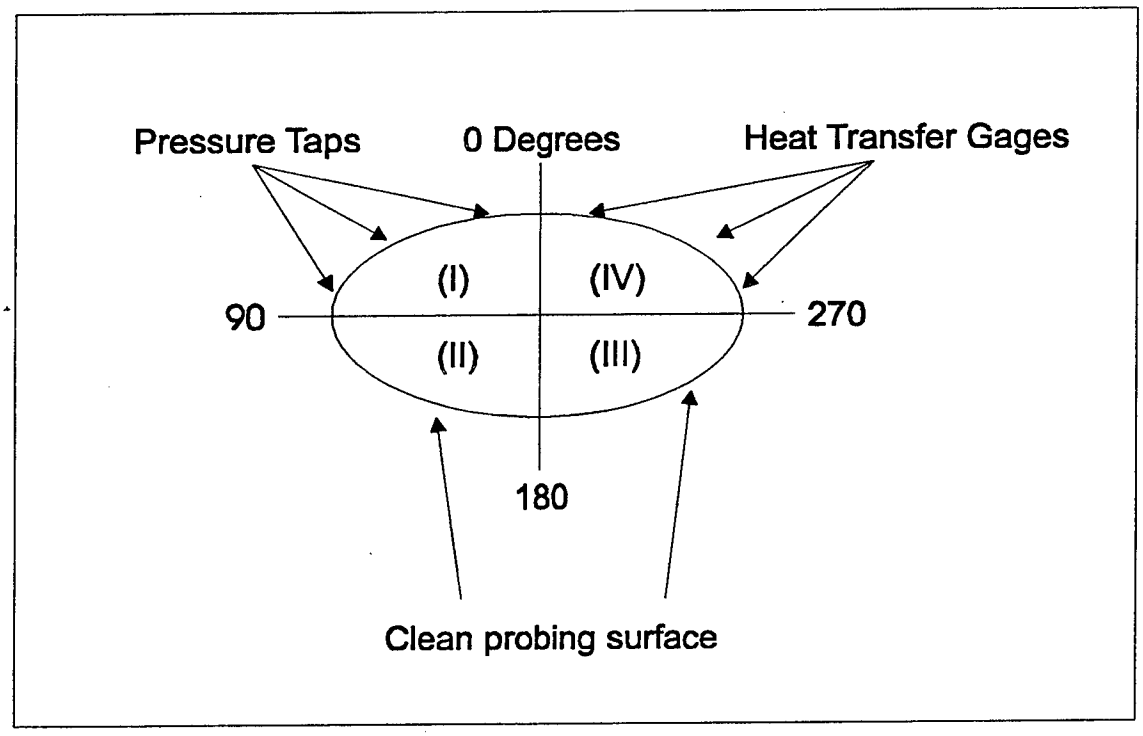

Figure 5. View of model cross section from nose, looking downstream

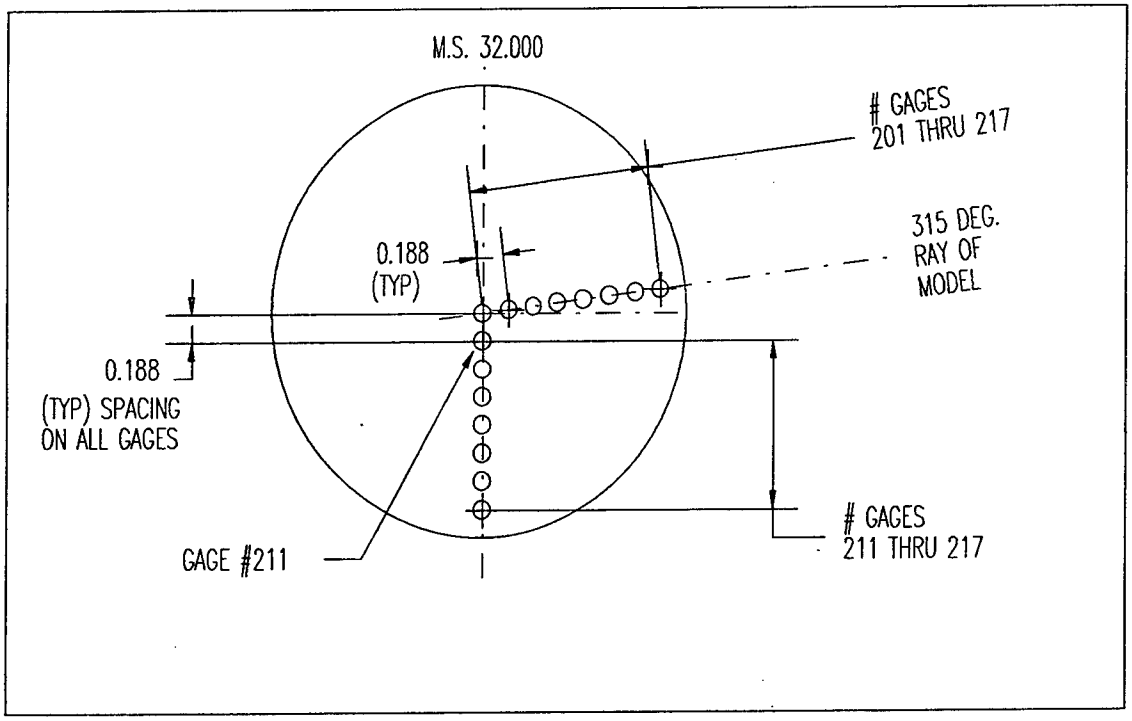

Figure 6. Thermocouple layout in ceramic insert. Viewed from top, normal to surface.

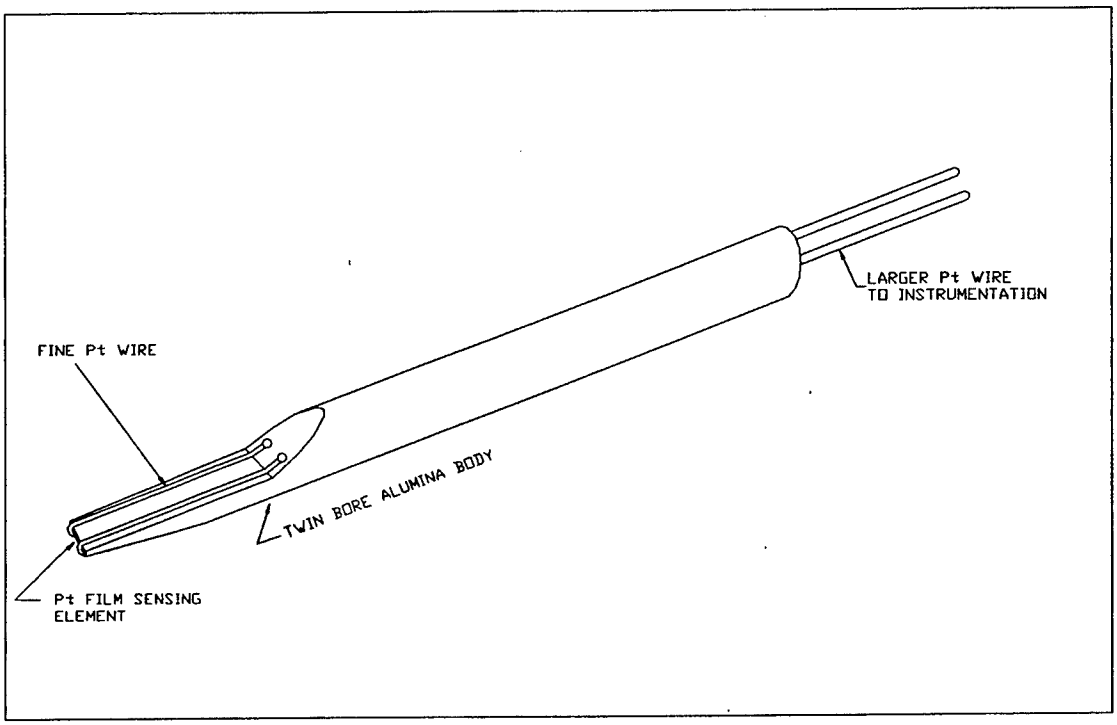

Figure 7. Sketch of film probes used for 3-D boundary layer study.

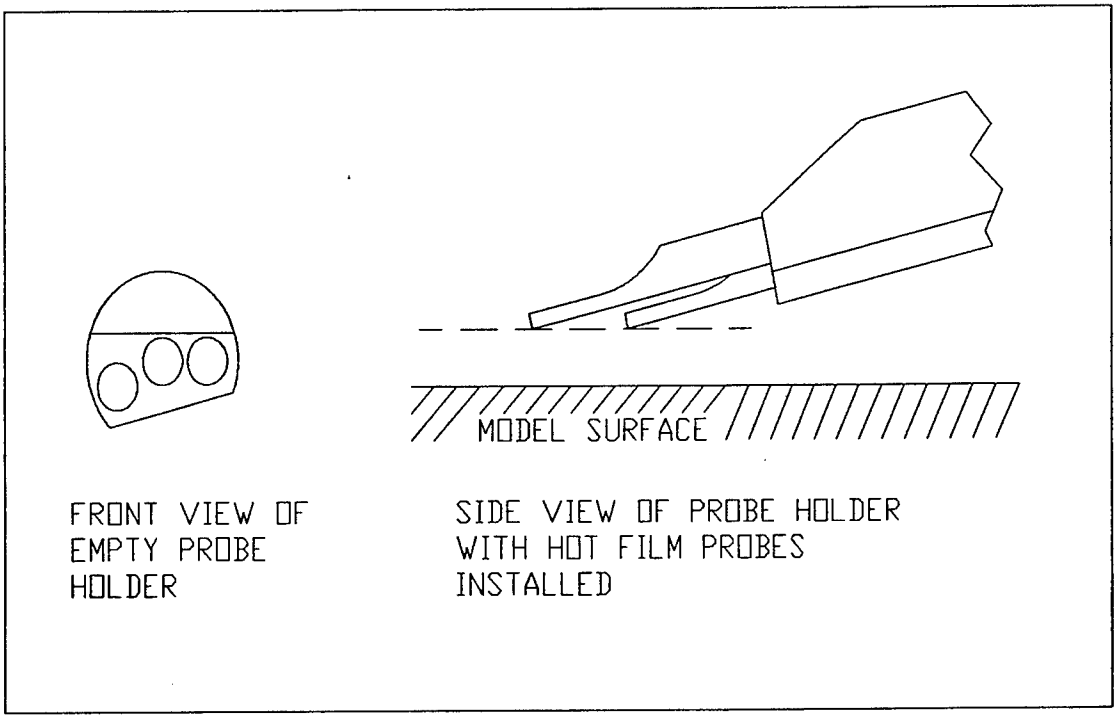

Figure 8. View of empty probe holder from front and side view of holder with film probes installed, positioned near model surface.

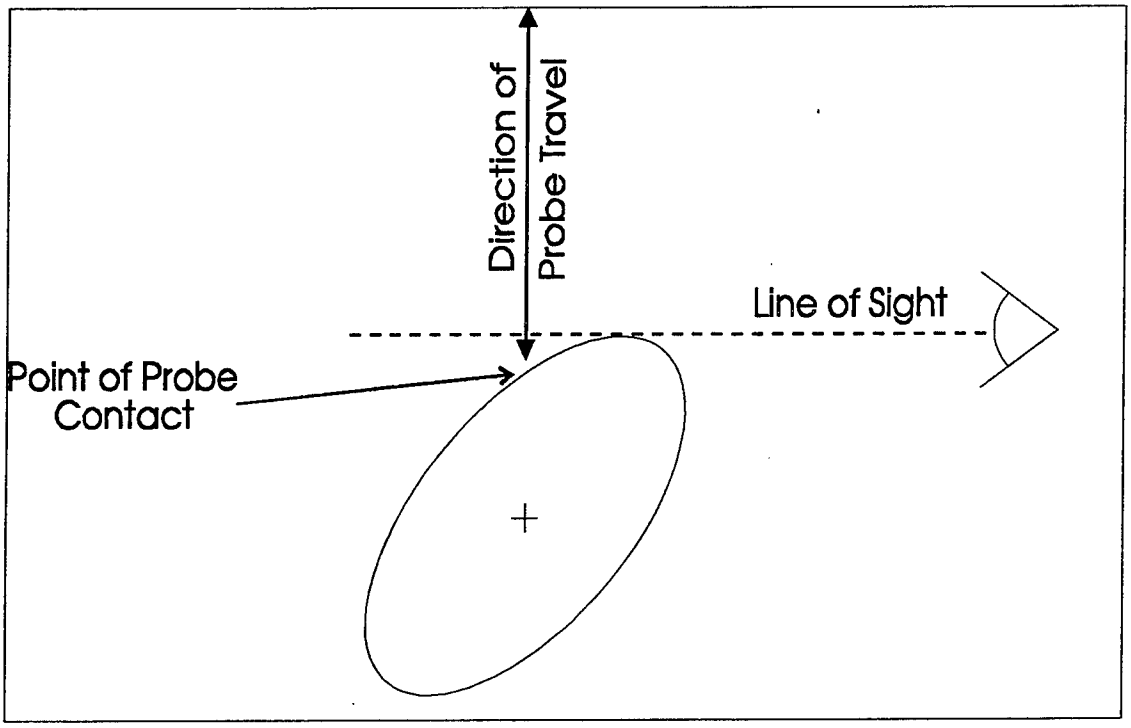

Figure 9. View of probing surface blocked due to model rotation.

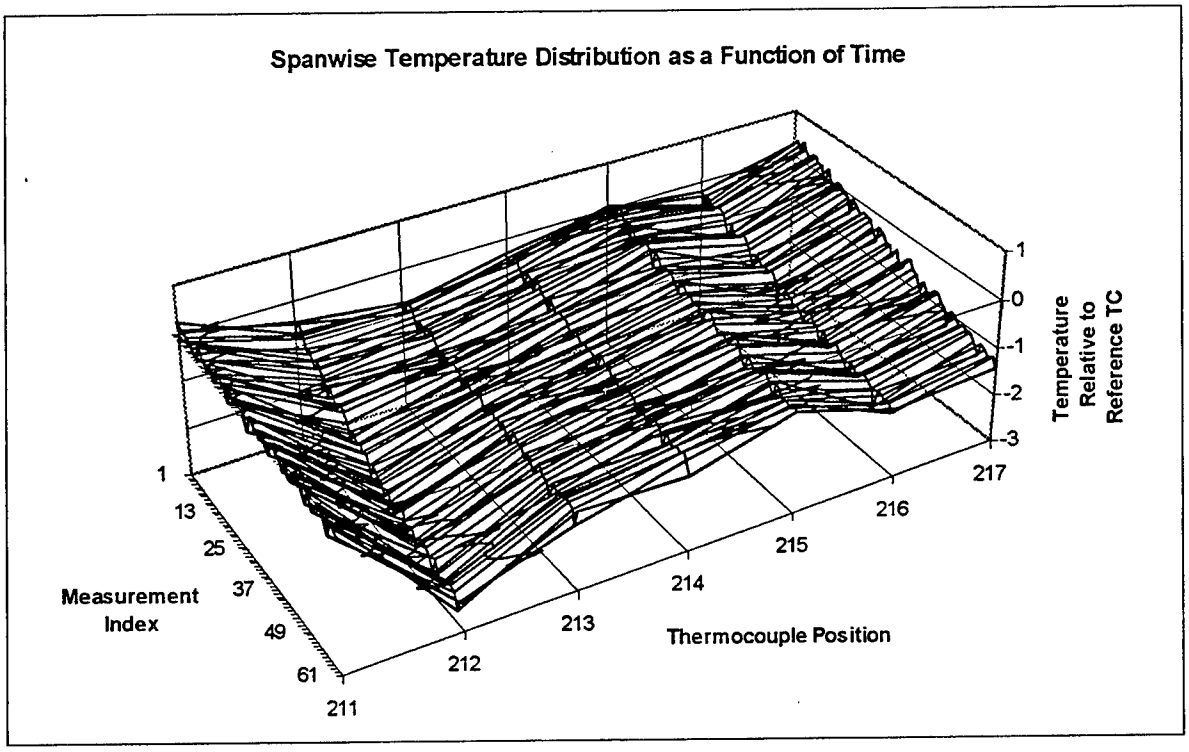

Figure 10. Spanwise temperature distribution as a function of time.

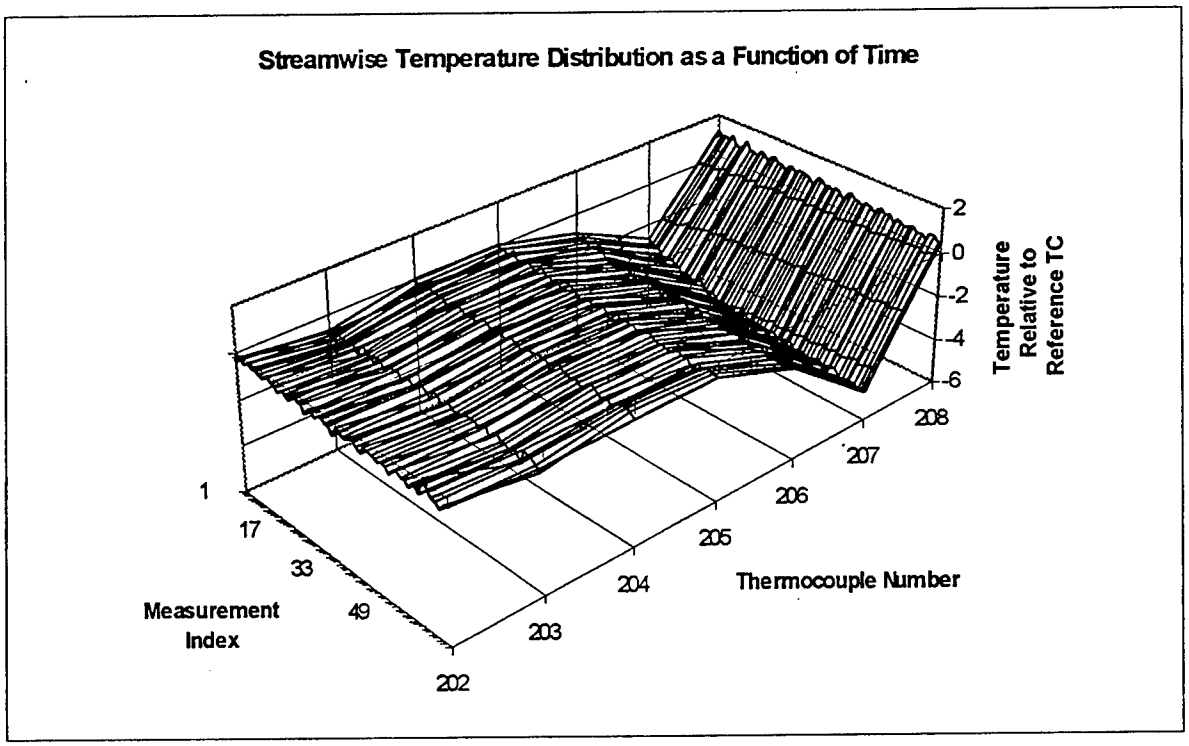

Figure 11. Streamwise temperature distribution as a function of time.

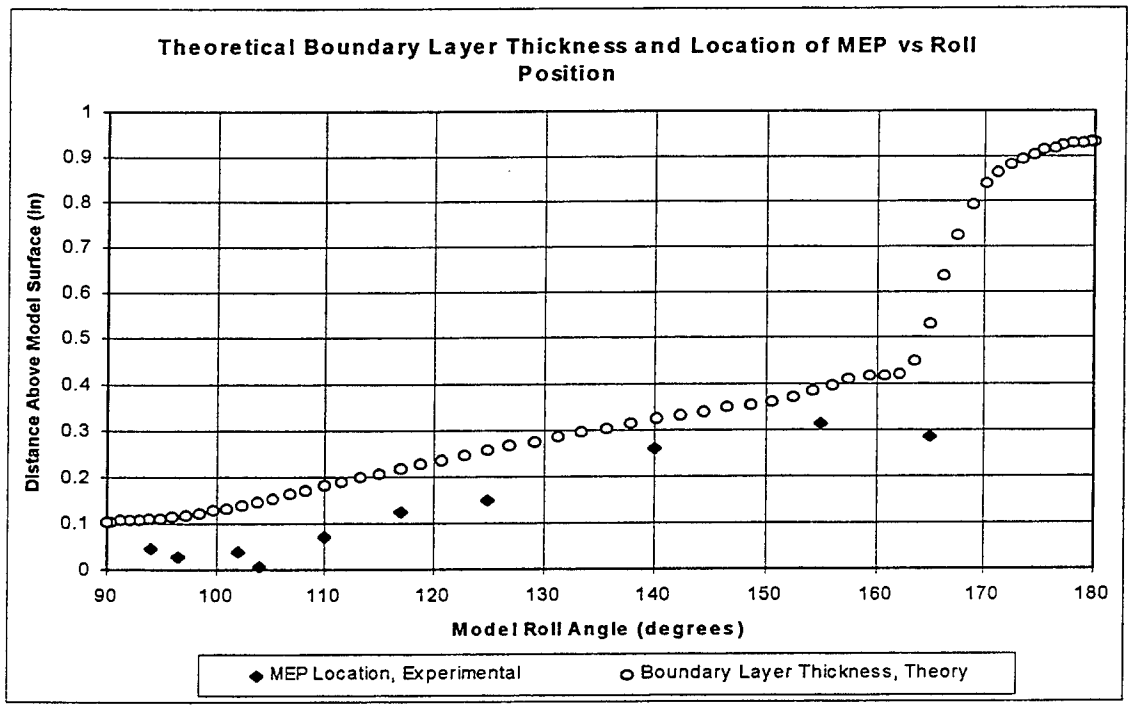

Figure 12. Boundary layer thickness and maximum energy point as a function of roll position

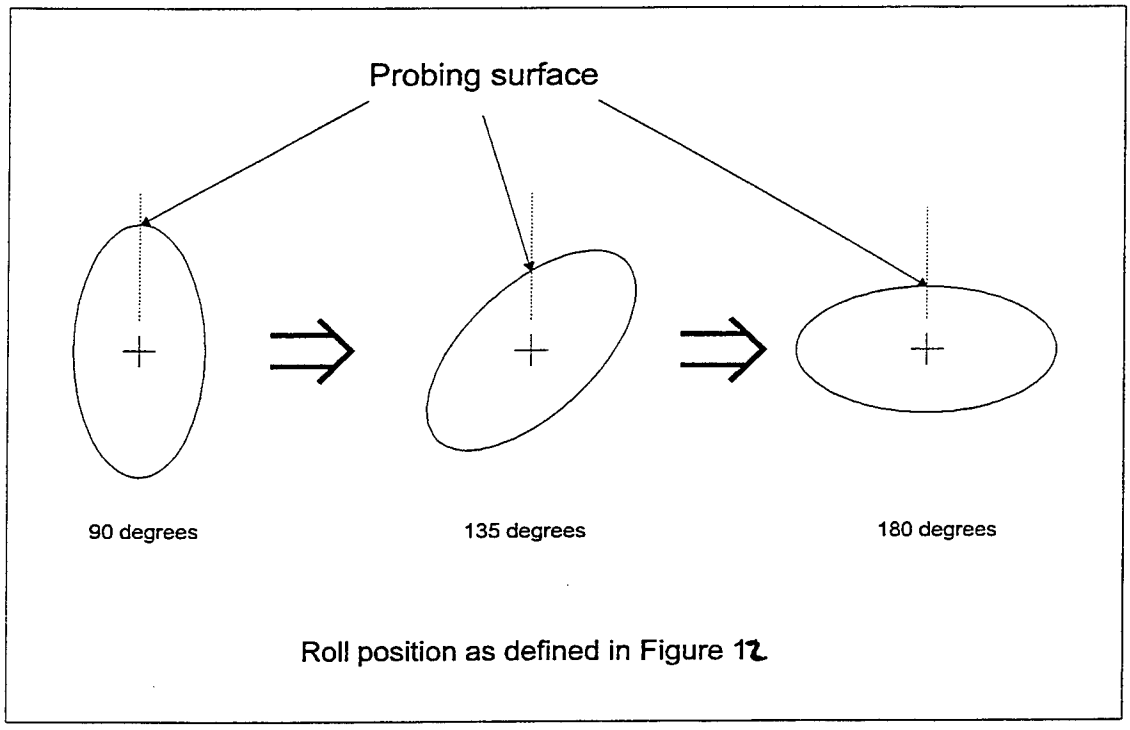

Figure 13. Convention used in Figure 12 to define roll angle.

USAFA TRISONIC WIND TUNNEL ANALYSIS FOR HEAT TRANSFER MEASUREMENTS: SUMMARY

Derek E. Lang
Graduate Student
Department of Aeronautics

University of Washington
Guggenheim Building
Seattle, WA 98195

Final Report for:
Graduate Student Research Program
U.S. Air Force Academy/Aeronautics Laboratory

Sponsored by:
Air Force Office of Scientific Research
Bolling Air Force Base, DC

and

U.S. Air Force Academy

September 1996

USAFA TRISONIC WIND TUNNEL ANALYSIS FOR HEAT TRANSFER MEASUREMENTS

Derek E. Lang
Graduate Student
Department of Aeronautics
University of Washington

Abstract

The United States Air Force Academy wishes to develop the capability to conduct heat transfer measurements as part of its high speed research program. This capability will enhance the educational aspects of its cadet technical training as well as support on-going research conducted in support of defense research programs. The study presented in this paper analyzed requirements for the application and implementation of heat transfer measurement techniques in the Academy's Trisonic Wind Tunnel facility. Specifically, experiments were conducted in the tunnel and assessed operational issues associated with the application of heat transfer measurements to the tunnel.

This study found that a model placed in the low enthalpy tunnel in its current configuration undergoes a relatively small temperature change. Moreover, this narrow temperature range has significant impact on the accuracy of the measurements. This problem is aggravated by unsteadiness in the total temperature of the flow. Potential solutions to this problem are implementing active control of the flow total temperature; changing of model materials from Stycast those with lower thermal conductivities, such as Plexiglas or RTV rubber; or selecting measurement techniques with higher accuracies. The recommended next phase to this development process is to conduct preliminary tests using thermal mapping in a selected temperature range.

USAFA TRISONIC WIND TUNNEL ANALYSIS FOR HEAT TRANSFER MEASUREMENTS

Derek Lang

Introduction

The United States Air Force Academy (USAFA) conducts high speed aerodynamic research to complement their educational mission as well as in support national defense programs. Researchers analyze supersonic flowfields and vehicle characteristics in the USAFA Trisonic Wind tunnel by evaluating pressure measurements, force and moment data, oil flow visualization, and schlieren photography. To increase their ability to investigate a broader range of aerodynamic problems, the USAFA wishes to develop the capability to measure heat transfer characteristics on models in the Trisonic tunnel. Heat transfer analyses and measurements have significant impact for a number of current military applications. For example, heat transfer measurements will assist in the Theater Missile Defense research for identifying missile heat signatures and in the Hypersonic Cruise Missile program for airframe-propulsion integration.

The selection of techniques for use at the USAFA must be consistent with the operational conditions of the facilities as well as the institution's capabilities. In particular, the chosen techniques must be accessible and usable in an undergraduate cadet environment. This research project conducted the initial analyses for developing heat transfer measurement techniques for the Trisonic tunnel. The project was composed of four areas: thermal characterization of the tunnel, analysis of data reduction techniques, examination of model materials selection, and evaluation of measurement techniques.

Discussion of Problem

Theory. Heat transfer occurs from the air to a body surface due to temperature gradients in the boundary layer. Changes in the boundary layer due to the nature of the flow (i.e., whether it is laminar, turbulent or transitional) or whether flow separation has occurred will affect the amount

of heat transfer between the fluid and body surface. The heat flux is quantified by the relation given in Equation (1):

$$\dot{q} = k \left. \frac{\partial T}{\partial y} \right|_{y=0} = h(T_{aw} - T_w) \tag{1}$$

Since the adiabatic wall temperature equals recovery temperature, T_r, as defined in Equation 2, it can be seen that heat transfer will indicate whether the flow is laminar, turbulent or transitional [Ref 1].

$$T_{aw} = T_r = \left(r + \frac{1-r}{1+\frac{\gamma-1}{2}M_e^2} \right) T_{tot,e} \tag{2}$$

where $r = \sqrt{Pr}$ for laminar flow, $r = \sqrt[3]{Pr}$ for turbulent flow

Thus, trends in heat transfer distributions can be used to provide qualitative assessments of the boundary layer or numerical computations of heat transfer or recovery factor can be used to determine the state of the flow quantitatively. The level of detail to which analysis is conducted is dependent on the problem to be solved, available facilities, measurement technique(s) utilized, the test conditions and geometries, and researcher resources and capabilities.

Measurement Techniques. Numerous experimental techniques are available for determining heat transfer. Detailed descriptions of these techniques can be found in most engineering measurement texts. Neumann presents an overview of the techniques typically used for measurements in high speed flows [Ref 2]. Global, or thermal mapping, techniques which provide information over the whole surface of a body are well suited toward the USAFA's needs to gain broad understandings of general flow characteristics or patterns that can validate more detailed analytical work or assist in the design of vehicles and models. These techniques, such as liquid crystals, thermographic phosphors, infrared thermography, or phase-change coatings,

measure temperature by color changes or phase changes on the model due to a temperature-sensitive coating or the radiation emitted from the surface.

Data Collection and Reduction. Temperatures may be measured and used for heat transfer computations by various approaches of increasing sophistication. In the simplest case, the time can be recorded when a single temperature-dependent event (such as a color change) occurs. More complex methods continuously monitor these events as hue changes over time and provide a temperature history [Ref 3]. Common techniques for reducing these data are given by Equations 3, 4, and 5 [Refs 4,5]. For discrete measurements, the semi-infinite wall method may be used; whereas the latter two require continuous data collection.

Semi-Infinite Wall

$$\frac{T_w - T_{aw}}{T_{w,0} - T_{aw}} = e^{\beta^2}\,\mathrm{erfc}(\beta) \qquad (3)$$

and $$h = \frac{\beta\sqrt{\rho c k}}{\sqrt{t}}$$

Cook-Felderman

$$\dot{q}(t_n) = \frac{2\beta_0}{\sqrt{\pi}} \sum_{i=1}^{i=n} \frac{T_{w,i} - T_{w,i-1}}{\sqrt{t_n - t_i} + \sqrt{t_n - t_{i-1}}} \qquad (4)$$

Kendall-Dixon and Hedlund

$$Q(t_n) = \frac{\beta_0}{\sqrt{\pi}} \sum_{i=1}^{i=n} \frac{\Delta T_{w,i} - \Delta T_{w,i-1}}{\sqrt{t_n - t_i} + \sqrt{t_n - t_{i-1}}} \Delta t \qquad (5)$$

where $\Delta T_w = T_w - T_{w,0}$, $\Delta t = t_n - t_{n-1}$

and $$\dot{q}(t_n) = \frac{dQ_n}{dt} = \frac{-2Q_{i-8} - Q_{i-4} + Q_{i+4} + 2Q_{i+8}}{40\Delta t}$$

Materials Selection. Another consideration in designing heat transfer experiments is the selection of the material that will be used to build the test model. Two major factors in the selection process are the material thermal and mechanical properties. The semi-infinite wall assumption is commonly used as a simple method for computing heat transfer. For the purposes of this research, the semi-infinite wall approaches will be used. This approach assumes: an

initially isothermal model; heat penetration is small compared to the wall thickness; thermal sensor is massless; heating step of constant magnitude; and material properties are known and constant over time. Generally, materials that are good insulators, i.e., low $(\rho ck)^{1/2}$, are well suited to these assumptions.

External factors that affect the properties of the final model are critical in the evaluation of materials. Factors such as batch consistency, thermal loads during machining, and shelf life may all affect the thermal properties of the final model configuration [Ref 6]. The strength of the material is another significant factor, since the model will be subjected to loads under supersonic flow conditions. The operating envelope of the tunnel can achieve steady state dynamic pressures up to 2.2 bars. But in addition, transient loads have been measured to exceed steady state values by up to 3500% for start-up and 500% for shut-down [Ref 7].

Methodology

Some simplified heat transfer experiments were conducted in the USAFA Trisonic Wind Tunnel in order to characterize typical heat transfer environments in the tunnel as well as identify operational issues that must be considered in planning future tests. The Trisonic tunnel shown in Figure 1 is a blow-down facility with a test section cross-sectional area of $1ft^2$ ($0.0923\ m^2$). Test section Mach numbers range from 0.24 to 4.28 for 1-7 minutes.

Tests were conducted on the spherically-blunted cone shown in Figure 2. The cone is made of a highly filled epoxy casting compound, called Stycast. Six Omega "Cement-On" Chromel-Constantan (type-E) foil thermocouples of 0.0005 inch thickness were attached to the surface of the cone to measure temperatures at discrete locations along the body. Test conditions are presented in Table 1. All tests were run at M=2.45.

Table 1: Test Conditions

Run	Tank Pressure (bars) (start/finish)	Tank Temperature (K) (start)	Stilling Chamber Pressure (bars)	Run Time (sec)
1	38.57/11.75	317	45	162
2	37.67/19.61	317	45	100
3	36.71/18.78	307	45	100
4	37.40/19.89	305	45	100

Heat transfer was computed using the USAFA RedHeat software. This program allowed the user to compute heat transfer using either Cook-Felderman (C-F), Kendall-Dixon (K-D), or Semi-Infinite (S-I) methods. The uncertainty for each method is shown in Table 2.

Table 2: Uncertainty Analysis

Parameter (x)	Typical Value	δx (+/-)	C-F (%)	K-D (%)	S-I (%)
T_{tot}	296.6K	.3K	1.5	1.9	1.3
T_0	295.7K	.3K	4.3	8.8	16.6
T_w	293.7K	.3K	35.4	10.1	17.8
$\sqrt{\rho ck}$	1594 $W.s^{1/2}/m^2.K$	35	2.4	2.8	2.2
t_n	12s	.0125s	0.8	2.4	0.1
		Total (%)	35.8	14.0	24.5

Results

The purpose of the experimental portion of this research was to analyze the thermal characteristics and operating issues of the Trisonic tunnel. An initial assessment of the Trisonic temperature data was conducted to determine whether the anticipated thermal environments were realized in actual operations. Focus was then placed on addressing specific issues that would impact future heat transfer measurements.

Thermal Characterization. Using Stycast material thermal properties and constant values of heat transfer coefficient, the Semi-Infinite Wall method of Equation 3 provided the temperature variations over time (Figure 3). The schlieren of Figure 4 verifies the expected shock formations for flow around the blunted cone. The resulting temperature history for this flow corresponds relatively well to Runs 2-4 in Figure 5. Immediately, it is seen that the overall temperature range is relatively small over the duration of the tests. Runs 3 and 4 which have the greatest temperature range have a reduction in temperature of less than 10°K. More importantly, the temperatures never come close to reaching the T_{aw}. The narrow temperature range will affect measurement uncertainty and constraints on tunnel operations. Approaches to reducing uncertainty therefore are to increase accuracy for small temperature ranges or increase the temperature ranges for a given accuracy [Ref 8]. The narrow temperature range also affects test design and operations. For example, the crystal may begin changing colors at 293 °K; pass through a narrow bandwidth color hue at 295 °K; and complete its color change at 303 °K. Besides considerations of the predicted temperature range for the test conditions, ambient indoor temperatures of the Trisonic tunnel facility can vary between 283-290°K depending on the season of the year and thus have an impact on the success of the test. Alternative methods for increasing temperature ranges for a given test duration include changing total temperature or changing material properties.

A key concern revealed in Figures 5(a), (c), and (d) is the unsteadiness of T_{tot}. Because of the small surface temperature range experienced during the tests, the total temperature as measured in the stilling chamber has significant impact on surface temperature measurements. Run 1 shows an increasing Ttot and wall temperatures that would suggest little heat transfer. Comparison of Run 2 to Runs 3 and 4 shows a significantly smaller temperature variation over time for the steady T_{tot} than for the unsteady cases. The T_{aw} is decreased in Runs 3 and 4 due to the lower T_{tot}, creating a stronger driving potential. Therefore, the lower wall temperatures are likely due to the lower T_{aw} moreso than the fluid heat transfer properties. Run 2 was conducted later in the day after Run 1, whereas Runs 3 and 4 were conducted on separate days in the

morning hours. A possible post-run heat soak may have resulted the more steady conditions in Run 2, suggesting a systemic cause for the steadiness in one case versus the others. Additional investigation into this area is necessary to achieve as steady temperature. Potential solutions identified in Reference 8.

Figure 6 shows the computed heat transfer coefficients to be on the same order of magnitude as the theoretical values. Note that the heat transfer coefficient increases over time by about 60 $W/m^2.K$ in the first 30 seconds due to the transient thermal boundary conditions. Based on these values of heat transfer coefficient, one can determine the recovery factors (note: in fact, one would evaluate the value of heat flux to determine the flow state since an assumption of recovery factor is part of the computation for heat transfer coefficient).

Data Reduction Methodologies. Figure 7 compares the application of the three methods for computation of heat flux. The Cook-Felderman method is a direct method which attenuates fluctuations in the heat transfer. Kendall-Dixon computes total energy transfer and then time rate of change of this energy to give heat transfer. It is used in conjunction with a finite-difference approximation by Hedlund to smooth fluctuations in heat transfer. Hollis [Ref 9] notes that over a given time interval, the averaged values of the two approaches will be equal. Since the Semi-Infinite Wall method is based only on an initial and current temperature, it will also tend to smooth the heat flux profile. The Semi-Infinite Wall method assumes constant heat transfer coefficient, and therefore is really only applicable in the linear range of the heat flux-temperature relations. The Semi-Infinite results in Figure 7 still appear to have good agreement with Kendall-Dixon.

If a single point measurement approach is applied, the Semi-Infinite wall method will be used to reduce heat transfer data. Figure 8 indicates the time range under these test conditions in which the Semi-Infinite will give accurate results. In this case, the Semi-Infinite result converges to the Kendall-Dixon after 70 seconds. Examining the convergence time of all the thermocouples will

provide an average length of time necessary before the Semi-Infinite method will give accurate results. This time corresponds to a temperature range which can be used to select an appropriate liquid crystal and at what temperature the single point measurement should take place.

Material Properties. A method for increasing the temperature range within the test duration is the selection of material properties. For the Trisonic Wind Tunnel conditions, Figure 9 shows that a smaller $(\rho ck)^{1/2}$ increases the rate at which the temperatures at the surface vary. This trend is consistent with the fact that materials, such as stainless steel, with higher $(\rho ck)^{1/2}$ have shorter diffusion times. The low $(\rho ck)^{1/2}$ infers that heat is slow to diffuse into the body, thus the surface experiences the greatest temperature rise. On the other hand, materials with high $(\rho ck)^{1/2}$ rapidly soak in the energy transferred to it. The energy is quickly distributed throughout the thermal mass - which in the case of the spherically-blunted cone includes the entire mass of the model. Thus, the rate at which the surface temperatures change is relatively slow. Table 3 lists the thermal properties of some typical materials.

Table 3: Example Material Properties [Ref 8]:

Material	Density (kg/m^3)	Specific Heat (J/kg.K)	Thermal Conductivity (W/m.K)	$\sqrt{\rho ck}$ ($W.s^{1/2}/m^2.K$)	Diffusion Time (s)*
Stainless Steel	7880	460	16.07	7594	1.6
Quartz	2192	728	1.30	1439	8.6
Fused Silica	2210	755	1.40	1528	8.6
Macor	2520	734	1.46	1644	9.1
Pyrex Glass	2230	712	1.09	1315	10.5
Stycast	2277	904	1.24	1594	12.0
RTV Rubber	1350	1381	0.35	810	38.1
Cast Epoxy	1150	1671	0.35	815	40.0
Plexiglas	1190	1462	0.19	571	66.8

* - based on a 6 mm thickness

Fabrication issues will also be critical selecting materials for the USAFA's experiments. To date, most of the USAFA's models have been machined from steel and aluminum. Glass ceramics such as Macor are machinable, but are very brittle. Pyrex glass requires glass blowing or other heat processing. Stycast and epoxies typically require curing in a mold, while rubber is molded, injected or extruded. A common approach used by AEDC was to insert a stiffener into the model geometry to provide structural support. One problem faced by AEDC when using Stycast and Macor was that here was a tendency for the model to crack when attached to a stiffener with different thermal expansion properties [Ref 10]. Based on the thermal characteristics and diffusion time, materials like RTV rubber and Plexiglas appear to be likely candidates for use with these heat transfer experiments [Ref. 8].

In addition to the fabrication of the model, the test and environment must also be evaluated with respect to the materials used. In high enthalpy wind tunnel, sharp leading edges must withstand significant heat loads. Depending on the temperatures involved, the material melting point may need to be considered. Stycast and rubbers may soften at these high temperatures as well as change thermal properties. If the same model is to be used for measurements other than heat transfer, each of these tests will have other constraints. For example, oil flow visualization requires relatively smooth finish, while it is easier to work with metals such as steel or aluminum to machine small pressure taps for models used in pressure tests.

Measurement Techniques. An understanding of the tunnel operating envelope and thermal characteristics provides the basis for further assessment of the various measurement techniques that may be selected for use by the USAFA. Clearly the factors that have been discussed above will have wide ranging implication on the measurement techniques that are available. Each technique when used in this environment will have its inherent advantages and disadvantages. While further analysis is necessary to determine the optimal technique, several observations can be made:

- The narrow temperature range will likely affect all techniques. Given the existing tunnel conditions then, one must consider how effective each technique might be within this current temperature range.
- Another problem that must be considered for all the thermal mapping techniques is that the one dimensional heat transfer assumptions used break down if the surface depth is not sufficient.
- The potential need to analyze complex model geometries may complicate the use of liquid crystals. Since the color of the crystal is dependent on the reflection of a light source, the orientation of the light source and relative position of the observer are critical to evaluating color changes in the crystals.
- One of the problems for liquid crystals that has been raised in discussions with NASA-Langley and AEDC is keeping the crystals intact on the model [Refs 6,10].

Several factors must be considered in selecting the measurement technique that will be useful for the Trisonic tunnel. In addition to further analysis of the impacts of the tunnel operating characteristics on the measurement technique, these factor must be prioritized.

Conclusions and Recommendations

This research assessed issues that must be addressed in the development of heat transfer measurement capabilities for the USAFA Trisonic wind tunnel. An investigation of measurement techniques and experimentation in the Trisonic tunnel provided qualitative and quantitative baseline data and tunnel characteristics that will be necessary in the selection of a measurement technique and design of future heat transfer experiments. As part of this research effort, a heat transfer measurement capability using thermocouples has been established for use as an independent technique or for use in conjunction with thermal mapping techniques. The implementation and assessment of several data reduction methodologies also support future transient heat transfer research for the Trisonic tunnel as well as other efforts in the USAFA Aeronautics Laboratory.

Based on the analyses and experiments conducted during the course of this research, the following conclusions can be drawn:

- The tunnel as configured will provide airflow that will produce a narrow range of temperature changes on the surface of the models.
- This narrow temperature range will affect measurement uncertainty and operational constraints of tunnel. For example, cooling the air storage tanks increased the temperature range.
- Stilling chamber temperature is unsteady and has significant impact on temperatures in the current range.
- Materials with low thermal properties products are desirable for heat transfer experiments, yet machinability and mechanical strength are also critical factors.
- The current tunnel operating conditions and geometry impact the effectiveness and even adequacy of all the heat transfer measurement techniques. There does not appear to be one ideal technique, but rather the selection of a technique will require prioritization of criteria and engineering trade-offs.

As a result, the following efforts are recommended which to advance the USAFA's efforts to develop a resident heat transfer measurement capability:

- Investigate options for increasing temperature range, including changes to total temperature and material selection.
- Investigate options for stabilizing stilling chamber temperatures. This study should analyze the heat transfer between the air storage tanks and stilling chamber as well as the incorporation of active temperature controls.
- Investigate further the suitability of RTV rubber and/or Plexiglas for model construction with particular focus on structural integrity in the supersonic flow environment.

Sample tests using thermal mapping should be conducted to gain operational experience. Key focus will be the effectiveness of the technique in the narrow temperature range.

Nomenclature

c	= specific heat (J/Kg.K)	$\dot{q}$	= heat flux (W/m^2)
h	= heat transfer coefficient ($W/(m^2.K)$)	r	= recovery factor
k	= thermal conductivity (W/m.K)	T	= temperature
M	= Mach Number	T_w	= wall temperature at a specific time (K)
Pr	= Prandtl Number		
Q	= total energy transfer (J/m^2)	t	= time (s)
α	= thermal diffusivity, $k/(\rho c)$ (m^2/s)	β_o	= thermal product, $\sqrt{\rho c k}$ ($W/(m^2.s^{1/2})$)
β	= non-dimensional heat parameter, $\sqrt{h^2 \alpha t / k}$		
ρ	= density (gm/cm^3)		

Subscripts

aw	= adiabatic wall	e	= boundary layer edge
tot	= total conditions	w	= wall conditions
0	= initial conditions	∞	= freestream conditions

References

1. Bertin, John J., Hypersonic Aerothermodynamics, American Institute of Aeronautics and Astronautics, Washington, D.C., 1994.
2. Neumann, R.D, "Aerothermodynamic Instrumentation," Special Course on Aerothermodynamics of Hypersonic Vehicles, AGARD-R-761, May 30-June 3, 1988.
3. Camci, C., et. al., "A New Hue Capturing Technique for the Quantitative Interpretation of Liquid Crystal Images Used in Convective Heat Transfer Studies," ASME Journal of Turbomachinery, Vol. 114, pp. 512-518, October 1992.
4. Cook, W.J. and Felderman, E.J., "Reduction of Data from Thin Film Heat Transfer Gages: A Concise Numerical Technique," *AIAA Journal*, Vol. 4, No. 3, pp. 561-562, March 1966.

5. Kendall, D.N. and Dixon, W.P., "Semiconductor Surface Thermocouples for Determining Heat Transfer Rates," *IEEE Transactions on Aerospace and Electronic Systems*, Vol. AES-3, No. 4, pp596-603, July 1967.

6. Telephone Conversation with Mr. Tom Horvath, NASA Langley, August 1996.

7. Busch, B. (C2C) and Wickramisinghe, V. (C2C), "Startup Loads in Trisonic Wind Tunnel," AE 471 Project, U.S. Air Force Academy, May 1996.

8. Lang, D.E., "USAFA Trisonic Wind Tunnel Analysis for Heat Transfer Measurements," U.S. Air Force Academy, To Be Published September 1996.

9. Hollis, B.R. and Perkins, J.N., "Hypervelocity Heat-Transfer Measurements in an Expansion Tube," AIAA 96-2240, 19th AIAA Advanced Measurement and Ground Testing Technology Conference, New Orleans, LA, June 18-20, 1996.

10. Telephone Conversation with Mr. Kenneth Nutt, Arnold Engineering Development Center, August 1996.

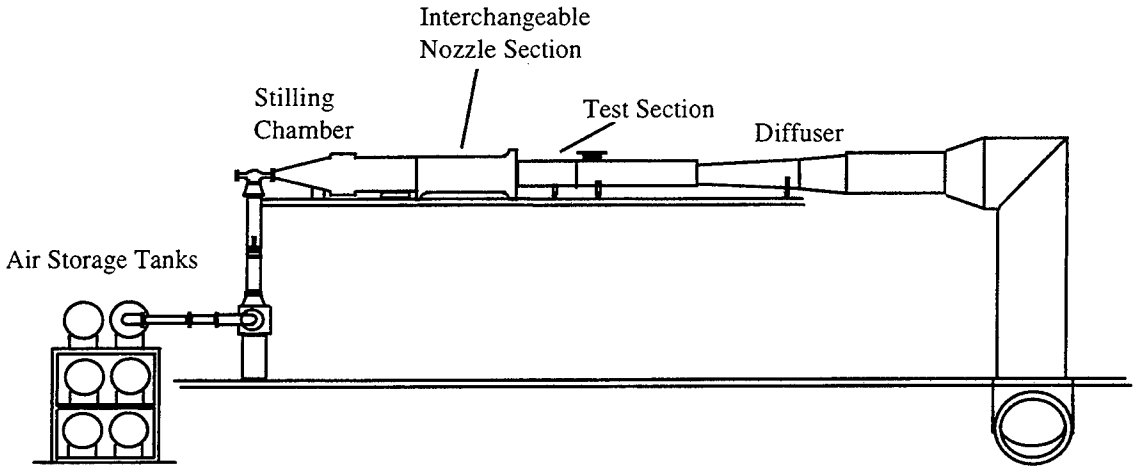

Figure 1: USAFA Trisonic Wind Tunnel

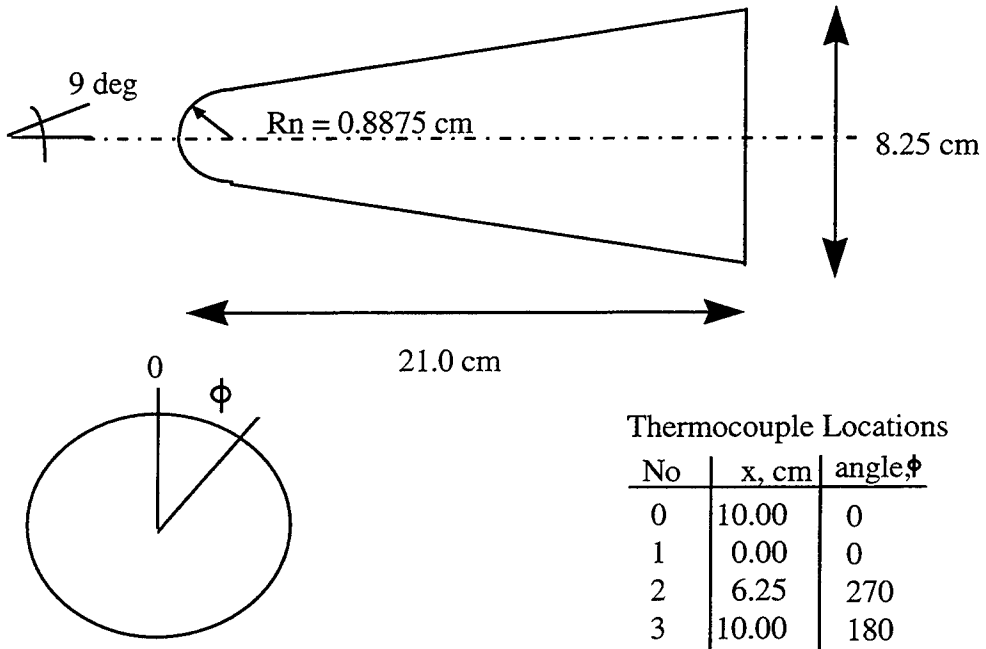

Thermocouple Locations

No	x, cm	angle,ϕ
0	10.00	0
1	0.00	0
2	6.25	270
3	10.00	180
4	8.75	45
5	3.75	90

Figure 2: Model Configuration

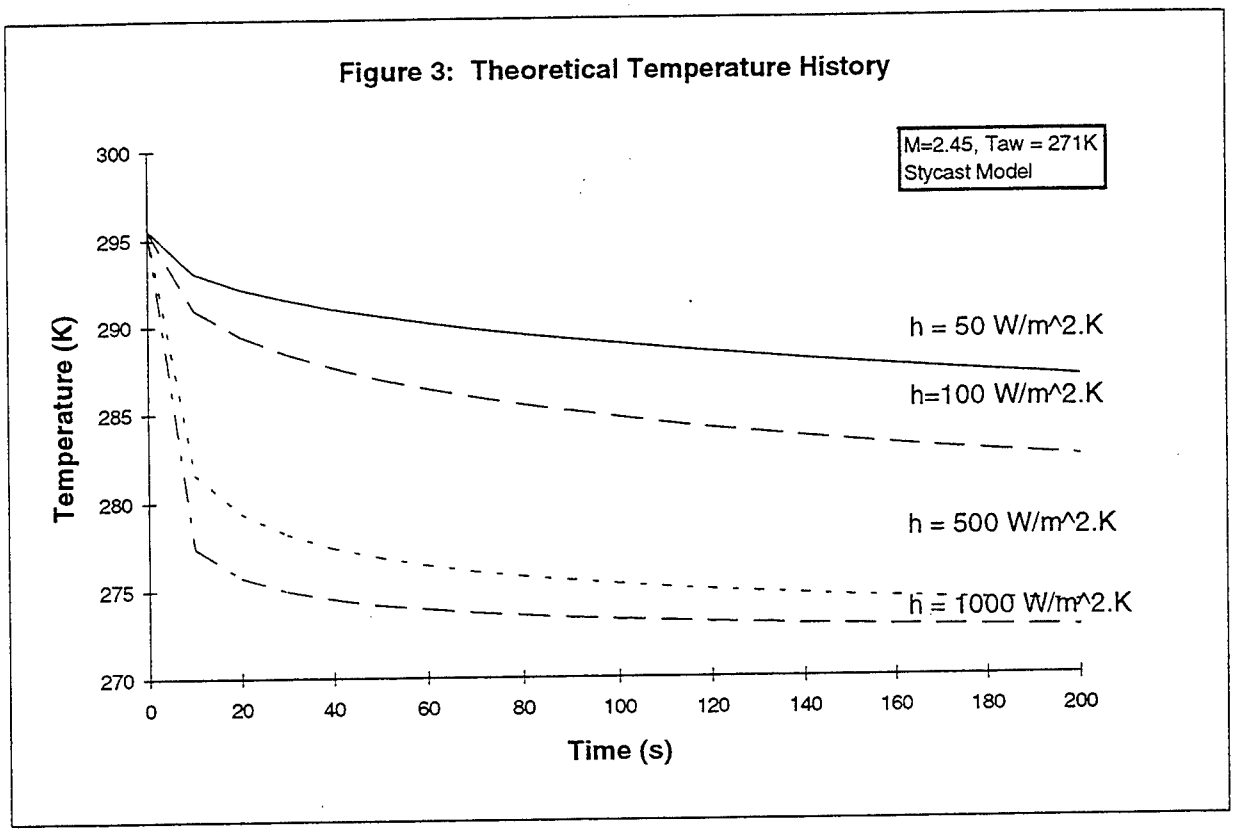

Figure 4: Schlieren of Cone at M=2.45

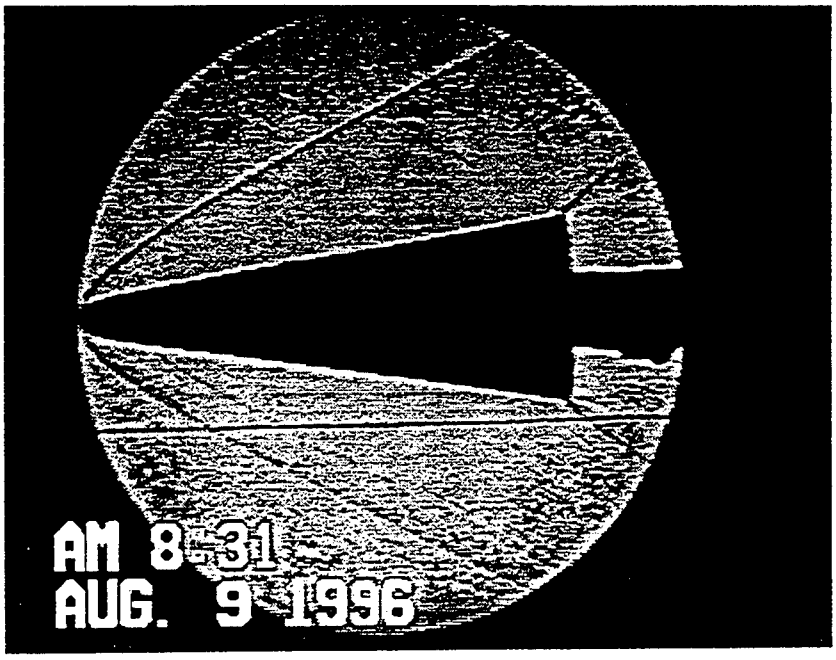

Figure 5(a): Experimental Temperature History - Run 1

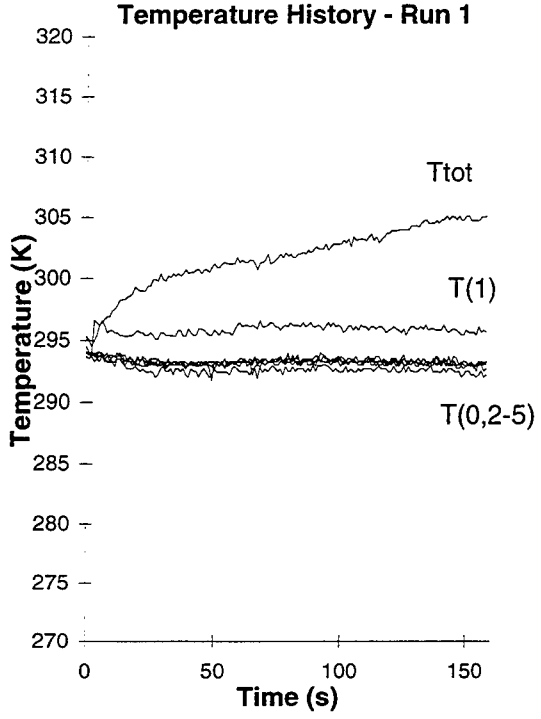

Figure 5(b): Experimental Temperature History - Run 2

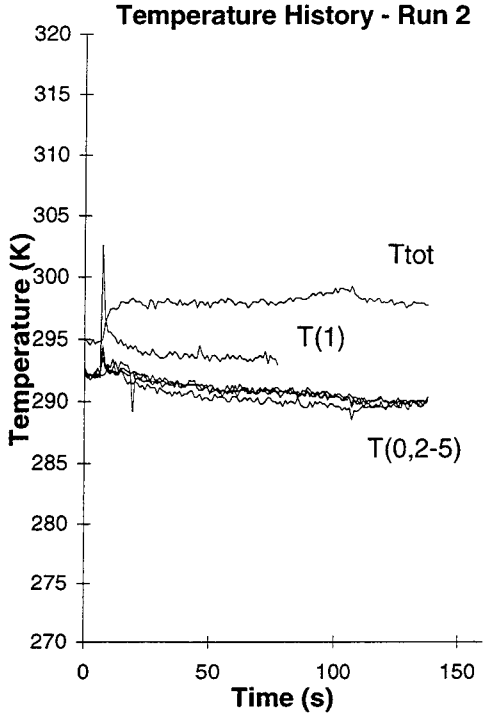

Figure 5(c): Experimental Temperature History - Run 3

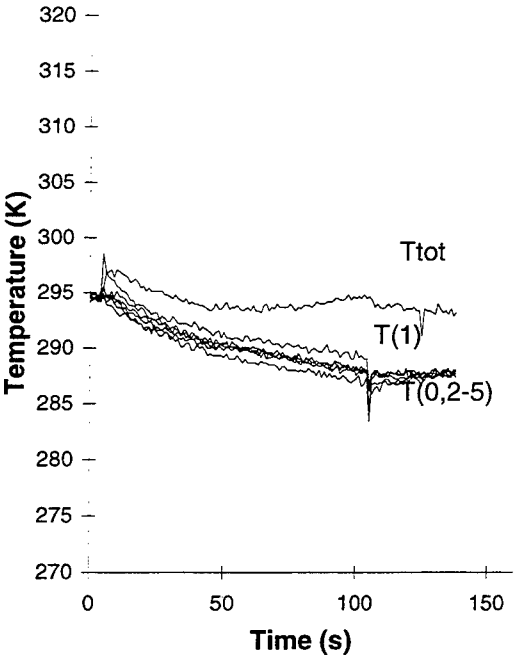

Figure 5(d): Experimental Temperature History - Run 4

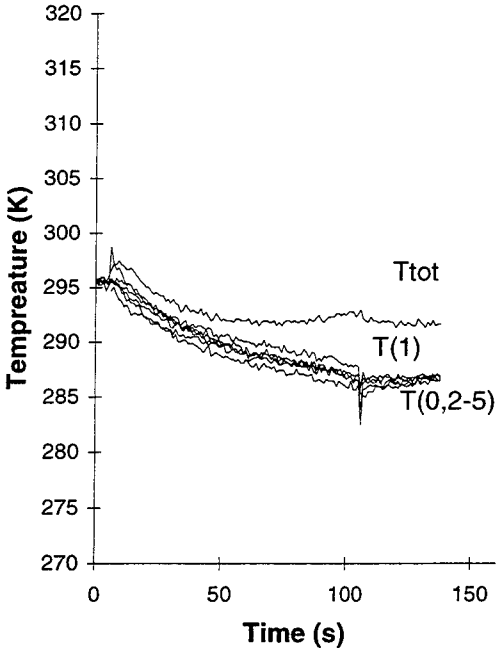

Figure 6: Experimental Heat Transfer Coefficient Distribution

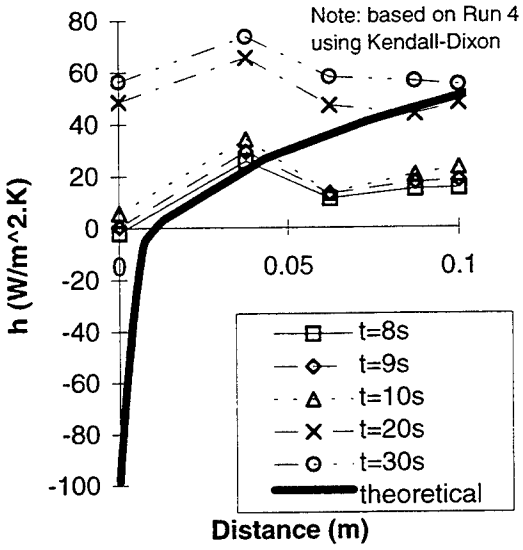

Figure 7(a): Cook-Felderman for Run 4

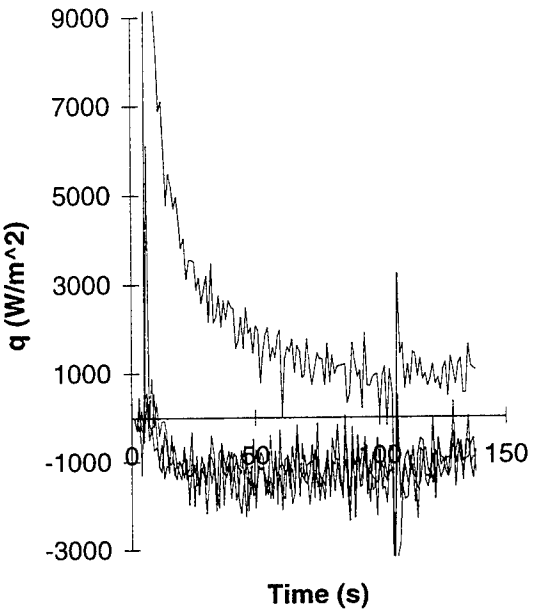

Figure 7(b): Kendall-Dixon for Run 4

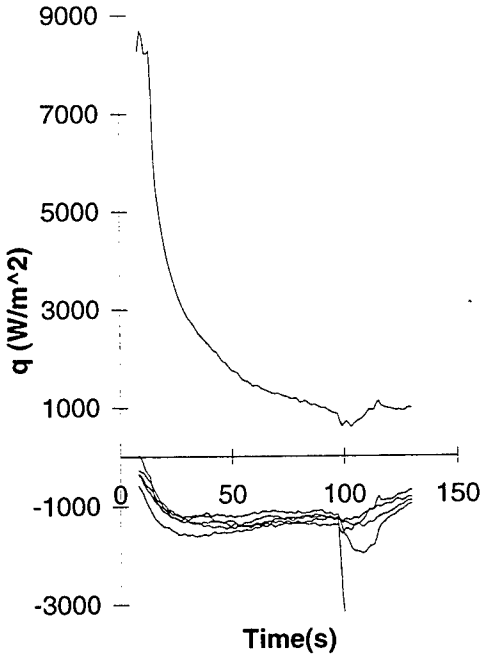

Figure 7(c): Semi-Infinite for Run 4

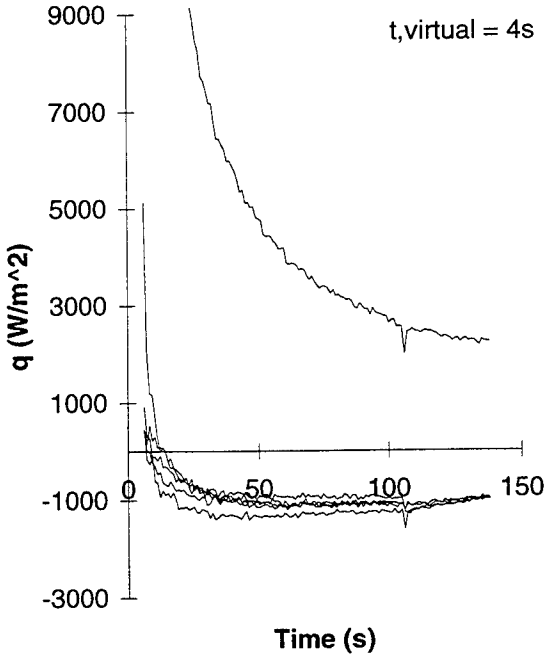

Figure 8: Comparison of Data Reduction for Specific Channel

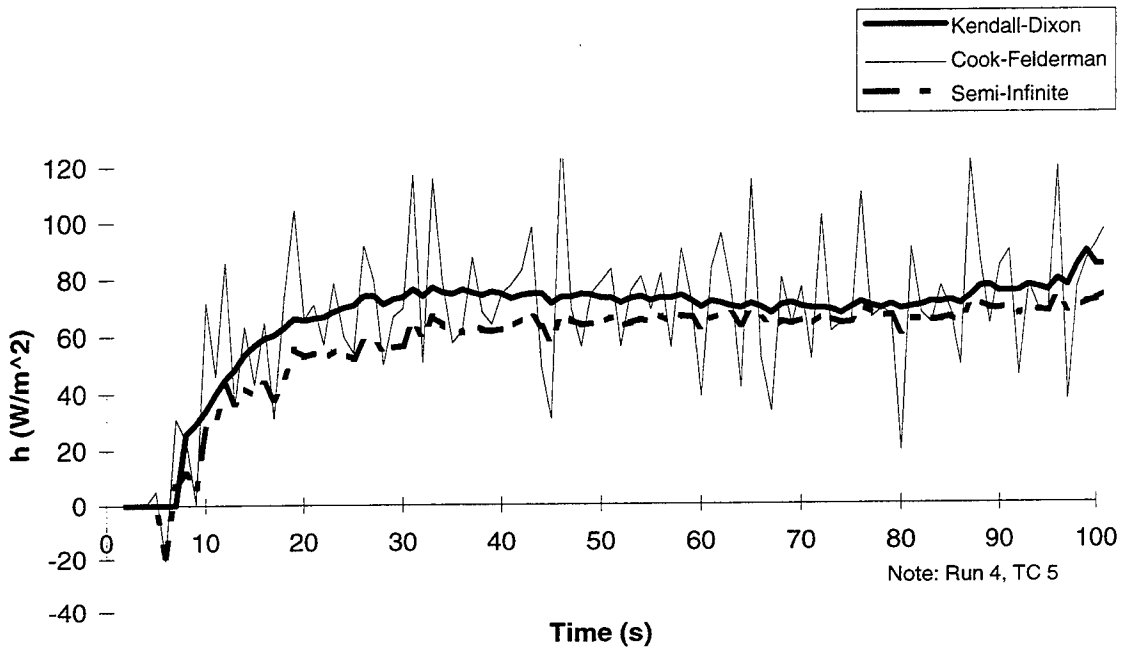

Figure 9: Temperature Histories for Various Material Properties

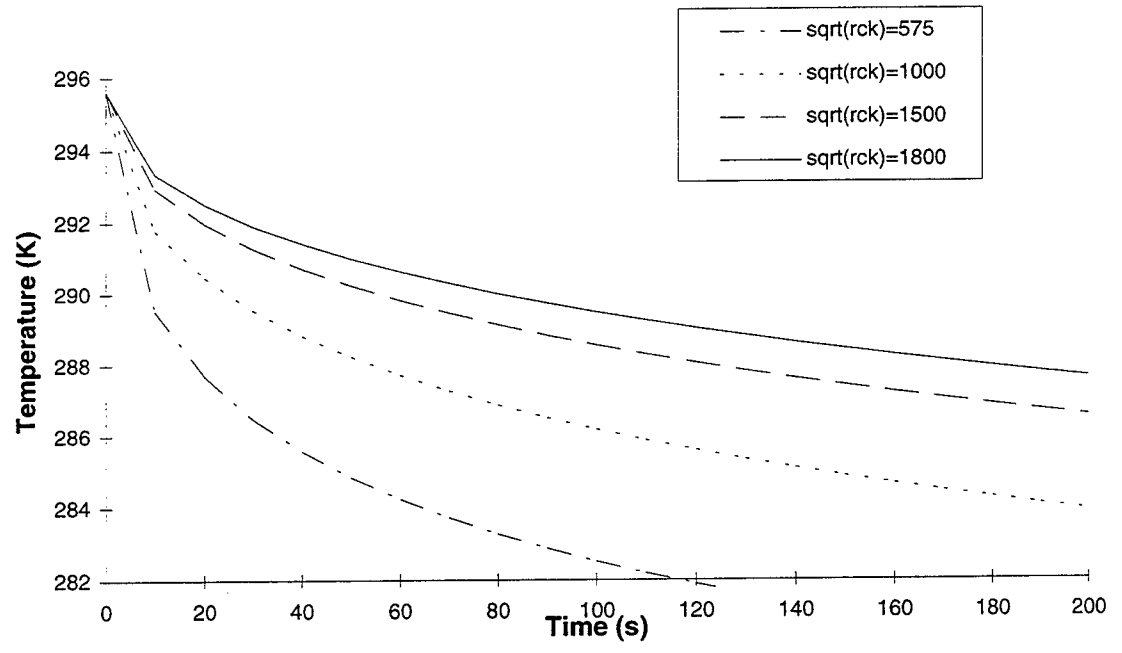

DETECTION OF AMPHETAMINE IN URINE FOLLOWING MULTI-DOSE ADMINISTRATION OF FENPROPOREX

Stedra L. Stillman
Graduate Student
Department of Justice Sciences

John T. Cody, Ph.D.
Deputy Director
Clinical Investigations

Sandra Valtier
Research Technologist
Clinical Investigations

University of Alabama at Birmingham
101 15th Street Office Building
901 South 15th Street
Birmingham, AL 35294-2060

Final Report for:
Graduate Student Research Program
Wilford Hall Medical Center

Sponsored by:
Air Force Office of Scientific Research
Bolling Air Force Base, DC

and

Wilford Hall Medical Center

October 1996

DETECTION OF AMPHETAMINE IN URINE FOLLOWING MULTI-DOSE ADMINISTRATION OF FENPROPOREX

Stedra L. Stillman
Graduate Student
Department of Justice Sciences

Abstract

The precursors of amphetamine and methamphetamine can be significant in interpreting results of positive amphetamine drug testing. There are a number of drugs that are known to produce amphetamine in the urine of users. Administration of one of these, fenproporex, was reported to be detected for hours, while amphetamine could be detected for days. Administration of fenproporex to five volunteers for a period of seven days resulted in the detection of amphetamine in the urine of all subjects. The concentration of amphetamine reached a steady state for all subjects, with peak concentrations ranging from 2851 to 4150 ng/ml of amphetamine. Peak concentrations were detected 54 to 86 hours after the first dose . Amphetamine was detected (> 5 ng/ml) for up to 177 hours after the last dose. The presence of both enantiomers of amphetamine was revealed in the analysis of the metabolically produced amphetamine. This can be important in establishing whether illicit amphetamine is involved. In addition, the parent fenproporex could be detected in samples where amphetamine was greater than or equal to 500ng/ml.

DETECTION OF AMPHETAMINE IN URINE FOLLOWING MULTI-DOSE ADMINISTRATION OF FENPROPOREX

Stedra L. Stillman

Introduction

The anorectic drug fenproporex, 3-[(1-methyl-2-phenylethyl)amino]-propanenitrile, is available in a number of countries (1). In Mexico, it is easily obtained with or without a prescription. Since ingestion of fenproporex results in urinary excretion of amphetamine, misinterpretation could occur in positive amphetamine drug tests. From previous studies, fenproporex was found to be detected for a few hours after administration, while amphetamine could be detected for days(2). A single dose study (3) resulted in peak concentrations of amphetamine being detected for up to 20 hours post-dose. The concentration of amphetamine reached a high of 2099 ng/ml.

The current study adopted a multi-dose approach. Like the single dose study(3), excretion characteristics included concentration level and detection period of amphetamine as well as amphetamine enantiomeric composition. This study also evaluated the accumulative effects of multi-dosing on the concentration of amphetamine.

Materials and Methodology

Amphetamine, amphetamine-d5, methamphetamine, methamphetamine-d5, and methamphetamine-d11 were obtained from Radian Corporation. The internal standards (amphetamine-d5 and methamphetamine-d5) used for the enantiomer analyses were racemic. Amphetamine-d6 was obtained from Alltech. Fenproporex, *d*-amphetamine, *l*-amphetamine, *d*-methamphetamine, *l*-methamphetamine and the derivatizing agent heptafluorobutyric anhydride (HFBA) were obtained from Sigma Chemical Company. The derivatizing reagent *N*-trifluoroacetyl-*l*-propyl chloride(*l*-TPC) was obtained from Regis Chemical Company. The

fenproporex (Fenisec) administered to the subjects was purchased in Mexico.

One Fenisec tablet, each containing 10 mg of fenproporex, was given to four healthy subjects for seven consecutive days. A fifth subject discontinued taking the drug after the fourth dose. A pre-dose urine specimen was analyzed to eliminate the possibility of previous use of amphetamine, methamphetamine, or fenproporex. Urine specimens were collected for seven days during administration of the drug and an additional seven days after the last dose. Samples were provided ad lib and refrigerated until analysis. As previously described (3,4), pH, specific gravity, creatinine, quantitative and enantiomeric analyses of samples were determined.

Results and Discussion

As previously reported (2,3,5,6,7,8,9), urinary excretion of amphetamine resulted after the administration of fenproporex. All samples were negative for methamphetamine (LOD for methamphetamine: 5 ng/ml), even though pseudoephedrine interference was apparent in the samples from one subject. No subject reported any feeling of stimulation during drug use. Tognoni et al (5) explained how ingesting fenproporex results in the production of amphetamine by cleaving the nitrogen-cyanoethylbond. See Figure 1. Figure 2 depicts a typical chromatographic result from the quantitative analysis of urine samples. The quantitative results of the samples are shown in Table 1. Linearity for fenproporex ranged from 5-2500 ng/ml. The limit of detection for this drug was determined to be 2 ng/ml.

In the single dose study (3), amphetamine was detected for up to 119:20 hours post-dose with a peak concentration level reaching up to 2099 ng/ml in one subject. This multi-dose study was able to detect amphetamine for up to 177:30 hours after the last dose. Peak concentrations of amphetamine were reached 54:15 to 86:00 hours following the first dose, and ranged from 2851 to 4150 ng/ml. As anticipated, the concentration of amphetamine increased

as dosage continued until it achieved a steady state. During drug administration, the valleys remained between 84.64 and 429.54 ng/ml. Results from the single dose study (3) established that fenproporex could be detected for a considerably longer period of time than previously reported.

In comparison to the single dose study, three inferences can be drawn: (1) As long as the drug was being administered, the concentration of amphetamine reached a peak level and remained relatively steady, instead of continuously increasing with each dose. (2) Throughout drug administration, the concentration of amphetamine was detectable, even though levels fell due to excretion. (3) Once the drug was no longer used, amphetamine concentration gradually decreased and urinary excretion simulated the rate of a single dose.

Conclusion

Multi-dosing of fenproporex can result in amphetamine being detected in the urine for up to 177 hours after the last dose. Peak concentrations reached as high as 4150 ng/ml for amphetamine. Instead of amphetamine concentration rising with each dose, it reaches a level and remains relatively steady. Interpreting analytical results can help to ascertain what involvement a drug may have with the subject. Since amphetamine metabolized from fenproporex is racemic, the presence of only the *d*-enantiomer would be incongruous with the use of fenproporex. Unfortunately, some illicit amphetamine is also racemic. Still the presence of the parent drug and its relative concentration is suggestive of its use.

All samples with a concentration of amphetamine at or above 500 ng/ml also showed detectable levels of fenproporex. Testing drugs not specified in HHS guidelines are prohibited, unless it's a 'for cause' testing of drugs under schedule I and II.

Since testing of the parent drug, fenproporex, is not always possible, enantiomeric analyses can be useful in the interpretation of positive amphetamine results. After

administration of racemic amphetamine, both enantiomers of amphetamine are equally distributed followed by an increase of *l*-amphetamine. However, following administration of fenproporex, the enantiomers were distributed in equal concentrations for a short period of time, followed by an increase in *d*-amphetamine.

Acknowdgements

The authors are grateful to Ms. Hensley for assistance with samples, TSgt Lorenzen for assistance with pH and specific gravity measurements, and to the staff of the Wilford Hall Medical Center clinical laboratory for assistance in creatinine analysis.

References

1. Schlesser JL Ed. Drugs available abroad-A guide to therapeutic drugs available and approved outside the US. MEDEX Books. Detroit 1991.

2. Beckett AH, Shenoy EVB, Salmon JA. The influence of replacement of the N-ethyl group by the cyanoethyl group on the absorption, distribution and metabolism of (+-)-ethylamphetamine in man. J Pharm Pharmacol. 24:194-202 (1972).

3. Cody JT, Valtier S. Detection of amphetamine following administration of fenproporex. J Anal Toxicol. 20(6):425-31 (1996).

4. Valtier S, Cody JT. Evaluation of internal standards for the analysis of amphetamine and methamphetamine. J Anal Toxicol. 19(6):375-80 (1995).

5. Tognoni G, Morselli PL, Garattini S. Amphetamine concentrations in rat brain and human urine after fenproporex administration. European J Pharmacol. 20:125-26 (1972).

6. Sznelwar RB. Chromatographic identification of amphetamine in urine of patients treated with fenproporex. European J Toxicol and Environmental Hygiene. 8:5-13. (1975).

7. Cody JT. Metabolic precursors to amphetamine and methamphetamine. Forensic Sci Rev. 5:109-27 (1993).

8. Cody JT. Issues pertaining to the monitoring the abuse of amphetamines in workplace drug testing. Forensic Sci Rev. 6:81-96 (1994).

9. Cody JT. Important issues in testing for amphetamine. In Handbook of workplace drug testing, RH Liu and BA Goldberger Ed. AACC Press. Washington, DC, 1995, pp. 239-88.

LIST OF FIGURES

I

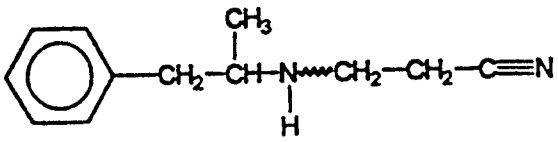

Fenproporex

II

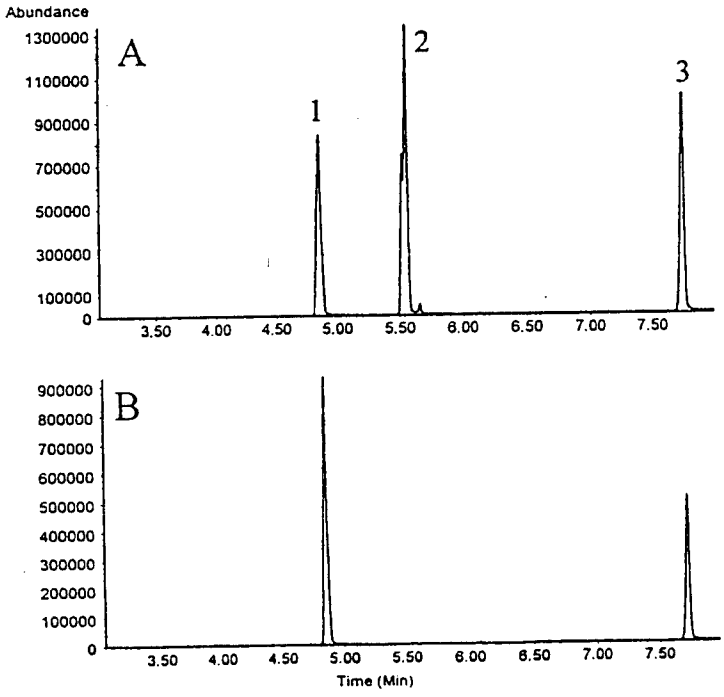

LIST OF TABLES

LEGEND: Limits of detection (LOD) and quantitation (LOQ) for analytes: Amphetamine - LOD = 5 ng/ml, LOQ = 5 ng/ml. Fenproporex - LOD = 2 ng/ml, LOQ = 5 ng/ml. Samples which indicated levels of > 2 ng/ml and < 5 ng/ml are annotated as "Detected" in the table.

Subject 1

Hours	pH	Specific Gravity	Creatinine	Concentration (ng/ml) Amphetamine	Fenproporex
00:00	7.0	1.004	41.5	0.00	0.00
07:45	8.0	1.009	80.5	230.67	219.50
10:45	7.9	1.008	64.9	458.09	78.80
12:45	7.6	1.004	32.1	319.28	15.17
14:45	8.1	1.004	20.1	97.25	5.71
21:45	7.2	1.010	90.5	600.59	10.92
25:45	6.1	1.010	105.5	669.23	11.88
31:15	5.7	1.011	124.0	2,206.93	1,152.44
33:45	7.3	1.005	36.8	598.68	48.05
38:15	7.1	1.011	105.5	1,123.73	34.02
41:15	5.4	1.007	57.0	1,440.40	75.02
46:15	5.2	1.006	42.5	904.73	51.64
51:15	5.3	1.014	118.0	1,443.72	50.46
54:15	5.8	1.010	122.0	2,850.58	2,159.07
59:15	5.2	1.009	77.6	2,210.94	270.44
60:45	6.9	1.004	29.6	331.47	13.21
65:15	5.8	1.009	59.8	930.15	40.70
69:45	5.6	1.016	97.0	1,829.81	58.85
75:45	5.4	1.016	105.5	1,606.25	392.87
80:15	5.4	1.009	70.0	1,877.59	475.41
86:15	5.3	1.013	115.0	2,670.29	191.57
93:45	5.4	1.013	119.0	1,980.04	74.64
97:45	5.3	1.019	181.0	1,670.27	27.99
103:15	5.4	1.014	119.0	2,398.26	473.56
106:45	5.4	1.014	154.0	2,453.95	369.01
110:15	6.9	1.006	48.6	612.13	36.48
117:45	5.8	1.016	132.0	1,588.64	29.64
125:45	5.8	1.022	228.0	2,178.34	1,162.67
128:15	6.2	1.004	31.6	887.70	121.73
134:45	5.4	1.015	136.0	2,520.77	122.61
141:45	5.8	1.010	86.5	1,313.23	29.24
147:45	5.2	1.012	111.1	1,354.59	253.74
151:45	5.9	1.012	100.8	1,602.40	174.29
156:15	7.4	1.012	86.9	841.96	15.84
161:45	6.8	1.011	64.4	734.40	8.62
165:45	6.3	1.014	113.8	1,291.63	9.47
171:45	5.9	1.010	69.7	801.29	6.62
175:45	5.4	1.008	73.3	751.92	6.55
179:15	5.1	1.013	145.0	1,122.42	12.36
183:15	5.3	1.011	114.0	730.29	6.12
189:45	5.8	1.007	89.5	437.61	Detected
194:15	6.2	1.011	129.0	327.68	0.00
197:15	6.9	1.004	38.7	123.59	0.00
201:45	7.3	1.008	65.1	114.26	0.00
207:15	8.0	1.013	100.5	27.78	0.00
213:45	6.3	1.009	91.5	133.08	0.00

219:15	5.6	1.017	163.0	315.71	0.00
221:15	5.5	1.004	24.1	60.64	0.00
222:15	5.6	1.006	34.2	56.75	0.00
227:15	5.1	1.013	107.0	127.82	0.00
230:15	7.3	1.007	56.4	28.21	0.00
237:45	6.1	1.015	145.0	61.21	0.00
243:15	5.3	1.012	89.0	46.42	0.00
246:15	6.1	1.008	46.3	21.18	0.00
249:15	5.8	1.008	60.9	20.05	0.00
253:45	5.7	1.007	60.7	18.19	0.00
257:15	8.2	1.006	35.4	0.00	0.00
261:45	7.7	1.007	52.7	0.00	0.00
266:15	7.8	1.008	71.0	0.00	0.00
268:45	7.7	1.007	47.7	0.00	0.00
270:15	7.4	1.004	23.1	0.00	0.00
271:45	8.1	1.005	30.4	0.00	0.00
277:45	7.4	1.009	100.0	0.00	0.00
285:45	7.9	1.011	102.0	0.00	0.00
291:45	8.2	1.010	92.0	0.00	0.00
296:45	8.1	1.010	94.0	0.00	0.00
301:15	7.6	1.009	73.4	0.00	0.00
302:45	7.1	1.005	36.9	0.00	0.00
309:45	5.7	1.008	89.0	9.34	0.00
314:45	6.4	1.008	56.8	0.00	0.00
317:45	5.9	1.012	89.1	0.00	0.00
322:15	7.2	1.009	71.1	0.00	0.00
327:45	7.4	1.006	46.3	0.00	0.00
333:45	6.5	1.012	125.0	0.00	0.00
338:15	6.5	1.008	56.8	0.00	0.00
342:15	6.3	1.017	166.0	0.00	0.00
344:15	6.5	1.005	34.4	0.00	0.00

Subject 2

Hours	pH	Specific Gravity	Creatinine	Concentration (ng/ml) Amphetamine	Fenproporex
00:00	5.4	1.005	28.0	0.00	0.00
03:30	5.1	1.009	44.6	427.81	516.31
09:00	5.1	1.014	134.0	2,002.56	572.59
15:30	5.2	1.023	214.0	2,178.79	107.17
22:00	5.5	1.019	157.0	890.40	42.10
24:30	5.4	1.022	179.0	666.20	14.05
31:00	5.3	1.014	92.0	1,580.99	505.84
34:30	5.7	1.018	116.0	1,452.37	113.35
39:30	5.5	1.021	127.0	1,713.76	115.10
46:30	6.1	1.018	93.0	726.86	13.88
51:30	5.3	1.020	109.0	1,706.99	348.04
58:00	5.3	1.018	127.0	3,074.31	463.11
63:30	5.5	1.013	81.0	1,224.81	35.36

67:30	6.2	1.010	54.8	420.94	9.12
70:00	6.0	1.014	76.2	574.86	11.44
76:30	5.7	1.013	75.0	577.62	81.56
79:30	6.7	1.009	57.2	797.79	120.34
86:30	5.5	1.018	223.8	2,605.95	67.03
94:00	5.8	1.021	202.7	1,831.92	24.65
102:00	5.7	1.022	186.0	2,060.41	738.33
108:30	5.9	1.028	238.0	2,282.52	75.26
115:30	6.4	1.012	83.5	992.72	20.42
119:00	6.1	1.010	64.2	736.00	14.17
122:00	5.6	1.010	58.3	549.89	6.78
124:00	7.0	1.006	28.8	176.39	33.48
129:30	5.8	1.011	66.9	681.91	143.43
138:00	5.5	1.017	129.0	1,741.98	69.69
144:30	6.3	1.008	50.6	626.56	17.38
147:00	6.6	1.015	88.0	359.13	Detected
150:00	5.9	1.012	76.3	811.86	213.57
159:30	5.5	1.022	198.0	2,476.32	176.08
166:00	5.8	1.011	80.4	856.22	55.85
173:30	5.3	1.019	143.0	1,151.67	47.75
183:30	6.1	1.026	178.0	468.30	6.33
190:00	5.7	1.011	76.4	309.07	10.75
194:00	5.5	1.012	79.7	197.37	Detected
198:00	5.4	1.017	133.0	241.08	0.00
205:00	6.0	1.011	85.0	86.06	0.00
214:00	6.1	1.014	107.0	76.12	0.00
221:30	5.5	1.018	136.0	90.19	0.00
227:30	5.9	1.005	39.0	16.32	0.00
225:30	5.9	1.011	79.0	35.52	0.00
237:30	5.9	1.007	54.9	17.96	0.00
243:00	6.7	1.010	67.9	10.50	0.00
245:30	7.3	1.011	68.0	0.00	0.00
256:30	5.8	1.014	157.0	33.08	0.00
264:00	6.4	1.024	182.0	11.43	0.00
269:00	5.9	1.006	41.4	0.00	0.00
272:30	5.9	1.008	55.9	6.20	0.00
274:30	6.7	1.009	64.7	0.00	0.00
282:00	5.6	1.018	140.0	10.65	0.00
287:30	5.7	1.012	98.0	7.40	0.00
290:00	5.7	1.005	36.5	0.00	0.00
291:30	6.8	1.005	27.1	0.00	0.00
294:30	6.2	1.007	54.6	0.00	0.00
300:00	6.9	1.020	120.0	8.73	0.00
301:30	6.8	1.020	149.0	0.00	0.00
305:30	5.5	1.015	143.0	6.31	0.00
313:00	6.5	1.011	89.0	0.00	0.00
316:00	6.3	1.005	42,6	0.00	0.00
323:30	5.3	1.020	164.0	0.00	0.00
327:00	7.1	1.008	46.5	0.00	0.00
329:30	6.4	1.005	29.6	0.00	0.00
334:00	5.9	1.009	65.4	0.00	0.00

Subject 3

Hours	pH	Specific Gravity	Creatinine	Concentration (ng/ml) Amphetamine	Fenproporex
00:00	7.3	1.006	33.2	0.00	0.00
02:30	7.5	1.004	19.3	160.92	81.46
05:00	6.4	1.006	37.0	725.79	58.54
07:00	8.0	1.004	15.2	92.85	Detected
10:00	7.6	1.007	47.1	122.89	5.40
15:00	6.8	1.014	141.0	683.22	Detected
22:30	5.7	1.008	84.0	860.03	9.54
26:30	7.7	1.010	88.0	369.41	110.37
29:30	7.0	1.010	59.7	735.99	99.22
38:00	5.5	1.023	315.0	3,581.64	45.15
45:30	6.6	1.010	80.2	689.98	Detected
52:00	7.7	1.013	122.8	736.03	149.29
54:00	7.4	1.005	36.2	717.13	17.38
56:00	7.3	1.005	32.7	651.82	8.06
61:00	6.4	1.019	174.0	1,877.53	17.48
63:30	7.2	1.008	52.0	525.52	Detected
68:30	5.9	1.007	50.6	939.97	8.02
75:30	5.8	1.013	139.2	1,911.56	178.49
77:30	7.6	1.006	29.0	288.35	12.81
80:00	6.5	1.008	44.9	1,032.46	25.28
86:00	5.1	1.017	168.9	3,600.01	75.16
92:30	5.4	1.018	153.2	2,084.25	88.47
97:30	6.2	1.012	80.2	765.72	88.47
103:30	5.9	1.008	76.8	1,445.11	104.97
105:30	5.9	1.005	45.8	867.81	13.58
110:00	5.8	1.022	238.2	2,063.82	25.02
117:30	6.4	1.008	63.2	641.15	Detected
122:00	6.5	1.006	55.7	562.79	113.73
127:00	5.3	1.015	184.0	2,981.95	135.53
130:30	5.9	1.016	156.0	2,181.35	45.27
134:00	5.9	1.008	70.4	688.87	8.84
135:30	5.8	1.009	57.9	624.47	11.88
141:00	6.8	1.008	53.6	326.98	6.22
146:00	6.9	1.010	70.7	506.19	169.78
151:00	6.0	1.013	119.0	1,796.00	262.60
154:00	6.5	1.011	84.0	1,037.34	28.72
160:00	5.4	1.021	140.0	1,944.20	18.40
165:30	5.6	1.007	50.4	608.91	15.33
168:30	5.5	1.020	177.0	997.22	5.52
171:00	6.8	1.005	28.1	110.04	0.00
175:00	6.7	1.008	78.4	199.40	0.00
180:00	7.0	1.005	35.8	69.95	0.00
189:00	6.6	1.014	87.0	129.64	0.00
194:00	6.4	1.011	65.8	74.28	0.00
196:30	6.9	1.005	27.8	25.12	0.00
200:00	6.8	1.005	29.8	15.13	0.00

204:00	6.4	1.009	85.0	31.88	0.00
221:00	6.7	1.025	238.0	23.56	0.00
224:00	6.6	1.007	40.7	8.82	0.00
225:00	6.0	1.005	24.4	6.75	0.00
230:30	5.9	1.012	95.0	15.61	0.00
237:00	5.2	1.019	65.0	19.16	0.00
243:00	5.4	1.023	208.1	11.44	0.00
246:00	7.1	1.007	38.8	0.00	0.00
261:00	5.5	1.012	44.0	5.65	0.00
269:00	5.9	1.017	129.0	0.00	0.00
274:00	6.7	1.008	64.9	0.00	0.00
278:00	5.2	1.024	230.0	9.19	0.00
279:00	5.7	1.031	306.0	8.17	0.00
286:00	6.2	1.007	44.4	0.00	0.00
299:00	6.4	1.020	208.0	0.00	0.00
311:30	5.5	1.023	191.0	5.00	0.00
314:00	5.8	1.005	34.5	0.00	0.00
316:30	6.1	1.008	56.7	0.00	0.00
317:30	6.3	1.004	17.9	0.00	0.00
319:30	6.7	1.006	29.4	0.00	0.00
327:30	6.4	1.017	134.0	0.00	0.00
333:00	6.1	1.012	68.4	0.00	0.00
337:30	7.0	1.008	48.6	0.00	0.00

Subject 4

Hours	pH	Specific Gravity	Creatinine	Concentration (ng/ml) Amphetamine	Fenproporex
00:00	6.3	1.021	124.0	0.00	0.00
02:02	8.0	1.007	35.3	84.64	163.43
03:02	8.2	1.008	42.9	151.35	154.70
04:02	7.8	1.008	43.4	141.15	72.76
05:32	7.7	1.008	49.0	148.71	39.16
06:02	7.6	1.004	15.4	98.92	18.53
07:02	6.7	1.004	28.0	195.04	29.75
11:02	7.1	1.008	144.0	460.69	40.50
21:02	5.5	1.008	294.0	1,468.06	35.65
25:32	6.7	1.015	117.0	256.40	27.52
27:02	7.3	1.006	38.7	278.30	214.63
29:02	7.8	1.013	88.0	250.84	104.10
32:02	7.2	1.021	220.0	545.29	97.25
37:02	6.2	1.028	282.0	1,250.29	55.67
45:02	5.9	1.025	212.0	1,488.93	21.37
49:02	6.7	1.022	213.4	492.74	Detected
49:32	7.3	1.009	50.7	131.73	81.29

50:02	7.3	1.005	27.5	209.85	216.76
51:32	7.4	1.007	46.0	248.22	155.14
53:02	7.1	1.012	86.4	496.68	103.39
56:02	7.6	1.020	182.5	416.19	73.43
59:02	7.5	1.023	198.5	277.29	28.54
61:32	7.0	1.023	164.2	630.22	16.51
69:02	6.6	1.023	152.5	753.74	7.46
72:02	6.7	1.016	91.5	463.81	400.59
73:02	7.1	1.006	29.7	155.12	9.48
74:02	7.0	1.008	39.6	264.02	137.82
75:02	7.0	1.005	22.8	299.76	141.20
76:02	6.8	1.009	48.3	443.20	111.86
78:32	5.4	1.016	181.2	2,291.45	444.41
84:02	5.3	1.026	330.0	3,643.90	126.43
87:02	5.6	1.031	336.0	2,502.91	916.49
94:02	5.7	1.029	240.0	1,703.25	79.84
96:32	6.2	1.028	214.0	857.06	5.93
101:02	5.7	1.025	208.0	2,105.82	294.19
104:02	6.1	1.030	256.0	2,341.72	124.13
106:32	6.0	1.029	222.0	1,857.76	49.64
110:02	5.4	1.027	198.0	2,659.01	167.22
116:02	—	1.029	256.0	2,208.05	171.72
120:02	5.9	1.024	136.0	821.52	6.37
122:32	6.7	1.020	90.0	564.19	131.24
123:32	6.7	1.013	66.2	893.72	293.26
126:02	6.8	1.020	138.0	951.76	106.40
131:02	6.5	1.025	206.0	1,294.75	224.97
135:02	5.8	1.023	168.0	1,474.87	36.68
141:32	5.6	1.024	205.0	1,625.16	28.33
144:32	6.4	1.018	120.0	405.65	8.58
145:32	7.5	1.016	32.3	86.80	24.64
146:02	6.9	1.008	22.6	151.11	455.85
146:32	7.1	1.008	29.1	191.96	716.08
147:02	7.3	1.006	20.3	145.17	367.68
147:32	7.2	1.004	15.1	118.23	113.10
148:02	7.3	1.007	34.6	211.10	70.76
149:02	7.2	1.009	49.8	292.21	50.48
151:02	6.3	1.014	105.0	771.17	226.89
154:32	6.5	1.021	103.0	925.37	48.32
157:02	5.6	1.026	378.0	2,520.27	47.66
165:02	5.8	1.032	432.0	2,239.86	31.61
167:02	6.1	1.023	170.0	722.48	5.81
168:32	7.1	1.013	77.0	202.49	0.00
169:32	7.2	1.008	46.5	115.63	0.00
170:32	7.4	1.006	25.0	69.96	0.00
171:02	7.1	1.004	28.2	99.46	0.00
172:02	6.5	1.013	89.5	220.83	0.00
173:32	6.5	1.014	98.5	217.33	0.00
181:02	5.5	1.027	278.0	776.41	Detected
195:02	5.6	1.022	364.0	207.97	0.00

199:32	7.4	1.024	380.0	56.77	0.00
203:32	7.3	1.023	130.0	54.76	0.00
212:32	5.9	1.028	196.0	169.47	0.00
214:32	6.1	1.022	127.0	76.64	0.00
216:32	6.6	1.018	110.0	36.12	0.00
217:32	7.0	1.007	31.8	9.63	0.00
219:02	7.2	1.007	36.1	11.30	0.00
221:32	6.5	1.014	109.6	21.48	0.00
222:32	5.7	1.007	44.5	22.72	0.00
225:32	5.9	1.019	201.5	44.02	0.00
229:02	5.8	1.028	268.0	69.83	0.00
237:02	5.5	1.028	212.0	53.52	0.00
240:32	5.8	1.023	189.0	21.67	0.00
242:32	6.1	1.012	78.0	7.65	0.00
243:32	6.8	1.004	20.2	0.00	0.00
245:02	6.0	1.006	50.0	0.00	0.00
250:32	5.5	1.026	273.0	18.91	0.00
252:32	6.0	1.023	210.0	12.33	0.00
255:02	5.6	1.026	348.0	26.91	0.00
262:32	5.7	1.027	228.0	15.67	0.00
266:02	6.4	1.027	183.0	9.91	0.00
269:32	6.1	1.027	162.0	8.26	0.00
271:32	5.9	1.031	246.0	11.07	0.00
274:02	6.9	1.027	190.0	0.00	0.00
277:02	6.4	1.025	156.0	0.00	0.00
286:02	6.0	1.027	207.0	7.55	0.00
288:02	6.3	1.025	136.0	5.09	0.00
291:32	6.0	1.025	156.0	5.38	0.00
297:02	6.5	1.027	177.0	0.00	0.00
298:32	6.5	1.028	64.0	0.00	0.00
301:32	6.1	1.032	237.0	6.74	0.00
309:02	5.7	1.029	156.0	6.12	0.00
312:02	5.7	1.026	151.0	0.00	0.00
313:32	6.5	1.009	46.0	0.00	0.00
315:02	6.9	1.005	18.5	0.00	0.00
315:32	6.9	1.008	36.3	0.00	0.00
316:32	6.9	1.008	39.4	0.00	0.00
317:32	6.6	1.011	64.8	0.00	0.00
319:02	6.2	1.011	68.2	0.00	0.00
322:02	6.7	1.016	117.0	0.00	0.00
323:32	7.0	1.012	67.0	0.00	0.00
325:32	6.5	1.021	168.0	0.00	0.00
333:02	5.7	1.023	171.0	0.00	0.00
336:32	6.0	1.020	147.0	0.00	0.00
338:02	6.5	1.015	73.0	0.00	0.00

Subject 5

Hours	pH	Specific Gravity	Creatinine	Concentration (ng/ml) Amphetamine	Fenproporex
00:00	5.2	1.030	284.0	0.00	
02:30	5.1	1.011	86.0	1,023.09	0.00
03:50	5.0	1.005	160.0	1,677.89	2,395.54
04:40	5.2	1.020	222.0	2,629.51	2,751.00
10:00	5.4	1.027	384.0	1,491.48	2,456.63
15:00	5.6	1.030	345.0	1,321.84	265.35
18:30	6.0	1.028	316.0	948.50	490.60
25:00	5.4	1.033	396.0	1,129.68	214.00
28:00	5.5	1.031	363.0	3,797.92	1,201.37
32:00	5.4	1.030	369.0	3,410.59	3,032.00
36:30	5.4	1.032	408.0	3,625.03	1,235.83
40:30	5.9	1.032	384.0	1,818.34	933.63
44:30	5.8	1.017	129.0	1,116.87	413.06
45:00	5.7	1.024	188.0	430.99	56.89
48:00	5.7	1.015	79.0	429.54	16.10
53:30	5.6	1.024	226.0	2,169.30	16.63
55:00	5.9	1.017	124.0	1,415.31	586.68
56:00	6.2	1.014	96.0	902.84	271.00
57:00	6.0	1.011	81.0	787.44	120.38
60:30	5.6	1.027	368.0	3,705.53	108.90
61:00	6.1	1.022	230.1	1,306.58	315.80
64:30	6.4	1.024	246.5	839.12	81.35
68:00	5.8	1.025	282.2	1,877.70	51.13
69:30	5.7	1.007	71.1	530.99	48.33
73:30	5.6	1.027	345.9	2,257.65	26.43
77:00	5.8	1.024	331.4	3,765.40	1,639.93
78:00	5.6	1.020	262.0	2,659.20	1,220.28
82:00	5.6	1.027	395.4	3,837	533.34
85:00	5.5	1.029	463.3	4,149.77	553.79
95:00	5.5	1.015	168.9	1,155.79	518.67
97:00	6.8	1.021	201.7	363.95	69.92
101:00	6.3	1.024	253.4	560.35	17.28
107:00	5.3	1.025	332.0	793.79	25.55
121:00	5.3	1.031	322.0	409.26	12.42
125:30	5.2	1.033	356.0	456.85	0.00
130:00	5.0	1.035	495.0	409.09	0.00
134:00	5.0	1.036	611.0	307.94	0.00
142:00	5.5	1.029	328.0	89.21	0.00
145:00	6.9	1.022	172.0	20.07	0.00
148:00	6.9	1.033	196.0	34.16	0.00
152:00	6.8	1.029	236.0	21.99	0.00
158:00	5.5	1.032	489.0	37.74	0.00
160:30	6.3	1.026	208.0	10.61	0.00
164:30	5.8	1.028	221.0	16.73	0.00
166:00	5.5	1.027	188.0	16.49	0.00

168:00	5.9	1.020	127.0	7.14	0.00
170:00	5.4	1.017	128.0	8.57	0.00
171:30	5.3	1.024	236.0	17.07	0.00
174:30	5.3	1.025	228.0	22.42	0.00
175:30	5.2	1.018	157.0	21.86	0.00
176:00	6.3	1.013	96.5	5.17	0.00
177:30	5.6	1.023	215.0	24.52	0.00
181:30	5.2	1.029	310.0	35.10	0.00
187:00	5.4	1.029	252.0	36.52	0.00
190:30	5.5	1.028	204.0	24.70	0.00
192:00	5.5	1.007	40.5	0.00	0.00
193:30	6.1	1.017	118.0	6.37	0.00
195:00	5.4	1.024	220.0	20.90	0.00
196:30	5.4	1.020	187.0	24.46	0.00
199:00	6.8	1.021	182.0	7.13	0.00
201:00	6.1	1.026	273.0	11.93	0.00
203:00	5.3	1.029	315.0	40.81	0.00
205:00	5.1	1.031	372.0	46.52	0.00
208:00	5.6	1.028	244.0	15.80	0.00
212:30	5.8	1.027	240.0	17.66	0.00
214:30	5.8	1.006	32.1	0.00	0.00
215:00	6.5	1.011	61.0	6.51	0.00
217:00	5.3	1.021	139.0	10.65	0.00
218:00	5.1	1.022	150.0	31.35	0.00
220:00	5.7	1.024	214.0	18.09	0.00
222:30	5.4	1.030	376.0	20.54	0.00
225:30	5.5	1.024	183.0	34.63	0.00
227:00	5.7	1.026	282.0	27.80	0.00
229:30	5.3	1.034	390.0	42.66	0.00
232:30	5.2	1.031	362.0	23.74	0.00
236:30	5.6	>1.035	304.0	36.21	0.00
238:30	5.6	1.033	217.0	18.08	0.00
241:00	5.4	1.029	197.0	10.92	0.00
243:00	5.5	1.017	110.0	9.36	0.00
248:00	6.6	1.023	179.0	0.00	0.00
252:00	6.0	1.023	105.0	12.13	0.00
257:00	6.3	1.021	170.0	7.00	0.00
258:30	6.2	1.016	122.0	7.59	0.00
260:30	5.6	1.022	130.0	16.48	0.00
262:30	5.6	1.017	111.0	9.15	0.00
263:30	6.1	1.011	66.8	0.00	0.00
265:30	7.1	1.020	127.0	0.00	0.00
268:00	6.8	1.018	116.0	0.00	0.00

Construction of Knowledge Bases Demonstrating Immune System Interactions

Jennifer A. Raker
Graduate Research Assistant
Department of Microbiology and Immunology

Wright State University
3640 Colonel Glenn Hwy
Dayton, OH45435

Final Report for:
Graduate Student Research Program
Wright Laboratory

Sponsored by:
Air force Office of Scientific Research
Bolling Air Force Base, DC

and

Wright Laboratory

September 1996

CONSTRUCTION OF KNOWLEDGE BASES DEMONSTRATING IMMUNE SYSTEM INTERACTIONS

Jennifer A. Raker
Graduate Student
Department of Microbiology and Immunology
Wright State University

ABSTRACT

Using the qualitative modeling program, The Scholar's Companion (TSC), knowledge bases were designed for general processes of the Immune System. The primary objective was to refine and extend the existing knowledge bases that modeled virus-stimulated cytokine production by immune cells. A qualitiative clock was designed and the four existing virus knowledge bases were developed to be compiled in TSC for envisionment building. When the knowledge bases were complete, envisionment graphics were compared and between experiment differences in process episode progressions were noted. A secondary objective was to develop a novel knowledge base and model for lymphocyte trafficking and cell adhesion molecules involved in the process. Much of this knowledge base was developed in the allotted time, and development will continue as an ongoing project. Both of these objectives are important to and a continuation of the wound healing model currently in development by Robert Trelease.

CONSTRUCTION OF KNOWLEDGE BASES DEMONSTRATING IMMUNE SYSTEM INTERACTIONS

Jennifer A. Raker

INTRODUCTION

As education approaches the 21st century, computer-based learning or computer-assisted instruction will play a major role in a child's development. Even now in the 1990's, schools are beginning to use computer technology to enhance learning. The computer is a powerful multimedia tool that the teacher can use any where from lecture presentations to individual work. Use of the computer can be incorporated as both an instructional and as a support tool. The needs of the students and teachers must be balanced with the curriculum and with the availability of computers (1). Computer-based learning in the classroom allows for an individual to interact with the computer which promotes active learning. Students not only enjoy using computers, they learn from them too. Computer-based modeling allows students to participate in active learning in guided and unguided approaches that will lead to creative play and learning. Science education is one educational area in which computer-based learning is being initiated. In science education, the computer-based modeling system leads to discovery-based learning because students have the freedom to explore and receive rapid feedback. In scientific research, in addition, can be a tool for novel discovery through artificial intelligence that can complement and to some extent reduce the need for "wet lab" research. One such computer-based modeling system used in science education and research is The Scholar's Companion (TSC). This program, developed by Think Along Software in California, is now being tested at the high school and professional scientist levels. Our primary objective of this summer project, using TSC, was to update, verify, and improve the virus knowledge bases started the previous year. A secondary goal was to investigate and establish a novel knowledge base for modeling the interactions of cell adhesion molecules with the immune system. The work on this knowledge base would be initiated this summer and continue throughout 1996-1997.

DISCUSSION OF THE PROJECT

A computer is a machine that can process information based on the instructions that are given. The computer then manipulates, changes, and processes the information before giving the output. As computers begin to be used routinely throughout the world, educators are advocating their use in the classroom. Many educators think that computers can contribute to a student's learning experience. Decker Walker, a veteran of "educational revolution" has identified many ways that computers could enhance education (3). These ideas are:

1) offering potential for a more active involvement in learning
2) use of sensory and conceptual modes
3) reduction of " mental drudgery"
4) individual learning based on the student's preferences and performances
5) independent thinking and learning
6) ability to make ideas come alive on the screen to increase creative thinking

The Scholars Companion is a discovery based learning computer system. This program development was fostered by Jack Park of Think Along Software, Inc., Brownsville, California. Jack Park hopes the program can eventually be used in "both interactive educational endeavors and in discovery research" (2). The reasoning behind this program came from cognitive theory and symbolic computer programming. These concepts were developed out of artificial intelligence research (4). An underlying motivation for TSC was a 1988 report published by the California School Readiness Task Force that determined "passive rote learning" was in need of improvement in United States' educational programs. TSC was developed to bring an active technology to the learning process. This would allow a student to have creative playtime especially in science. TSC can be operated in two learning systems namely, the guided and unguided approaches to learning. The guided system would allow TSC to detect student problems when developing the qualitative model and coach the student along. While the unguided system has TSC acting as a listener to student's inputs and then transforming the information into a model. The guided approach would be appropriate for grades K-6 and the unguided would allow the student to explore and serve as a reward.

Overall TSC can be used to discover missing knowledge and use that as information. These two aspects are valuable tools to professional scientists and to students in science education.

TSC provides a student the opportunity to learn in an active fashion. This allows for an interactive form of learning especially in science education. Education is enhanced by hands on experience which can be provided through qualitative modeling development using The Scholar's Companion.

I was originally introduced to The Scholar's Companion by Dr. Nancy Bigley at Wright State University (Dayton, Ohio). TSC was being used as an educational tool with two Dayton area highschools to determine how effective the program was for learning. Simple models of phagocytosis and inflammation were set up to show the basic steps involved in each process (5,8,10) (Fig. 1). At this time work has progressed to starting a knowledge base for infection and immunity with the help of highschool students.

Previous wet lab work conducted in Dr. Bigley's lab was the basis for the virus-stimulated cytokine production knowledge bases (7). Cytokines are proteins made by and secreted by cells that affect itself and other cells (8). Examples are interleukin-10 (IL-10), interleukin-12 (IL-12), and interferon-gamma (IFN-gamma). The interaction of the two strains of virus (EMCV-D and EMCV-MM) with the murine immune system and the cytokines produced as a result of infection. These virus knowledge bases fit under inflammation and immune responses as an addition to an existing wound healing knowledge base and model.

Methodology

Qualitative process theory allows for reasoning about the physical world. Although knowledge is usually common sense oriented, qualitative process theory allows one to formalize the knowledge and make it precise (9). The knowledge from the physical world can be encoded by the qualitative process theory which enables methods to reason with that information (9). The idea is based on physical objects and properties of those objects. The physical processes that the objects encounter actually cause the change. These physical processes can directly or indirectly cause change in the physical world. In order to observe change, not only have to look at the physical objects, but also the processes causing the change must be considered. If a certain change is desired, one has to look for the physical processes involved and modify those processes to have an affect on the physical object.

When using qualitative process theory, a pattern of behaviors and general processes can be generated referred to as qualitative states (9). The use of this set of general rules or behaviors can produce an envisionment that shows all possible combinations of qualitative states and the interactions between these states. The envisionment can be based on an initial set of conditions or initial experiment or set up to analyze a repeated process.

The Scholar's Companion software is based on the ideas of qualitative process theory. TSC starts with a taxonomy that lists all the physical objects. The knowledge bases are the physical processes composed of IF-THEN statements that determine how the objects interact and the relations between objects. A set of initial conditions is used to start the process building. The resulting envisionment is composed of individual boxes that are assembled in a tree-like branching pattern. Each box represents an episode or a firing of a process rule while each branch of the tree is called a history.

All work for this project was performed on two Power PC Power Macintosh computers (9500/132 & 8100/100AV). The TSC version used for this project was TSC3b0NL. All software used for the project was compatible with the Macintosh computer system. The existing knowledge bases of virus-stimulated cytokine production need to be redefined. Literature searches were performed to determine if the cytokine information in the models was current (6,10,11). One area that needed improvement was the concept of time in the qualitative model. Several different ways of dealing with time were tried with each model. The overall goal of developing these models was to determine if there were any gender-based differences in cytokine production within twenty-four hours after infection with two variants of encephalomyocarditis virus, namely EMCV-D and EMCV-MM, using TSC (7).

Another goal was to initiate development of a novel model for cell adhesion molecules which are cell-surface proteins that are involved in binding of cells together in tissues and organs (8). The underlying concept was to this was to generate a generic model of the involvement of cell adhesion molecules in the disease process in an animal at the level of virus-infected cells. General information on cell adhesion molecules was obtained along with the limited amount known about the organs affected by the viruses (5,8,12). Organ-specific and lymphocyte-specific cell adhesion molecule

expression were identified before modeling could begin. Once sufficient information was obtained a simple model was formulated. This model is in the process of further development as the project was coming to a close. Robert Trelease (UCLA, SFRP) is continuing the ongoing work with the cell adhesion molecule model and the wound healing models.

RESULTS

Problems Encountered and Solutions to Problems

When it was time to develop the models in TSC, computers had to be left running for extended periods of time. Many times there were power failures. This was frustrating because it was taking weeks for an envisionment to build. Once electrical outlets were grounded, no further problems were encountered. A problem with the knowledge bases was it would take weeks to run one consisting of over 3,000 episodes. This was due to our concept of time. The concept of time in the knowledge bases was streamlined and modified several times. Finally, time resulted in a qualitative clock. At time zero, once all events had occurred at that timepoint the clock jumped to three hours and so forth. This concept greatly reduced the time to run and the number of episodes in each envisionment. Using the qualitative clock, allowed results to be observed in a number of hours instead of weeks. It was easier to see the end results.

Research Outcomes

I. Virus-Cytokine Model

After comparing the virus-cytokine production envisionments there were significant differences in the outcomes. There were differences between experiments virus.E1 and virus.E2 verses virus.E3 and virus.E4. Experiments E1 and E2 were male murine splenocytes infected with EMCV-D and EMCV-MM respectively (Fig. 2 & 3). Both of these envisionments show different outcomes. At twelve hours post-infection, the virus.E1 experiment had helper T2-cell secreting no interleukin 10 (IL-10) and macrophage secreting IL-12 while the natural killer cell (NK-cell) secreted some of interferon-gamma (IFN-gamma). For the virus.E2 experiment at twelve hours post infection the helper T2-cell secretes IL-10, the macrophage secreted IL-10 and IL-12, and NK-cell secreted a small amount of IFN-

gamma. Finally at 24 hours the significant difference is shown by no IL-10 production in virus.E1 while in virus.E2 there is IL-10 secreted by the macrophage and helper T2-cell.

Experiments with virus.E3 and virus.E4 were those using splenocytes from female mice infected with EMCV-D and EMCV-MM respectively (Fig. 4 & 5). At first glance, both envisionments appear to be identical. The differences are subtle and are located within individual episodes of the envisionment. For example, at twelve hours post infection in the virus.E3 experiment there was a large amount of IFN-gamma produced while in virus.E4 there is only a small amount of IFN-gamma being secreted. There was not expected to be large differences between the two female experiments. Overall, the differences come when comparing the male envisionments to the female envisionments. The fact is there are gender-specific cytokine patterns produced when splenocytes are infected with either virus.

II. Cell Adhesion Model

The model for cell adhesion molecules expressed during lymphocyte trafficking began with a great deal of searching and reading. Once enough information was collected, the knowledge base was constructed. There was some difficulty expressing the idea of circulating immune cells. Once this part was established, the process of cell activation and the cell adhesion molecules involved were added to the model. The end result was a nice and relatively simple envisionment demonstrating the activation of a naive T helper 1 cell and once activated, circulating to and binding to the coronary vascular system (heart) (Fig. 6). This envisionment has potential for becoming very complex with the ongoing work.

Discussion and Conclusions

The Scholar's Companion provides students and professional scientists a way to study scientific universes in a qualitative manner. A professional scientist can make predictions about an experiment using TSC and then go into the laboratory and conduct the actual experiment for validation of the model. Once validated, this process can reduce costs and saves time experimentally. The results obtained from the lab experiments can be compared with the results obtained from TSC to discover if there are any similarities or differences or even new views of knowledge not perceived beforehand.

Programs similar to TSC can become valuable tools in science education and research in the future. These types of programs can allow students to have an active learning experience while also helping scientists conduct what-if studies and construct qualitative models to obtain conceptual views of the research project before going into the lab.

The four virus knowledge bases revealed the different cytokine patterns possible when splenocytes are infected with two different strains of virus. The obvious difference was the gender-specific cytokine patterns. This represented a difference in immune response between splenocytes from males verses those from females. The major accomplishment made with this objective was the establishment of the qualitative clock. This concept of time can be used in any knowledge base model. The qualitative clock was innovative and allowed for envisionment building within practical time period.

The cell adhesion molecule knowledge base is a general or generic one that can be applied to various experiments. This knowledge base also has the potential for becoming very specific and more complex. At present, the model is at the stage of having an immune cell circulate, become activated, and proceed to various organs based on the expression of the cell adhesion molecules. Eventually this novel computer-based model can be used to test hypothesis and predictions for actual laboratory research. This general model of lymphocyte activation is important in the concept of innate immunity. Cells in the innate immune system have a crucial role initiating and directing the adaptive immune response (8). This is the first line of host defense against common microorganisms and aids in controlling infection before the adaptive immunity takes effect four to five days after infection. It is important to learn what is going on in the early stages of infection to better understand the process and to develop ways to help fight off infection. The cell adhesion molecule model is a first step in that direction allowing for the collection of known information into a knowledge base. The use of this knowledge base, would allow for many predictions to be proposed before laboratory testing. The computer-based model could aid in narrowing or changing the predictions based on the envisionment. This novel model has the potential to be of great use for many years as more becomes known about cell adhesion molecules and the healing process.

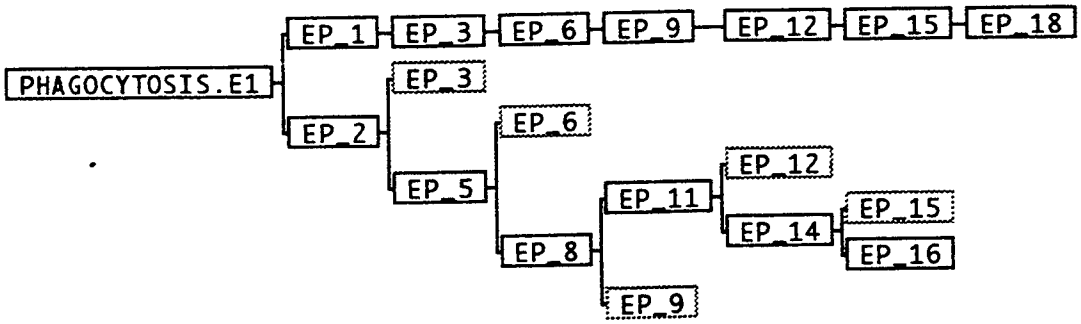

Episodes:

1 & 3	Phagocyte.binds.particle
6	Phagocyte.engulfs.particle
9	Lysosome.migrates.to.phagosome
12	Lysosome.fusion.with.phagosome
15	Phagolysosome.releases.enzyme
18	Enzyme.digests.particle

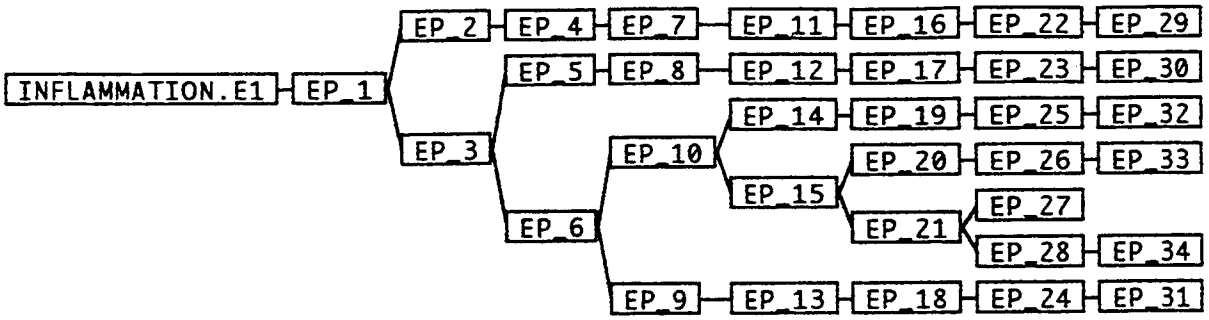

Figure one. Two envisionments used to teach immunology to highschool students.

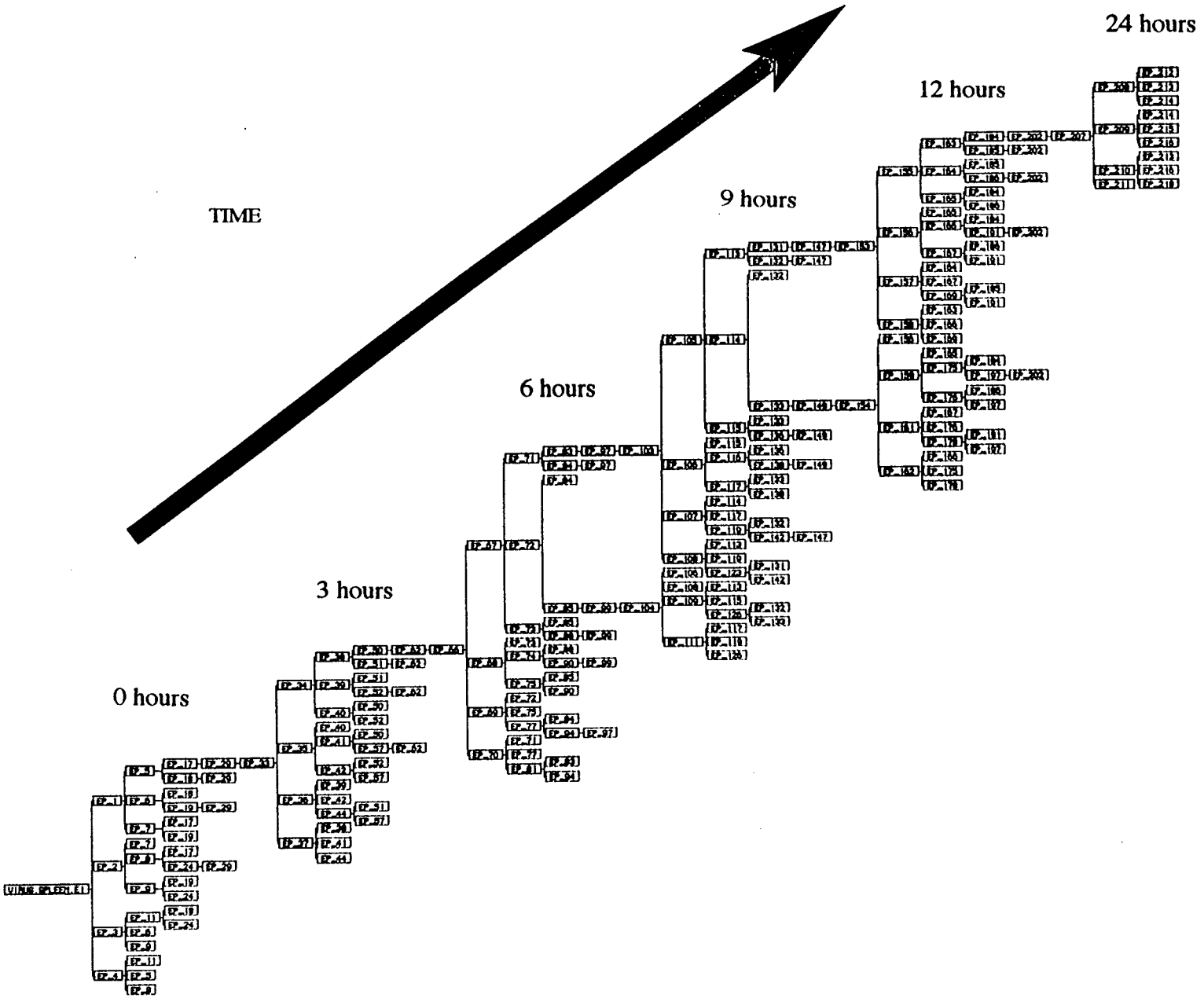

Figure two. Virus.E1 Envisionment. Splenocytes from male mice infected with EMCV-D.

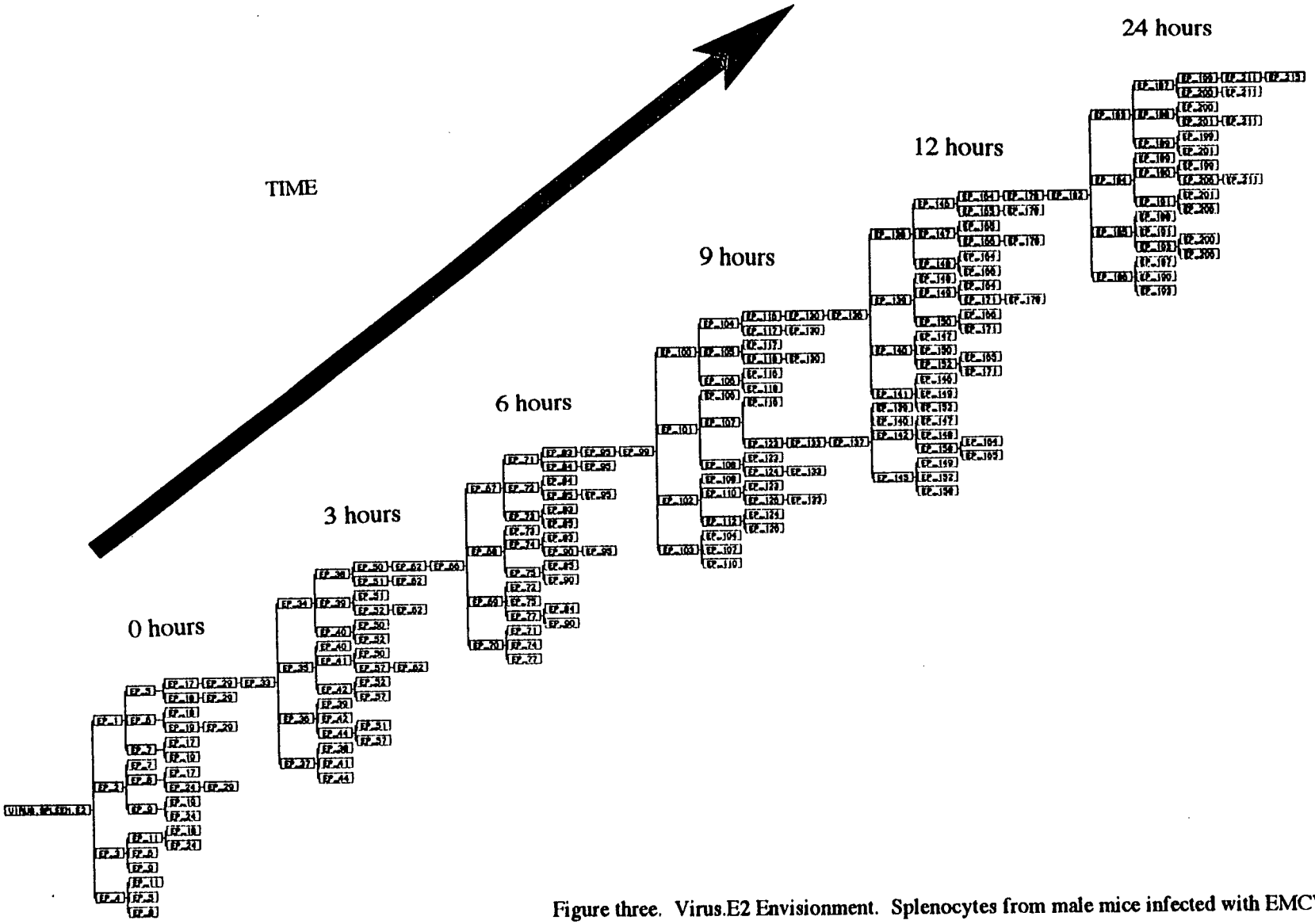

Figure three. Virus.E2 Envisionment. Splenocytes from male mice infected with EMCV-MM.

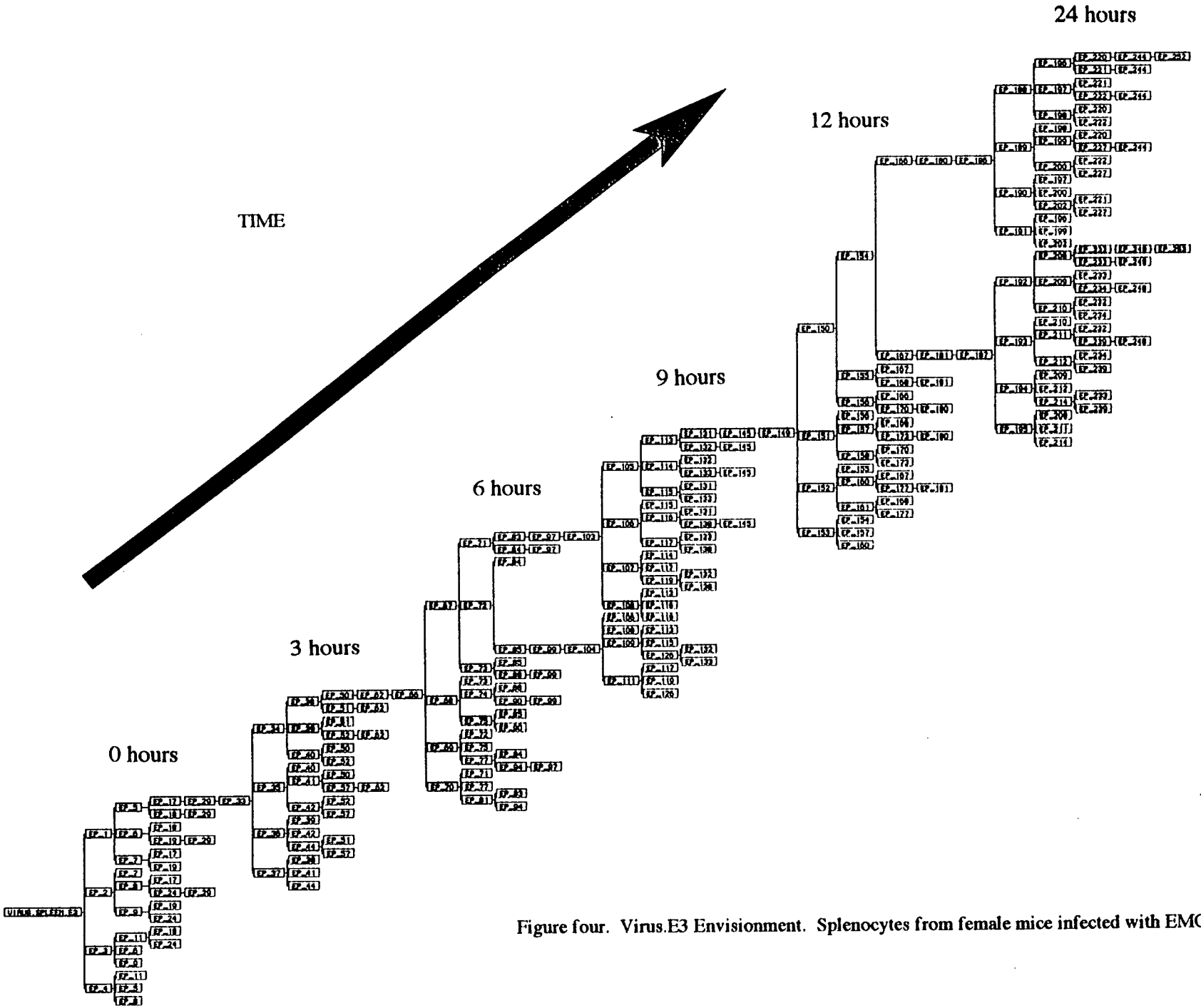

Figure four. Virus.E3 Envisionment. Splenocytes from female mice infected with EMCV-D.

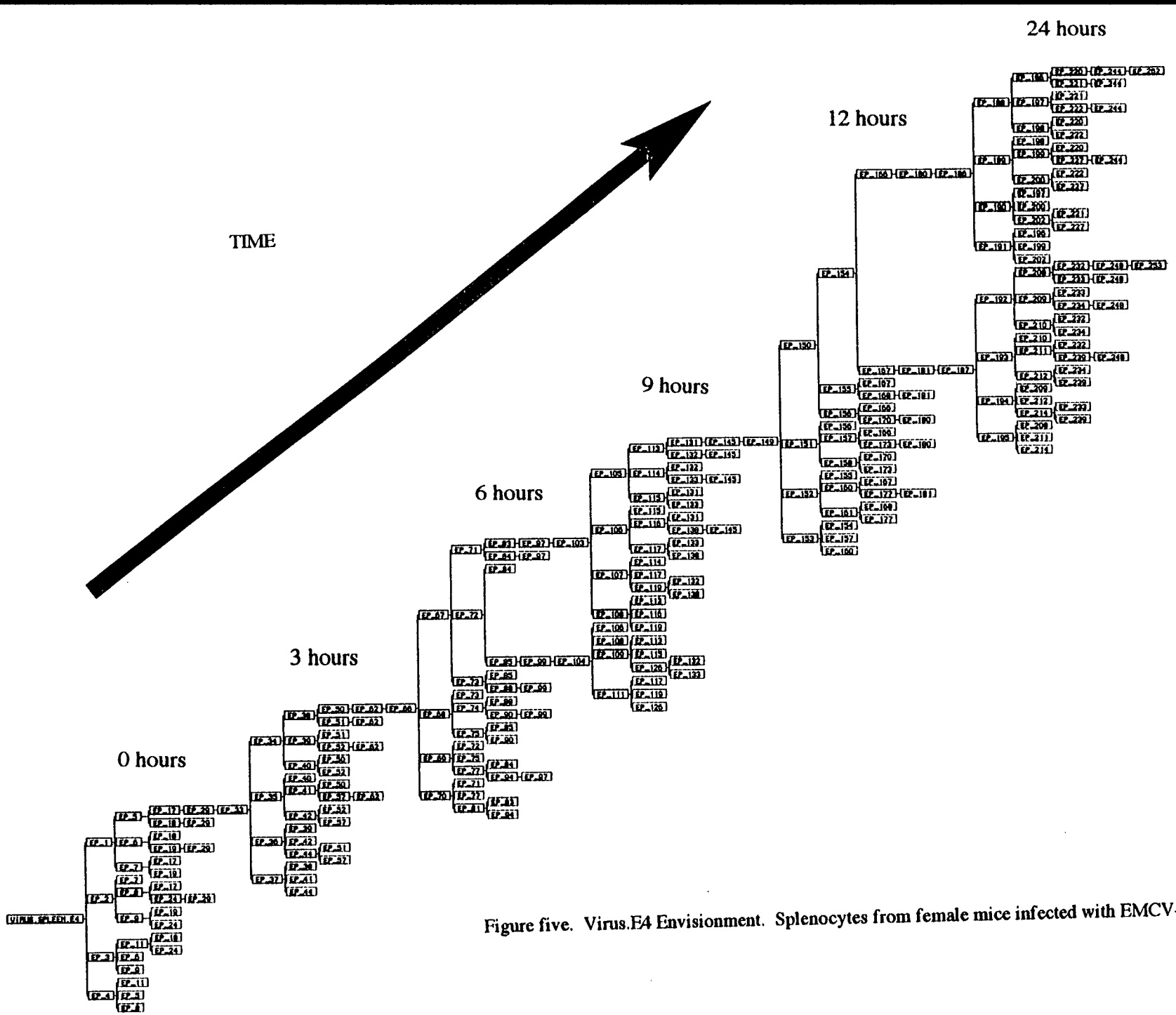

Figure five. Virus.E4 Envisionment. Splenocytes from female mice infected with EMCV--MM.

Figure six. ImmuneCAMs1.E1 Envisionment. Cell Adhesion Molecule Model

Naive T cell circulates freely to different organs.

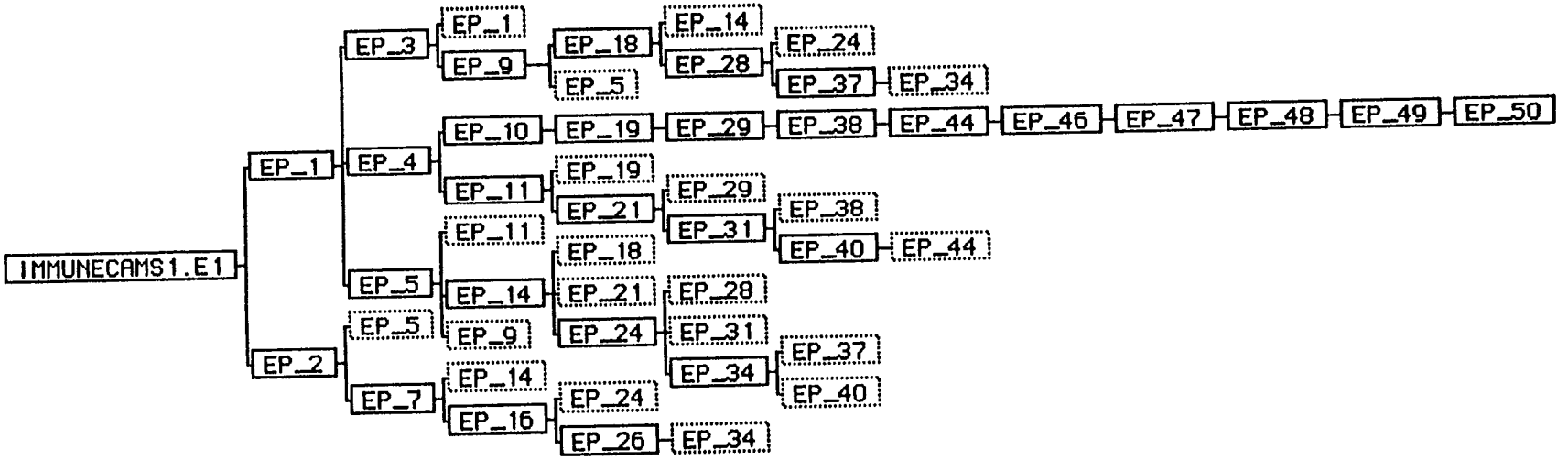

Episodes:

44	Diapedesis of naive T cell
46	Macrophage activates Th1
47	Activated Th1 expresses CAMs and leaves lymph node
48	Activated Th1 circulates freely to different organs
49	Activated Th1 cell binds to heart
50	Diapedesis of activated Th1 cell into heart

Future Aspects

The cell adhesion molecule model is an ongoing project that will continue on into next summer. A possible future project would be to combine that model with the virus knowledge bases to determine the manner in which the adhesion molecules exert an affect on cytokine patterns in response to virus or vice versa. Even the use of two knowledge bases used to teach highschool students some immunology are of value in determining the changes when combined with the cell adhesion model. This is true especially in the inflammation process where these kind of interactions are necessary for cells to come into contact with one another. Overall, TSC has the potential to model a great variety of scientific systems and perhaps other areas, it is just a matter of learning to use the program.

REFERENCES

1) Marsh, George, E.II. 1993. Computers: Literacy and Learning. Newbury Park, California: Corwin Press, Inc.

2) Small Business Research Program Phase 1 Grant Application Nancy Bigley, Ph.D. 1994.

3) Sewell, David. 1990. New Tools For New Minds. New York: St. Martin's Press. pp 1-14.

4) Trelease, Robert and Jack Park. 1995. "Qualitative Process Modeling of Biological Systems: Methods and Experiments in Cellular Immunology". Unpublished manuscript.

5) Kuby, Janis. 1994. Immunology. New York: W. H. Freeman and Company.

6) Nicola, Nicolas, A. 1994. Guidebook to Cytokines and Their Receptors. New York: Sambrook and Tooze Publication at Oxford University Press.

7) Curiel, R.E. 1995. Cytokine(s) expressed by cultured splenocytes during the first 24 hours of picornavirus infection reflect the disease susceptibility or resistance of the spleen cell donors. Wright State University, Dayton, OH Ph.D. Thesis.

8) Janeway, C.A. Jr., and Travers, P. 1996. Immunobiology: The Immune system in Health and Disease. New York: Garland Publishing Inc.

9) Forbus, K. D., and De Kleer, J. 1993. Building Problem Solvers. Cambridge Massachusetts: The MIT Press.

10) Sigal, L.H., and Ron, Y. 1994. Immunology and Inflammation: Basic Mechanisms and Clinical Consequences. New York: McGraw-Hill, Inc.

11) Mosmann, T. R. And Sad S. 1996. The expanding universe of T-cell subsets: Th1, Th2, and more. Immunology Today. 17(3):138-146.

12) Cerutis, D.R., Bruner, R.H., Thomas, D.C., and Giron, D.J. 1989. Tropism and Histopathology of the D, B, K, and MM Variants of Encephalomyocarditis Virus. Journal Of Medical Virology. 29:63-69

13) Imhof, B.A., and Dunon, D. 1995. Leukocyte Migration and Adhesion. Advances in Immunology. 58:345-416.